Carbohydrate and Metabonomic Studies by NMR Spectroscopy

Gustav Nestor
Faculty of Natural Resources and Agricultural Sciences
Department of Chemistry and Biotechnology
Uppsala

Doctoral Thesis
Swedish University of Agricultural Sciences
Uppsala 2014

Acta Universitatis agriculturae Sueciae
2014:6

Cover: $^{1}H,^{1}H$-TOCSY NMR spectra of a hyaluronan hexasaccharide at -10 °C (purple), -5 °C (blue), 0 °C (green), and 5 °C (red). The mixing time was 20 ms. The spectra show cross peaks between hydroxy protons and ring protons.

ISSN 1652-6880
ISBN (print version) 978-91-576-7960-4
ISBN (electronic version) 978-91-576-7961-1

Print: SLU Service/Repro, Uppsala 2014

Carbohydrate and Metabonomic Studies by NMR Spectroscopy

Abstract

NMR spectroscopy can be used to investigate organic and biomolecular structures, both as pure compounds and in complex mixtures. In this thesis NMR spectroscopy was used for carbohydrate and metabonomic studies.

Lipopolysaccharides are major components of the outer cell membrane of Gram-negative bacteria and are involved in pathogenic interactions. The structure of a lipopolysaccharide from the human pathogen *Plesiomonas shigelloides* was analyzed by NMR spectroscopy and mass spectrometry. The structure contained an O-specific polysaccharide with a tetrasaccharide repeating unit. The core oligosaccharide was an undecasaccharide with previously not reported heterogeneity within the carbohydrate backbone.

Hyaluronan is a glycosaminoglycan with high viscosity and water-retaining ability. Hydroxy protons of hyaluronan oligosaccharides were studied by NMR spectroscopy in aqueous solution to investigate hydrogen bonding interactions and hydration. Weak hydrogen bonding was observed between hydroxy protons and the ring oxygens over the β(1→3) and β(1→4) glycosidic linkages. A chemical exchange interaction was also identified between O(4)H of *N*-acetylglucosamine and O(3)H of glucuronic acid across the β(1→3) linkage. The interaction could be mediated through water bridges and thus contribute to the water-retaining ability of hyaluronan.

Polyunsaturated fatty acids are essential nutritional components of marine lipid sources. A ^{1}H HR-MAS NMR method was developed to determine the amount of essential polyunsaturated fatty acids in fish muscle without any pretreatment. Additionally, the small metabolite profile of the fish muscle was obtained, which can be used to determine fish quality.

Caloric restriction is known to increase the lifespan of rats. In order to evaluate the metabolic responses to graded caloric restriction in rats, blood serum was analyzed by NMR spectroscopy. Multivariate analysis showed a decrease in blood lipids and alanine, and an increase in creatine and 3-hydroxybutyrate as a response to caloric restriction.

Keywords: NMR spectroscopy, carbohydrates, metabonomics, lipopolysaccharides, hyaluronan, fish, fatty acids, caloric restriction, *Plesiomonas shigelloides*

Author's address: Gustav Nestor, SLU, Department of Chemistry and Biotechnology, P.O. Box 7015, 750 07 Uppsala, Sweden
E-mail: gustav.nestor@slu.se

Dedication

Till mamma

The seemingly impossible is possible.
Hans Rosling

Contents

List of Publications

This thesis is based on the work contained in the following papers, referred to by Roman numerals in the text:

I Nestor, G., Lukasiewicz, J. and Sandström, C. (2014). Structural analysis of the core oligosaccharide and the O-specific polysaccharide from *Plesiomonas shigelloides* O33:H3 (Strain CNCTC 34/89) Lipopoly-saccharide. *European Journal of Organic Chemistry* doi 10.1002/ejoc.201301399 (in press).

II Nestor, G., Kenne, L. and Sandström, C. (2010). Experimental evidence of chemical exchange over the β(1→3) glycosidic linkage and hydrogen bonding involving hydroxy protons in hyaluronan oligosaccharides by NMR spectroscopy. *Organic and Biomolecular Chemistry* 8(12), 2795-2802.

III Nestor, G., Bankefors, J., Schlechtriem, C., Brännäs, E., Pickova, J. and Sandström, C. (2010). High-resolution ^{1}H magic angle spinning NMR spectroscopy of intact Arctic char (*Salvelinus alpinus*) muscle. Quantitative analysis of *n*-3 fatty acids, EPA and DHA. *Journal of Agricultural and Food Chemistry* 58(20), 10799-10803.

IV Nestor, G., Sandström, C., Malmlöf, K. and Eriksson, J. Metabolic responses to graded levels of short term caloric restriction in rats as measured by NMR spectroscopy (manuscript).

Papers I-III are reproduced with the permission of the publishers.

Paper not included in this thesis:

V Rydén, A., Nestor, G., Jakobsson, K. and Marsh, G. (2012) Synthesis and tentative identification of novel polybrominated diphenyl ether metabolites in human blood. *Chemosphere* 88(10), 1227-1234.

The contribution of Gustav Nestor to the papers included in this thesis was as follows:

I Planning of the project, all experimental work, analysis and writing of the manuscript.

II Planning of the project together with Corine Sandström. All experimental work, interpretation and writing of the manuscript.

III Discussion of the problem to be solved together with Corine Sandström, Johan Bankefors, and Jana Pickova. Designed the execution of the project together with Corine Sandström. Parts of the experimental work and most of the analysis. Writing of the manuscript together with Corine Sandström and Johan Bankefors.

IV Parts of the experimental work, most of the analysis and writing of the manuscript.

Abbreviations

BPP-LED	bipolar-pair longitudinal eddy-current delay
CID	collision induced dissociation
CNCTC	Czechoslovak national collection of type cultures
COSY	correlation spectroscopy
CP-MAS	cross-polarisation magic angle spinning
CPMG	Carr-Purcell-Meiboom-Gill
CR	caloric restriction
DHA	docosahexaenoic acid
DMSO	dimethyl sulphoxide
DNA	deoxyribonucleic acid
DOSY	diffusion ordered spectroscopy
DQF	double-quantum filtered
EI	electron ionization
EPA	eicosapentaenoic acid
ESI	electro-spray ionization
FA	fatty acids
FAME	fatty acid methyl ester
FID	free induction decay
FT	Fourier transformation
Gal	galactose
GalA	galacturonic acid
GalN	galactosamine
GalNAc	*N*-acetylgalactosamine
GC	gas chromatography
Glc	glucose
GlcA	glucuronic acid
GlcN	glucosamine
GlcNAc	*N*-acetylglucosamine
HA	hyaluronan

Hex	hexose
HMBC	heteronuclear multiple-bond correlation
HR-MAS	high-resolution magic angle spinning
HSQC	heteronuclear single-quantum coherence
INEPT	insensitive nuclei enhanced by polarization transfer
Kdo	3-deoxy-D-*manno*-oct-2-ulosonic acid
L,D-Hep	L-*glycero*-D-*manno*-heptose
LDL	low-density lipoprotein
LED	longitudinal eddy current delay
LPS	lipopolysaccharide
MALDI	matrix-assisted laser desorption ionization
MD	molecular dynamics
MS	mass spectrometry
NEFA	non-esterified fatty acids
NMR	nuclear magnetic resonance
NOE	nuclear Overhauser effect
NOESY	nuclear Overhauser effect spectroscopy
OPLS-DA	orthogonal-partial least square discriminant analysis
OS	oligosaccharide
PC	principal component
PCA	principal component analysis
PFG	pulsed field gradient
PLS-DA	partial least square discriminant analysis
PMAA	partially methylated alditol acetate
PS	polysaccharide
PUFA	polyunsaturated fatty acids
ROE	rotating-frame nuclear Overhauser effect
ROESY	rotating-frame nuclear Overhauser effect spectroscopy
RU	repeating unit
STE	stimulated echo
TOCSY	total correlation spectroscopy
TOF	time of flight
TQF	triple-quantum filtered
UV	ultraviolet
VLDL	very low-density lipoprotein
WATERGATE	water suppression by gradient tailored excitation

1 Introduction

Nuclear magnetic resonance (NMR) spectroscopy is used in many different chemical contexts, from structure analysis of biomolecules, to structure determinations of small organic molecules, and analysis of metabolites in biological systems. Since the first observation of NMR signals from paraffin (Purcell *et al.*, 1946) and water (Bloch *et al.*, 1946), NMR spectroscopy has expanded to one of the major techniques in chemistry.

However, the history of structural biology and chemistry goes back all the way to the ancient Greece, where the word atom, from 'atomos' meaning indivisible, first appeared. Molecules were later introduced in the nomenclature in the 18th century. In 1806 the Swedish chemist Jöns Jacob Berzelius made the first distinction between organic and inorganic chemistry (Berzelius, 1806), which came to be the start of the development of organic chemistry.

In the early 20th century, molecular structures were still two-dimensional, but a number of new techniques for structural analysis were being developed, mainly by physicists. X-ray crystallography made it possible to determine the three-dimensional structure of small organic compounds, as well as of macromolecules like proteins and nucleic acids. The early use of X-ray crystallography on biomolecules led to breakthroughs like the discovery of α-helices and β-sheets as secondary structural elements of proteins (Pauling & Corey, 1951; Pauling *et al.*, 1951) and the double-helix of DNA (Watson & Crick, 1953).

An intrinsic property of X-ray crystallography is that it requires crystals of the sample. If the molecule does not crystallize, which is the case for most complex carbohydrates and membrane proteins, NMR spectroscopy is a good alternative. NMR spectroscopy can be used to analyze the structure of a molecule in solution and since most biomolecules occur and interact in aqueous solution that is an advantage. NMR spectroscopy has become one of the most common techniques for the determination of protein structures and it is crucial in the analysis of complex carbohydrates.

This thesis is a contribution to the broad area of NMR spectroscopy of biomolecules and biological systems, with emphasis on carbohydrates and metabonomics. NMR spectroscopy will be briefly introduced in chapter 2, followed by the structure analysis of carbohydrates in chapter 3. Also other techniques for structure analysis of carbohydrates will be mentioned. In chapter 4 the conformational analysis of carbohydrates is presented, with special focus on NMR spectroscopy of hydroxy protons. Metabonomics as an approach to analyze metabolites in biological systems is then introduced in chapter 5.

The introduction ends up in four applications of NMR spectroscopy, which are the basis for this thesis. Chapter 6 and paper I describe the structural analysis of a lipopolysaccharide (LPS) from the bacterium *Plesiomonas shigelloides* by NMR spectroscopy and mass spectrometry (MS). This analysis of the primary structure of a carbohydrate is followed by the analysis of hydrogen bonding in hyaluronan oligosaccharides by NMR spectroscopy of hydroxy protons (chapter 7 and paper II). A metabonomics approach is then exemplified by the quantitative analysis of *n*-3 fatty acids (FA) in intact Arctic char (*Salvelinus alpinus*) muscle by high-resolution magic angle spinning (HR-MAS) NMR spectroscopy (chapter 8 and paper III) and the analysis of blood serum from obese rats under caloric restriction (CR) by NMR spectroscopy and multivariate analysis (chapter 9 and paper IV).

2 NMR spectroscopy

This chapter will give a short introduction to NMR spectroscopy, with emphasis on the experiments that I have been using throughout the work presented in this thesis. NMR is a physical phenomenon with several different applications from liquid NMR spectroscopy and solid-state NMR spectroscopy to magnetic resonance imaging. This introduction will be limited to liquid NMR spectroscopy and HR-MAS NMR spectroscopy, which is used for semi-solid samples.

2.1 Nuclear magnetic resonance

Elementary particles possess three quantum numbers defined by the Schrödinger equation: The principal quantum number (n), the angular quantum number (l), and the magnetic quantum number (m_l). A fourth quantum number, the spin quantum number (m_s), was described by Dirac (1928) through a combination of quantum mechanics and Einstein's theory of relativity.

The spin quantum number is a fundamental property of elementary particles, making the difference between quarks and leptons (m_s = ½) which constitute matter, and elementary bosons (m_s = 1 or 0 for the Higg's particle) which represent the forces that bind quarks and leptons together. When quarks are merged into protons and neutrons the overall spin is ½. They are therefore called spin-½ particles, where also electrons are included. Adding protons and neutrons together to different atomic nuclei can result in integer or half-integer spins. Spin ½ (^{1}H, ^{13}C, ^{15}N), spin 1 (^{2}H and ^{14}N), and spin 0 (^{12}C and ^{16}O) are among the most common in biomolecules.

When the spin is non-zero, there is an angular magnetic moment (μ), defined by m_l and m_s. This is a vector where the size and direction are quantized, thus restricted to certain numbers. The maximum value of the z-component of μ is described by

$$\mu_z = \gamma \hbar I$$

where γ is the gyromagnetic ratio, ħ is the reduced Planck constant and I is the spin state of the nucleus. There are $2I+1$ different values of I, varying from $+I$ to $-I$ in integer steps. Hence spin-½ particles have two allowed spin states: +½ and –½.

By applying an external magnetic field, B_0, along the z axis an energy difference between the spin states will arise. The energy difference, ΔE, between two adjacent energy levels is

$$\Delta E = \gamma \hbar B_0$$

The splitting into multiple states affects the distribution between the spin states according to the Boltzmann distribution

$$\frac{N_{-½}}{N_{+½}} = \mathrm{e}^{-\Delta E/kT}$$

in which N is the population of a spin state, k is Boltzmann's constant, and T is the absolute temperature. Since the spin state +½ is slightly lower in energy (if γ is positive) it will be slightly more populated.

The magnetic moments are actually not lined up parallel to the z direction, but are circulating with a defined frequency, called the Larmor frequency (v_0). This motion, called precession, is due to the force generated by B_0 and is related to ΔE by the Planck relation $E = hv$, in which h is Planck's constant.

Like other kinds of spectroscopy, NMR spectroscopy is based on the absorption and emission of electromagnetic radiation due to an energy difference. This energy difference, ΔE, is equivalent to radiation of v_0, which for atomic nuclei is in the radiofrequency region. For a proton in a magnetic field of 14.1 T the frequency is 600 MHz, which is called the resonance frequency.

Some NMR active nuclei that are common in biomolecules are summarized in Table 1. Nuclei with high natural abundance, spin-½, and a high γ are advantageous in NMR spectroscopy, since they give rise to high sensitivity. ^{1}H and ^{31}P are perfect choices in biomolecular NMR spectroscopy, because of high natural abundance and high γ. ^{13}C is more difficult to study because of the low natural abundance and ^{15}N has both a low natural abundance and a low γ. However, there are techniques to observe ^{13}C and ^{15}N via ^{1}H (*e. g.* by polarization transfer), and ^{13}C and ^{15}N are also extensively studied in *e. g.* proteins and nucleic acids by labeling.

Table 1. *Properties of some NMR active nuclei found in biomolecules.*[1]

Nuclide	Natural abundance (%)	Spin (I)	$\gamma/10^7$ rad T^{-1} s^{-1}	Frequency[2]/MHz
^{1}H	99.99	½	26.75	600.00
^{2}H	0.01	1	4.11	92.10
^{13}C	1.07	½	6.73	150.87
^{15}N	0.37	½	-2.71	60.82
^{31}P	100.00	½	10.84	242.88

1. Values were taken from Harris *et al.* (2001).
2. In a magnetic field of 14.1 T.

2.2 The chemical shift

The electron clouds surrounding the nuclei induce local magnetic fields. The actual field in the microenvironment of a specific nucleus is thus determined by the electrons surrounding that nucleus, neighboring atoms and solvent atoms. This property, called shielding, affects the resonance frequency so that nuclei with different microenvironments have small differences in their resonance frequencies. The actual resonance frequency is expressed by

$$\nu = \frac{\gamma B_0(1-\sigma)}{2\pi}$$

where σ is the shielding constant. The variation of the resonance frequency with shielding is measured by the chemical shift, δ, and is expressed as the difference in resonance frequency compared to a reference standard. To avoid that the chemical shift is dependent on the magnetic field B_0, it is derived as the ratio between the difference in frequency of an arbitrary nucleus i and the reference r, and the frequency of the reference (Harris *et al.*, 2001):

$$\delta = \frac{\nu_i - \nu_r}{\nu_r}$$

Since the numerator is expressed in Hz and the denominator in MHz, chemical shifts are normally expressed in ppm (Harris *et al.*, 2001). In ^{1}H and ^{13}C NMR spectroscopy, tetramethylsilane (TMS) is used as a reference, but in D_2O solutions sodium 3-(trimethylsilyl)-1-propanesulfonate (DSS) is an alternative reference (Harris *et al.*, 2001) because of better solubility.

2.3 Excitation and relaxation

Protons in a magnetic field of 14.1 T (600 MHz) have a difference in energy (ΔE) of $4.0 \cdot 10^{-25}$ J. According to the Boltzmann distribution, at 25 °C this corresponds to a population difference of 1 in about 10.000. Compared to other

spectroscopic techniques like X-ray, UV and IR, this is a very small energy difference and the population difference could seem to be negligible. Nevertheless, the net magnetization, which is the sum of all individual spins, can be used in NMR spectroscopy. The net magnetization is a vector in the $+z$ direction, but when a frequency pulse is applied that is identical to the Larmor frequency the magnetization will be shifted from the z axis on to the y axis. The relaxation of the magnetization from the xy plane back to the z axis can then be detected as the resonance.

Relaxation is divided into one component parallel to the z axis, known as spin-lattice relaxation with time constant T_1, and a second component perpendicular to the z axis, known as spin-spin relaxation with time constant T_2. The "lattice" is the surroundings of the nuclei, to which energy can be transferred if there is a magnetic field fluctuating at the Larmor frequency. Since the frequency range of the lattice is wide, the probability of a certain spin to be able to transfer its magnetization is low, and thus the NMR relaxation times are long compared to other spectroscopic techniques (Freeman, 1988).

The main mechanisms for spin-lattice relaxation are dipole-dipole relaxation, relaxation due to shielding anisotropy, and spin-rotation relaxation (Freeman, 1988). Dipole-dipole relaxation is due to the motion of neighboring magnetic dipoles, which causes fluctuating magnetic fields. Shielding anisotropy arises because the shielding of the nucleus depends on the orientation of the molecule with respect to the B_0 field direction. Spin-rotation relaxation is due to small magnetic fields induced by the moving charges of the electrons as the molecule rotates.

Dipole-dipole relaxation of one spin can enhance the signal of another spin. This, so-called, nuclear Overhauser effect (NOE) is used to enhance the weak signals of low-abundance ^{13}C and to measure proximity of protons through space (Freeman, 1988). The latter application is used in conformational studies of biomolecules to measure inter-proton distances (r) by the dependence of the NOE intensity to r^{-6}.

Spin-spin relaxation is due to the gradual loss of phase coherence of the precessing spins over time. This does not alter the energy of the spin system, but the NMR signals become broader. Mechanisms of spin-lattice relaxation also affect spin-spin relaxation, but there are additional interactions that solely have an effect on T_2 relaxation. One such interaction is chemical exchange, where one nucleus is replaced by another nucleus with random precession, but without affecting the energy of the system. Another source of signal broadening is inhomogeneities of the magnetic field B_0, which causes chemically equivalent nuclei to precess with slightly different Larmor frequencies and thus a loss of phase coherence.

Molecules with slow molecular tumbling, such as macromolecules or solids, are dominated by T_2 relaxation ($T_2 < T_1$), whereas molecules with fast molecular tumbling are influenced in the same manner by spin-lattice and spin-spin relaxation and $T_2 = T_1$ (Freeman, 1988). The rate of different relaxation mechanisms determines the time-scale of the NMR experiment, which is usually in the range of milliseconds to seconds for ^{1}H and milliseconds to minutes for ^{13}C.

2.4 One-dimensional NMR

NMR experiments are carried out by applying a strong radiofrequency pulse with a short duration (microseconds) close to the resonance frequency. The magnetization is pushed from the *z* axis towards the *y* axis (a 90° pulse) or, for a longer pulse, further to the *-z* direction (a 180° pulse). The induced magnetization along the *y* axis is detected as the free induction decay (FID). This time domain function is converted into the frequency domain (the spectrum) by a Fourier transformation (FT; Figure 1).

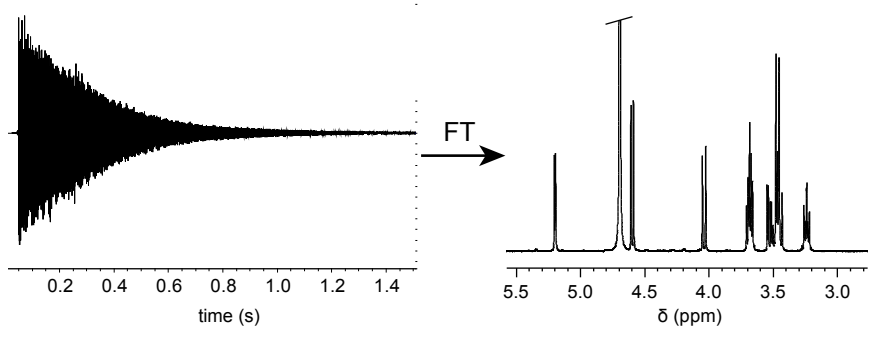

Figure 1. Signals in the time domain (FID) and in the frequency domain from a ^{1}H NMR experiment of glucuronic acid in deuterated water (D_2O). The truncated signal at 4.7 ppm originates from HDO.

The information that can be extracted from a ^{1}H NMR spectrum is not restricted to the chemical shift, which is used to determine the chemical surrounding of a proton due to differences in electronic shielding, but also involves coupling constants, the linewidth, and the relative intensities of the signals (Figure 2).

Coupling constants have their origin in the influence of neighboring spins on the nucleus being observed. This scalar spin-spin coupling is transferred through the electrons of chemical bonds and can yield additional structural information. Scalar coupling constants can be homonuclear or heteronuclear.

The one-bond scalar coupling between ^{1}H and ^{13}C ($^{1}J_{CH}$) is only visible in a ^{1}H NMR spectrum as small ^{13}C satellites, due to the low abundance of ^{13}C and ^{12}C being magnetically inactive (spin 0). On the other hand, homonuclear ^{1}H-^{1}H coupling strongly affects the spectrum by splitting of the signals into multiplets.

The area under a ^{1}H NMR signal is proportional to the abundance of that proton in the sample. This is essential in structural analysis and makes quantitative NMR possible.

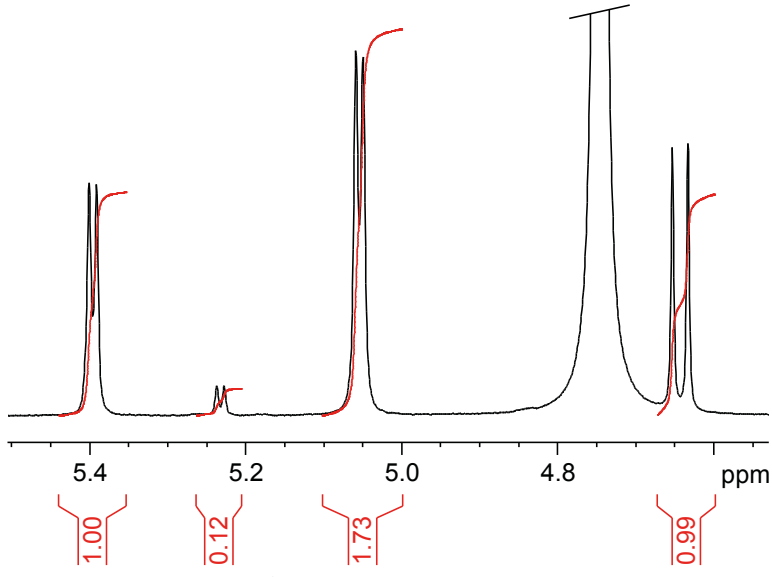

Figure 2. The anomeric region of a ^{1}H NMR spectrum of a mixture of maltose and β-cyclodextrin in D_2O, showing signals with differences in chemical shifts, coupling constants, and intensities. The truncated signal at 4.75 ppm originates from HDO.

2.4.1 Spin echoes

The manipulation of spins by applying different pulse sequences is the basis of NMR spectroscopy. One common spin sequence is the spin echo experiment, or the CPMG experiment, named by its inventors Carr and Purcell (1954), and Meiboom and Gill (1958). It allows the phase coherence that is lost by magnetic field inhomogeneity to be refocused by a 180° pulse in the *xy* plane – an effect similar to an echo. The pulse sequence can be described as $90°\text{-}(\tau\text{-}180°\text{-}\tau)_n$, where τ is a time delay for the evolution of the precession and $n > 1$ gives a 'train' of spin echoes, which removes effects of molecular diffusion (Figure 3A).

The CPMG experiment was originally developed to measure T_2 relaxation times (Meiboom & Gill, 1958), but it has also been used extensively to im-

prove linewidths by removing effects of field inhomogeneity. The spin echo sequence is an important tool for spectral editing, for instance by eliminating unwanted resonances from the spectrum. Signals with short T_2 relaxation times can be eliminated by the CPMG experiment to filter out the broad lines of macromolecules. Modulation of coupling constants (J modulation) and suppression of solvent signals (see section 2.4.3) can also be achieved by spin echo applications.

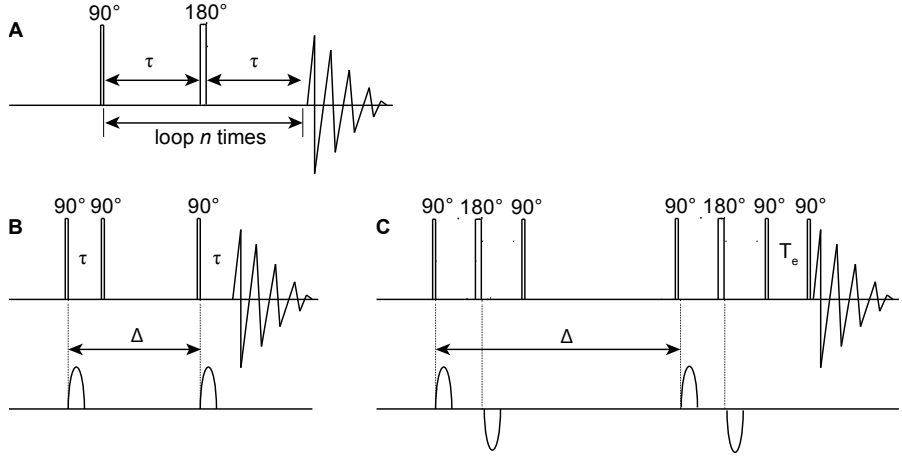

Figure 3. Schematic representations of the following pulse sequences: **A**) the CPMG experiment, **B**) the STE experiment with pulsed field gradients, and **C**) the BPP-LED experiment.

2.4.2 Diffusion NMR

The use of spin echoes to determine diffusion coefficients was realized already by Hahn (1950). Instead of removing the effects of molecular diffusion by repeating the spin echo sequence, the fact that spins are spatially labeled by the application of magnetic field gradients can be utilized. Originally, continuous gradients were used, but the advantage of pulsed field gradients (PFG) was later demonstrated (Stejskal & Tanner, 1965).

Hahn (1950) described the appearance of a stimulated echo (STE) after three 90° pulses, with a delay, Δ, between the two gradient pulses that is correlated to the diffusion coefficient of the observed molecule. The inclusion of PFG for defocusing and subsequent refocusing of the spins in the xy plane (Figure 3B) further improved the experiment (Stejskal & Tanner, 1965).

However, the use of gradient pulses induces eddy currents in the surrounding metal structures of the probe and the magnet, which leads to spectral distortions (Johnson, 1999). Gibbs and Johnson (1991) introduced the longitudinal eddy current delay (LED) sequence to diminish the effects of eddy currents by the additional element 90°-T_e-90°, where T_e is an eddy current delay.

The eddy currents were further reduced by replacing the PFG pulses with two gradient pulses of different polarity, separated by a 180° pulse (Wu *et al.*, 1995) – the so-called bipolar pulse LED (BPP-LED) sequence (Figure 3C).

Diffusion NMR experiments can be used for spectral editing purposes. Resonances from small molecules with fast diffusion can be filtered out, leaving signals from large molecules.

A pseudo-2D version of the diffusion experiment, DOSY (diffusion ordered NMR spectroscopy; Figure 4), has been developed, where the differences in diffusion coefficients can be clearly visualized by increasing gradient strength in the F1 dimension (Johnson, 1999). This technique can be used to investigate complex mixtures (Novoa-Carballal *et al.*, 2011) and intermolecular interactions (Brand *et al.*, 2005).

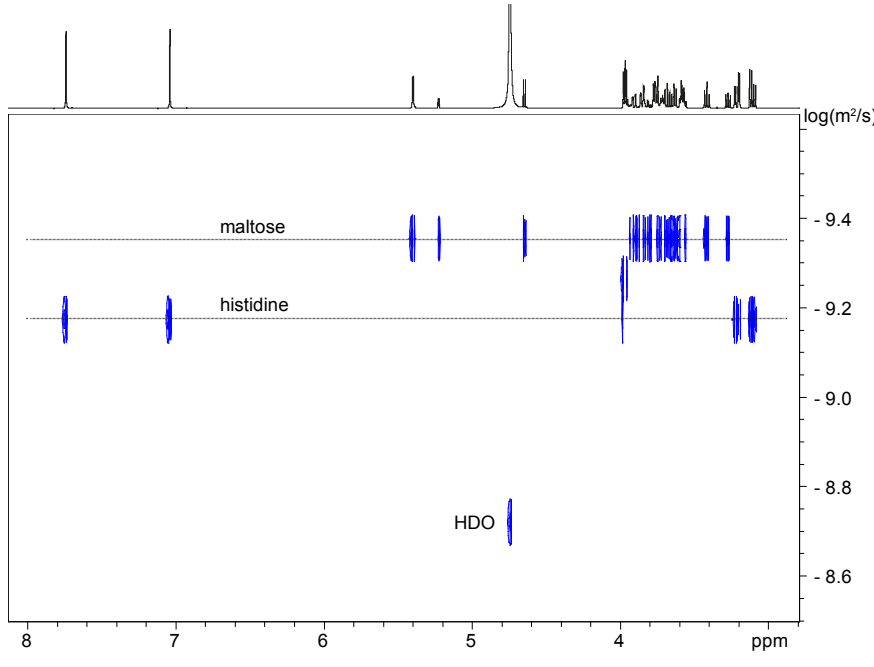

Figure 4. DOSY spectrum (BPP-LED sequence) of a mixture of maltose and histidine in D_2O.

2.4.3 Water suppression

NMR samples are often dissolved in deuterated solvents, such as D_2O or deuterated chloroform ($CDCl_3$), to prevent the appearance of a huge solvent peak in the spectrum. However, biological fluids, used in metabonomic NMR applications, are most often H_2O solutions. Exchangeable protons of biomolecules are

also observed in H_2O solution, because they are replaced with deuterium in D_2O solution.

The water signal of 110 M water protons in an aqueous solution introduces problems with the dynamic range and its broad appearance masks other signals of the sample. However, the water signal can be removed from the spectrum by water suppression.

The simplest way to achieve water suppression is by presaturation of the water peak. The transmitter frequency is set on the water resonance and a long, weak pulse is applied before the acquisition pulse (Figure 5A and 6A). Nearby proton resonances are, however, also partly presaturated, as well as signals which are in exchange with water (Freeman, 1997).

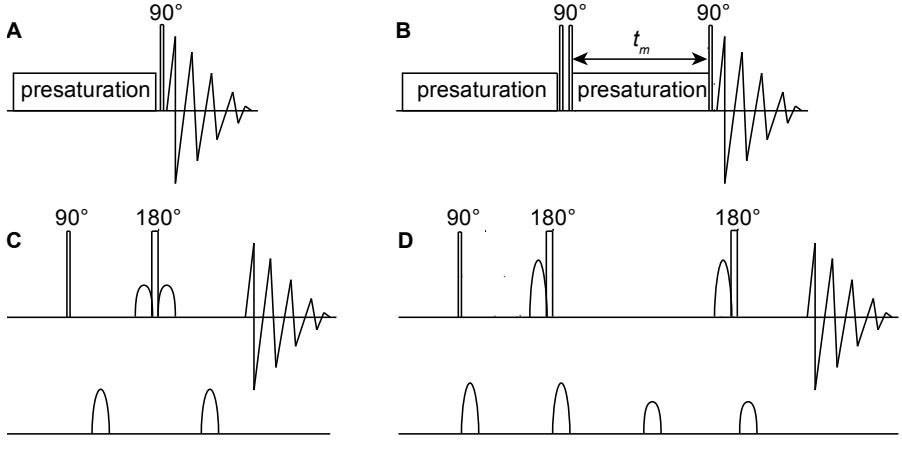

Figure 5. Schematic representations of the following water suppression pulse sequences: A) water presaturation, B) NOESY presaturation, C) WATERGATE, and D) excitation sculpting.

Presaturation techniques suffer from residual "humps" from the water signal. These can be suppressed by application of a 1D nuclear Overhauser effect spectroscopy (NOESY) experiment (Figure 5B and 6B), where presaturation is applied during the relaxation delay and the mixing time (Neuhaus *et al.*, 1996).

The use of pulse field gradients has further improved water suppression experiments (Freeman, 1997). Water suppression by gradient tailored excitation (WATERGATE) is a way to defocus the spins by a gradient pulse, followed by refocusing of all signals except the water signal by a second gradient pulse (Piotto *et al.*, 1992), thus a gradient spin echo (Figure 5C and 6C). In contrast to presaturation techniques, the WATERGATE sequence retains signals in exchange with water.

A drawback of the WATERGATE sequence is the inclusion of phase distortions caused by the selective pulses for the water signal. By doubling the

WATERGATE sequence, hence using a double pulsed field gradient spin-echo (DPFGSE), these phase distortions could be minimized (Hwang & Shaka, 1995). This sequence, known as excitation sculpting (Figure 5D and 6D), is as the WATERGATE sequence used for water suppression in many 2D experiments.

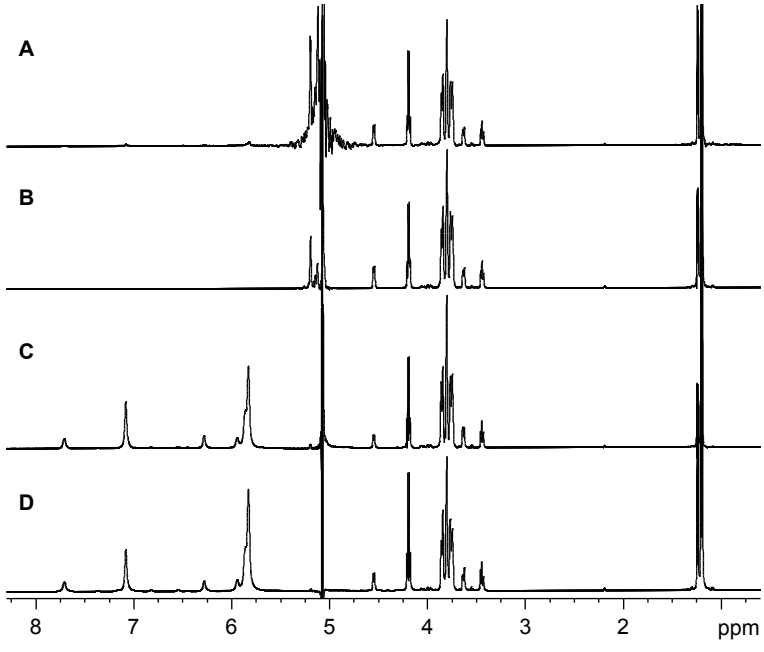

Figure 6. Spectra of fucose (0.2 M) in H_2O/acetone-d_6 (85:15) at 0 °C with the use of **A**) water presaturation, **B**) NOESY presaturation, **C**) WATERGATE, and **D**) excitation sculpting.

2.5 Two-dimensional NMR

The introduction of a second dimension (or even higher dimensions when using labeled samples) is essential for the structure analysis of biomolecules. The most common 2D NMR experiments in the structure analysis of unlabeled material (*e. g.* carbohydrates, peptides or natural products) will be described briefly.

2.5.1 Homonuclear 2D experiments

Homonuclear through-bond correlations can be detected by chemical shift correlation spectroscopy (COSY), where the pulse sequence is 90°-t_1-90° (Figure 7A). The two 90° hard pulses are separated by a variable period (t_1) for evolution of scalar couplings by coherence transfer (Freeman, 1997). COSY

requires that the scalar couplings are large enough to allow coherence transfer during t_1 and usually only correlations due to geminal and vicinal couplings are observed.

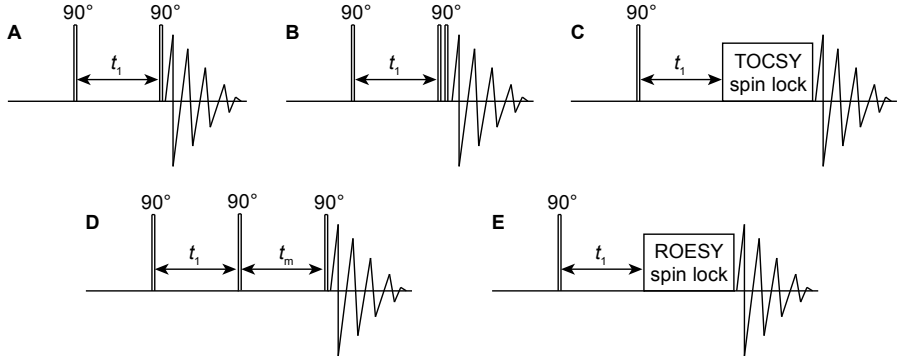

Figure 7. Schematic representations of the basic pulse sequences of the: A) COSY, B) DQF-COSY, C) TOSCY, D) NOESY, and E) ROESY experiments.

The use of a double-quantum filter (DQF) by an extra 90° pulse and phase cycling or gradients, converts double quantum coherences into observable magnetization (Figure 7B). In a DQF-COSY spectrum, signals from single quantum coherence, including singlet diagonal peaks and the solvent (HDO) peak, are absent. The triple-quantum filtered (TQF) COSY experiment can be used to eliminate resonances from both singlets and two-spin systems, but the sensitivity is decreased compared to DQF-COSY.

To observe all proton-proton correlations within the entire spin system the total correlation spectroscopy (TOCSY) experiment is used. After an initial 90° pulse and a variable evolution period, a spin lock with a defined mixing time is introduced (Figure 7C). The spin lock is achieved by a broadband decoupling scheme, such as MLEV (Bax & Davis, 1985a) or decoupling in the presence of scalar interactions (DIPSI) (Shaka *et al.*, 1988). Different mixing times can be used to observe parts of or the entire spin system.

The NOESY pulse sequence consists of three 90° pulses, separated by a variable period (t_1) and a fixed period (t_m, the mixing time; Figure 7D). During the mixing time, magnetization is transferred between neighboring spins via dipole-dipole interaction, and protons close in space (less than *ca.* 5 Å) will show NOE. The mixing time can be adjusted to observe NOE to spins at various proximity. Interactions through chemical exchange also show cross-peaks in NOESY spectra.

The magnitude of the NOE is dependent on the correlation time of the molecule under investigation. Small molecules with short correlation time exhibit a positive NOE, whereas medium-sized molecules exhibit a very small

or even no NOE. Larger molecules, on the other hand, display large but negative NOE. To overcome the problems with medium-sized molecules, rotating-frame nuclear Overhauser effect spectroscopy (ROESY) can be used.

The pulse sequence of the ROESY experiment is similar to TOCSY, with an initial 90° pulse and a variable evolution period, followed by a spin lock (Figure 7E). However, the spin lock is optimized for magnetization transfer through NOE rather than through scalar couplings. In the rotating frame the NOE remains positive over all correlation times and can be distinguished from chemical exchange by different signs of the cross-peaks. Whereas NOEs give rise to negative cross-peaks (compared to diagonal peaks), chemical exchange cross-peaks are positive.

There are several possible artifacts in NOESY and ROESY spectra that have to be considered. COSY-type peaks due to coherence transfer through scalar couplings can be observed, but in ROESY spectra they are out-of-phase compared to other cross-peaks. TOCSY-type peaks can be observed in ROESY spectra due to the similar spin lock pulses, but they can be distinguished from NOEs by their different sign of the cross-peaks (Bax & Davis, 1985b).

Magnetization can also be transferred by two subsequent NOE steps during the mixing time, so-called spin diffusion. This is a problem in both NOESY and ROESY spectra. However, cross-peaks related to spin diffusion can be distinguished from direct NOEs by their different build-up curves from NOESY spectra or by their different signs in ROESY spectra (Bax *et al.*, 1986).

2.5.2 Heteronuclear 2D experiments

The observation of ^{13}C resonances is difficult due to the low natural abundance of ^{13}C (1.1%). 2D NMR experiments have been developed to utilize the high abundance of ^{1}H resonances for the determination of ^{13}C resonances through heteronuclear coupling.

One extensively used heteronuclear 2D experiment is the ^{1}H-^{13}C heteronuclear single-quantum coherence (HSQC) experiment, where $^{1}J_{CH}$ couplings are used to monitor C-H correlations. It is based on double INEPT (Insensitive nuclei enhanced by polarization transfer) steps (Figure 8A), which is based on transfer of magnetization from one nuclei to another by inversion of their populations. Polarization is transferred from ^{1}H to ^{13}C, and then back to ^{1}H by a reversed INEPT step. ^{13}C resonances are thus detected by ^{1}H, which gives an enhancement of the ^{13}C responses due to the favourable polarization and relaxation properties of protons (Freeman, 1997).

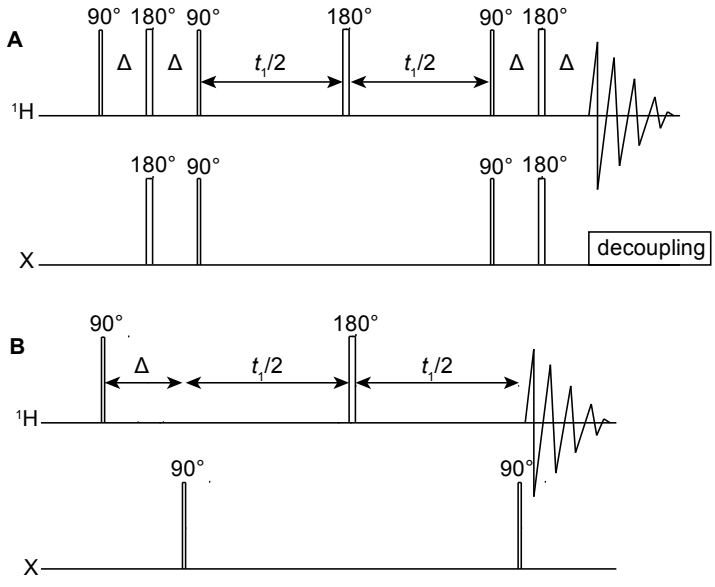

Figure 8. Schematic representations of basic **A**) HSQC and **B**) HMBC pulse sequences.

To investigate two- and three-bond heteronuclear connectivities, and thus also carbons without any attached protons, the heteronuclear multiple bond correlation (HMBC) experiment is used. The pulse sequence is, as in the HSQC experiment, based on magnetization transfer from ^{1}H to ^{13}C and then back to ^{1}H again (Figure 8B). However, the mechanism is not polarization transfer, but rather coherence transfer and the delay for evolution of C-H couplings is adjusted to the small long-range C-H couplings (*ca.* 0-20 Hz), instead of the much larger one-bond couplings (*ca.* 100-300 Hz).

2.6 HR-MAS NMR

Line broadening effects become a big problem if the conditions for liquid state NMR spectroscopy are used for solid or semi-solid samples. These effects arise primarily from dipole-dipole interactions, chemical shift anisotropy, differences in magnetic susceptibility, and, in the case of quadrupolar spins ($I > ½$), quadrupolar interactions. They all contain the factor $(3 \cos^2 \theta - 1)$, where θ is the angle between the spin and the B_0 field. In a liquid sample this factor is averaged by molecular tumbling and narrow lines can be observed. However, fast rotation of a solid sample at an angle where $(3 \cos^2 \theta - 1)$ becomes zero can be used to mimic the molecular tumbling and thus to eliminate the effects of dipole-dipole interaction and chemical shift anisotropy (Hennel & Klinowski, 2005). This angle $\theta = 54.7°$ is called the magic angle and is equiva-

lent to the angle between the edge of a cube and the adjacent space diagonal (Figure 9).

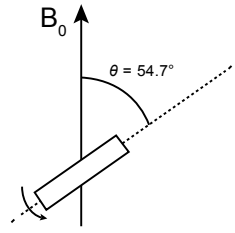

Figure 9. Schematic representation of a HR-MAS NMR rotor.

In solid state NMR spectroscopy there are additional challenges because the rate of rotation required to average the dipolar interactions is very high (several tens of kHz). This has limited the use of solid state NMR to mainly ^{13}C NMR with high power ^{1}H decoupling to remove the ^{1}H-^{13}C dipolar couplings and cross-polarisation (CP-MAS) to improve the ^{13}C sensitivity. The introduction of very fast MAS probes with spinning rates up to 70 kHz has made it possible to apply solid state NMR to biomacromolecules, such as membrane proteins (Varga & Watts, 2008).

In HR-MAS of semi-solid samples, *e. g.* gels, cell cultures, or tissue samples, the anisotropic interactions are partially averaged by molecular tumbling and spinning of just a few hundred Hz is required to remove residual dipolar interactions and variations in magnetic susceptibility (Lindon *et al.*, 2009). Spinning sidebands are still observable at those frequencies of rotation and spin rates in the range of the sweep width of the spectrum (typically 4-6 kHz) is used to remove them (Hennel & Klinowski, 2005). In contrast to CP-MAS, the same experiments as in liquid NMR can be used.

HR-MAS NMR spectroscopy is increasingly applied in the analysis of *e. g.* bacterial cells (Li, 2006), foodstuff (Valentini *et al.*, 2011), and in metabonomic studies (Lindon *et al.*, 2009).

3 Carbohydrate analysis

Carbohydrates are one of the most important classes of biomolecules, together with proteins, nucleic acids and lipids. The origin of carbohydrates can be traced to the light-independent reactions of photosynthesis, where plants and algae produce hexoses from carbon dioxide and water through the Calvin cycle. These monosaccharides are then used as energy deposits in plants and animals, in the form of starch and glycogen, respectively. Carbohydrates are also used for structural purposes: Cellulose, arabinoxylans and pectins are used in plant cell walls, chitins in fungi cell walls and in exoskeletons of insects, and glycosaminoglycans are used to maintain hydration in animal tissues. A third use of carbohydrates in biological systems is for adhesion and signaling, especially on cell surfaces. Many antigens, recognized by the immune system, are carbohydrates that are conjugated to proteins or lipids. Blood group antigens and LPSs on the surface of Gram-negative bacteria are examples of glycoproteins and glycolipids, respectively.

As the name indicates, carbohydrates were originally regarded as hydrates of carbon, with the empirical formula $C_n(H_2O)_n$, but later investigations found out that they are not hydrates of carbon, but polyhydroxy aldehydes and ketones. The molar ratio 2:1 between hydrogen and oxygen is only true for the most common monosaccharides like glucose ($C_6H_{12}O_6$).

Carbohydrates are divided into mono-, oligo- and polysaccharides. Monosaccharides are the monomers, which are building blocks for oligo- and polysaccharides. There is no strict borderline between oligo- and polysaccharides even though a chain of more than 10 monosaccharides is usually regarded as a polysaccharide (Kamerling, 2007). However, the difference can also be regarded as structure dependent, where polysaccharides are usually built up of several repeating units (RU), whereas oligosaccharides are restricted to a few RU or a non-repeating structure.

The primary structure of an oligo- or polysaccharide is, as in proteins, the sequence of the building blocks. There is no simple carbohydrate sequencing method,[1] like there are efficient protein, RNA and DNA sequencing methods. This is due to several facts: Carbohydrates constitute of more than 100 different sugar residues, whereas proteins are built up of 20 amino acids and nucleic acids of 4 canonical nucleotides. Carbohydrates can be branched and have several different available positions for substitution, whereas proteins and nucleic acids are linear chains with only two possible linkage positions. In addition to these structural differences the biosynthesis of carbohydrates is different from that of proteins and nucleic acids. Instead of one ribosome or polymerase catalyzing the linking of different templates, carbohydrates are synthesized by several different enzymes, responsible for different substitutions.

Hence the determination of primary carbohydrate structures is not a high-throughput process. It usually involves NMR spectroscopy and/or mass spectrometry, with parallel use of chemical analysis. If the material is a polysaccharide, the first step is often a chemical degradation to provide oligo- or monosaccharides, which are easier to study by NMR spectroscopy and mass spectrometry.

3.1 Chemical degradation

Chemical degradation of carbohydrates can be divided into 1) hydrolysis of the linkage between a carbohydrate chain and another molecule, for example the protein in a glycoprotein or fatty acyl chains in a glycolipid, 2) hydrolysis of glycosidic linkages, connecting carbohydrate residues, and 3) breakage of the ring structure of carbohydrate residues.

A complete acidic hydrolysis of an oligo- or polysaccharide yields the monosaccharides. This is done with a strong acid, like hydrochloric acid or trifluoroacetic acid, at high temperatures (≥100 °C) for several hours. The monosaccharide structures can then be determined by gas chromatography (GC) or liquid chromatography (LC) analysis.

Some glycosidic linkages are more easily hydrolyzed than others. For example, 3-deoxy-D-*manno*-octulosonic acid (Kdo) is more susceptible to hydrolysis than other monosaccharides, due to its acid labile ketosidic linkage.

1. There are attempts to construct a carbohydrate sequencing method and this has been achieved for proteoglycans (Li *et al.*, 2012) by a combination of enzymatic cleavages and mass spectrometric analysis. However, it has only been used for glycosaminoglycans so far, which have a disaccharide RU with different degrees of sulphation.

Thus, a mild acidic hydrolysis with acetic acid (1% in water) can be used for hydrolysis of Kdo only, which is used for delipidation of LPSs (see section 6.1.1).

3.2 Chemical analysis

Chemical analysis with comparison to known reference samples is still important for the determination of carbohydrate structures, in spite of more modern techniques like NMR spectroscopy and MS/MS analysis. The most common chemical analysis methods are sugar analysis, methylation analysis and determination of absolute configuration from 2-butyl glycosides.

Sugar analysis is usually performed by reduction of the monosaccharides, or the pre-hydrolyzed oligo- or polysaccharide, with sodium borohydride to alditols and subsequent acetylation with acetic anhydride and pyridine to alditol acetates (Sawardeker *et al.*, 1965), which can be analyzed by GC (Figure 10). One sugar gives rise to one peak in the chromatogram and the retention time and mass spectrum can be compared to reference standards. Uronic acids cannot be determined by this method because they form unvolatile sodium salts after reduction with sodium borohydride.

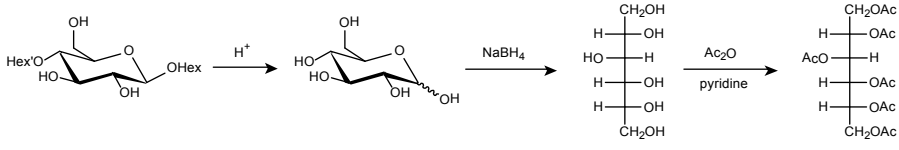

Figure 10. Procedure for sugar analysis exemplified by D-glucose.

An alternative method for sugar analysis is the use of methyl glycosides after methanolysis of the sample. The oligo- or polysaccharide is dissolved in dry methanol and hydrochloric acid or acetyl chloride is added to catalyze the formation of methyl glycosides. The methyl glycosides are then usually trimethylsilylated to yield volatile compounds that are useful for GC analysis. However, the equilibrium caused by the acidic methanolysis will facilitate the formation of all possible anomers. Hence peaks from both α- and β-pyranosides, as well as α- and β-furanosides, will be observed in the GC chromatogram.

Monosaccharides are divided into D- and L-sugars, depending on the configuration of the highest-numbered chiral carbon atom. To determine this absolute configuration, diastereomers can be formed, which will have different retention times even on an achiral GC column. By using (*S*)-2-butanol to form the (*S*)-2-butyl glycosides from methyl glycosides, this can be achieved in a

simple way (Figure 11). The trimethylsilyl derivatives can then be used for GC-MS analysis (Gerwig *et al.*, 1978).

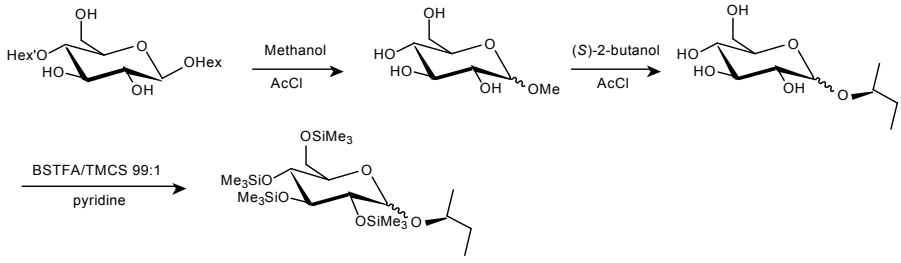

Figure 11. Procedure for the determination of absolute configuration by preparation of (*S*)-2-butyl glycosides, exemplified by D-glucose. BSTFA stands for *N*,*O*-bis(trimethylsilyl)trifluoroacetamide and TMCS stands for trimethylchlorosilane. The furanosides are also formed to some extent in the methanolysis and butanolysis steps. *N*-Acetylated sugars are re-*N*-acetylated after methanolysis and butanolysis.

The linkage pattern of oligo- and polysaccharides is traditionally studied by methylation analysis. The sample is first methylated by treatment with dimsyl sodium and then methyl iodide (Hakomori, 1964) or with methyl iodide in a sodium hydroxide solution (Ciucanu & Kerek, 1984). These permethylated sugars are then hydrolyzed, reduced and acetylated in the same way as in a sugar analysis, to obtain partially methylated alditol acetates (PMAA; Figure 12). The position of *O*-acetylation is either the position of a glycosidic linkage, or the position for ring-closure before reduction was performed. *O*-Acetylation on position 5 indicates a pyranoside, whereas *O*-acetylation on position 4, but not on position 5, indicates a furanoside.

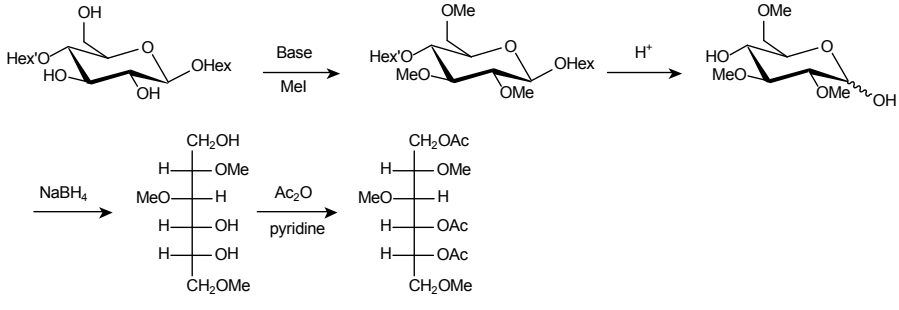

Figure 12. Procedure for methylation analysis, exemplified by 4-substituted D-glucose.

3.3 NMR spectroscopy

NMR spectroscopy has become one of the most important techniques for structural analysis of carbohydrates. Carbohydrates are rich in the NMR active

nuclei ^{1}H and ^{13}C. However, most of carbohydrate protons and carbons resonate in a narrow spectral range of δ_H 3.2-4.5 ppm and δ_C 61-76 ppm.

The determination of carbohydrate structures has therefore focused on signals appearing outside this crowded region, referred to as "structural-reporter groups" (Vliegenthart *et al.*, 1983). These signals correspond for example to anomeric protons at 4.4-5.5 ppm, methyl groups of *N*-acetylated sugars at ~2 ppm and H-6 of 6-deoxy sugars like rhamnose and fucose at 1.1-1.3 ppm.

Another approach is to use computer-aided techniques to overcome the complexity of carbohydrate NMR spectra. CASPER is a database that is used to predict chemical shifts of carbohydrates and can be used to rule out irrelevant structures (Lundborg & Widmalm, 2011; Roslund *et al.*, 2011).

3.3.1 Monosaccharide constituents

The number of different residues in a given carbohydrate can be determined by inspection of the anomeric region of a 1D ^{1}H spectrum or a $^{1}H,^{13}C$-HSQC spectrum. Anomeric protons resonate at 4.4-5.5 ppm and anomeric carbons at 91-109 ppm. Even though a ^{1}H spectrum can give information about the number of residues, there are also other resonances that can interfere with the anomeric signals, including signals from ring protons next to *O*-acetylations, which are shifted downfield to the anomeric region. Also H-2 of HexNAc and H-4 and H-5 of GalA can be mistaken for the upfield part of the anomeric region. Furthermore, there are monosaccharides without any anomeric proton, including ketoses and ulosonic acids (*e. g.* Kdo).

The number of sugar residues with anomeric protons (thus aldoses) is best determined by a $^{1}H,^{13}C$-HSQC experiment, where other possible protons are sorted out by the downfield shift of the anomeric carbon signals, due to the hemiacetal character of this carbon.

The anomeric configuration can be deduced by the chemical shift of the anomeric protons, where α-anomers resonate at higher frequencies than β-anomers. However, the chemical shifts of the anomeric protons are also affected by other factors, especially glycosylation to other sugars, thus making this method less reliable. The vicinal coupling constant between H-1 and H-2 of aldopyranosides indicates whether the orientation of the two protons is axial-axial (7-8 Hz), equatorial-axial (~4 Hz), axial-equatorial (<2 Hz) or equatorial-equatorial (<2 Hz) (Jansson *et al.*, 1987). To determine the anomeric configuration of aldopyranosides unequivocally the one-bond proton-carbon coupling constants ($^{1}J_{C\text{-}1,H\text{-}1}$) can be measured with a non-decoupled $^{1}H,^{13}C$-HSQC experiment. For D sugars in the $^{4}C_1$ conformation, a $^{1}J_{C\text{-}1,H\text{-}1}$ of ~170 Hz indicates an α-anomeric configuration whereas $^{1}J_{C\text{-}1,H\text{-}1}$ of ~160 Hz indicates a β-anomeric configuration (Duus *et al.*, 2000).

The configuration of the different monosaccharides can be obtained from vicinal scalar coupling constants between ring protons. $^{3}J_{\text{H-1,H-2}}$ has already been mentioned for the determination of the anomeric configuration. In a similar way all ring protons can be investigated, thus giving information about their respective axial or equatorial orientation. This can be determined by a TOCSY experiment with long mixing time (100 ms or more), where sugar residues with *manno*, *galacto* and *gluco* configurations can be distinguished by a qualitative inspection of the cross-peak intensities (Gheysen *et al.*, 2008). Sugars with *manno* configuration can be followed from H-1 to H-2, *galacto* configuration from H-1 to H-4, whereas sugars with *gluco* configuration can be followed all the way from H-1 to H-6.

To complete the assignment of ^{1}H and ^{13}C signals from each monosaccharide, HSQC-TOCSY, NOESY, ROESY and HMBC experiments can be used. HSQC-TOSCY is especially useful on complex carbohydrates, where the carbon dimension helps to solve the overlap of different spin systems. NOESY and ROESY experiments are used to complete the assignment when the coupling constants between ring protons are too small to give rise to cross-peaks in TOCSY spectra, such as between H-2 and H-3 in mannose and between H-4 and H-5 in galactose. 1,3-Diaxial correlations are than used to "jump over" this bottleneck of a TOCSY experiment. In parallel, HMBC experiments can be used to support the ^{13}C assignments.

3.3.2 Linkage and sequence

Glycosylation leads to a 4-10 ppm downfield shift of the carbon signal at the substitution position compared to an unsubstituted monosaccharide (Bubb, 2003). The most reliable method to determine which sugar residues that are linked together and at which position, is to look for correlations over the glycosidic linkages in HMBC spectra. NOEs over the glycosidic linkage can also be helpful, but should be used with some care due to possible NOEs occurring between sugar residues that are close in space, but far away from each other in the carbohydrate chain (Bubb, 2003).

3.3.3 Position of substituting groups

Many sugars are substituted by acetyl, sulphate, phosphate and other groups. Substitutions affect the chemical shift of the proton and carbon resonances where the group is located. The determination of this, usually downfield, shift should be accompanied by HMBC experiments to observe $^{3}J_{\text{C,H}}$ (acetyl group) or $^{3}J_{\text{P,H}}$ (phosphate group) couplings between the ring proton and the substituent. Acetyl groups show characteristic methyl signals at ~2 ppm, which can be traced to ring protons by NOE.

3.4 Mass spectrometry

In structural elucidations of an unknown compound, it is advantageous to confirm a structure derived from NMR data using a complementary technique. For carbohydrates this second (or first) technique is typically MS. MS data can provide accurate information about the mass of a carbohydrate molecule and MS analysis requires much smaller amounts of sample compared to the analysis by NMR spectroscopy.

MS analysis of fragments of the carbohydrate molecule can yield information about the sequence of sugar residues, possible branching, glycosylation sites and substitution pattern. Different isomers of sugars can be difficult to distinguish without the inclusion of a chromatographic step prior to the MS analysis.

Mass spectrometers contain an ion source, a mass analyzer, and a detector. In the ion source the sample molecules are converted into ions of some charge state, z. Ions are subjected to an electric field that guides them towards the mass analyzer and away from the ion source. The mass analyzer separates the ions in space or time according to their respective mass-to-charge (m/z) ratios, before they reach the detector. The mass spectrum is the resulting detector signal intensity for each m/z. There are several different ways of designing mass analyzers. The quadrupole filter, quadrupole trap and time-of-flight (TOF) are common for analysis of carbohydrates.

The choice of ionization method is determined by the volatility of the sample. For volatile samples, electron ionization (EI) is the most common ionization method. Mass spectrometers using EI are often coupled on-line with gas chromatography (GC-MS). In the EI ion source sample molecules are bombarded with electrons to generate positively charged ions, which are often immediately fragmented further.

$$M + e^- \rightarrow M^{+\cdot} + 2e^-$$

Less volatile compounds can be ionized with electrospray ionization (ESI). In ESI a solution of the sample is sprayed at atmospheric pressure through a capillary placed in a strong electric field. Charged droplets are generated in the spray, which gradually become smaller by evaporation of the solvent. The droplets are transported towards the ion source and a region with lower pressure. When the droplets are small enough for the electrostatic repulsion between ions at the surface to exceed the surface tension of the liquid, free ions are formed. ESI is a soft ionization technique typically producing protonated or deprotonated molecular ions without fragmentation. However, these ions can be fragmented by a subsequent step, often a collision induced dissociation (CID). In CID the ions are allowed to collide with a gas (nitrogen or helium

gas) and depending on the collision energy, which is controlled by electrical potentials, the amount of fragmentation can be adjusted.

Non-volatile compounds can also be ionized by matrix-assisted laser desorption ionization (MALDI). In MALDI the sample is prepared by mixing the analyte molecules with a solution of UV absorbing matrix molecules. A small amount of the mixture is placed on a metal plate and as the mixture dries the analyte molecules co-crystallize with the matrix molecules. The sample plate is transferred to the ion source of the mass spectrometer, where it is irradiated by a pulsed UV laser beam. The matrix is excited by the laser energy that causes matrix and analyte molecules to simultaneously desorb from the surface into the gas phase. Charge exchange with the matrix leads to the formation of free analyte ions, which can eventually be detected, often by a TOF detector. MALDI-TOF is especially advantageous when working with carbohydrates of high mass.

3.4.1 EI fragmentation

EI is a hard ionization technique and carbohydrates usually do not give any molecular ion, but primary fragments can be used for identification.

The fragmentation of alditol acetates yields primary fragments by elimination of an acetyloxy group $(M - AcO)^+$ or by cleavage of the alditol chain (Lönngren & Svensson, 1974). The symmetry introduced by converting sugars to alditols can be avoided by reduction with sodium borodeuteride, which labels C-1 with a deuterium atom (Cui, 2005).

PMAA form primary fragments by α-cleavage. Cleavage between two methoxylated carbons occurs rather than cleavage between two acetyloxylated carbons (Figure 13). The methoxylated carbon carries the positive charge, rather than the acetyloxylated carbon (Lönngren & Svensson, 1974). Secondary fragments are formed by elimination of methanol, acetic acid and ketene (CH_2CO).

The fragmentation of PMAA of different 2-deoxy-2-(*N*-methylacetamido)-hexoses obey the same fragmentation rules, with the difference that cleavage between C-2 and C-3 is favored, producing a main diagnostic ion at *m/z* 158 (Schwarzmann & Jeanloz, 1974). This ion readily eliminates ketene to produce its daughter ion at *m/z* 116.

3.4.2 CID fragmentation

The major fragments produced by CID fragmentation of oligosaccharides are the result of cleavage at the glycosidic linkages. In positive ion mode the oxygen in a glycosidic bond is protonated and the bond is cleaved preferentially so that the glycosidic oxygen is retained on the reducing sugar moiety and a gly-

cosyl cation (B ion) is formed (Domon & Costello, 1988). If the positive charge instead is maintained on the reducing fragment a Y ion is formed (Figure 14).

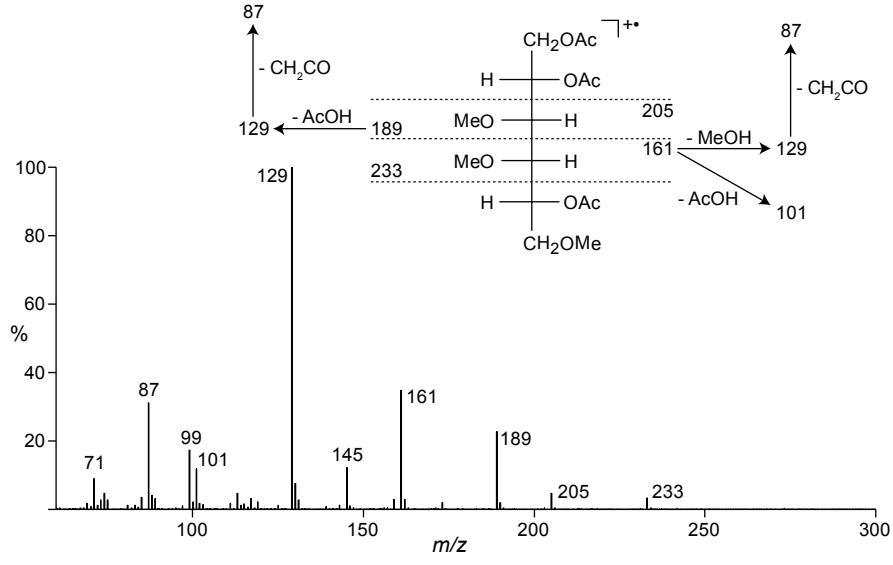

Figure 13. Mass spectrum of 1,2,5-tri-*O*-acetyl-3,4,6-tri-*O*-methylgalactitol, corresponding to 2-substituted Gal*p*. Typical primary fragments are indicated, as well as some abundant secondary fragments.

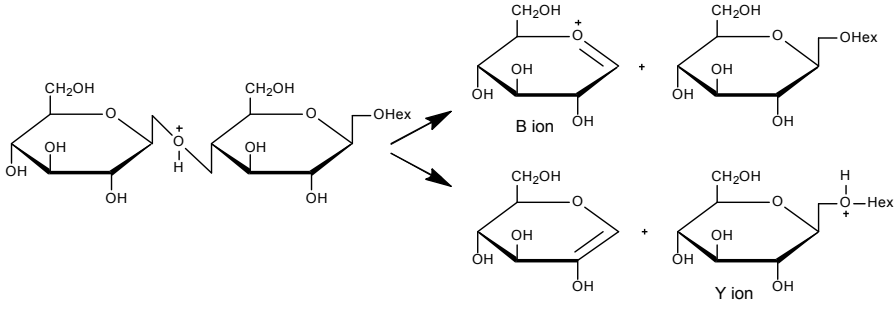

Figure 14. Formation of B and Y ions in positive ion mode.

In negative ion mode (Figure 15), B and Y ions are formed by accommodation of the negative charge on the glycosidic oxygen (Y ion) or on a hydroxyl group (B ion). However, fragmentation in negative mode also produces ions where the glycosidic oxygen is retained on the non-reducing fragment, yielding C ions with the negative charge on the glycosidic oxygen and Z ions with the negative charge on a hydroxyl group of the reducing fragment (Domon & Costello, 1988).

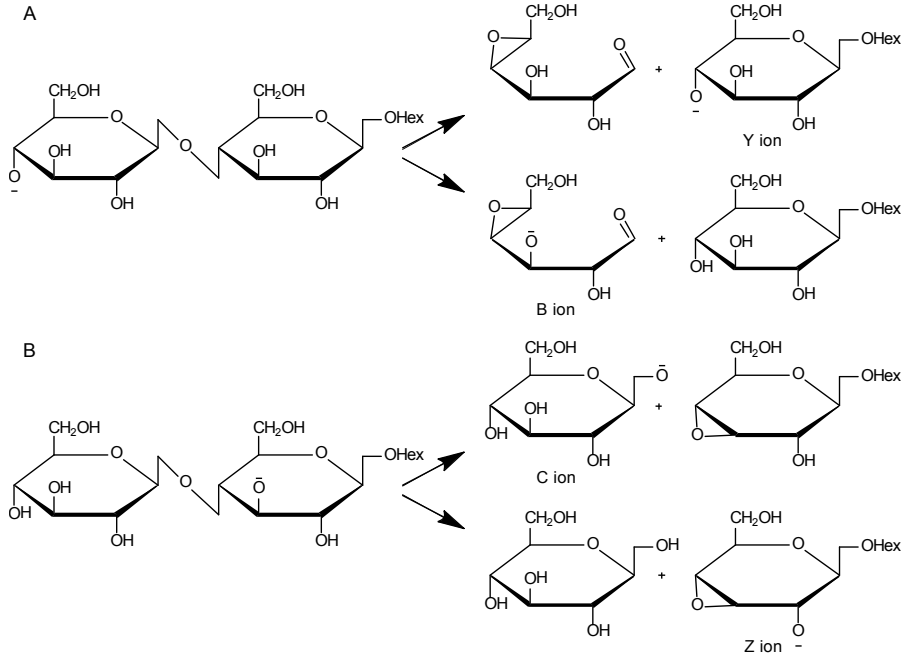

Figure 15. Formation of A) B and Y ions, and B) C and Z ions in negative ion mode.

In addition to cleavage of glycosidic linkages, fragments can also be formed by cleavage across the sugar ring. Such fragments with the charge on the reducing or non-reducing part of the oligosaccharide are termed X and A ions, respectively. To determine where the ring has been broken a superscript (^{k,l}A or ^{k,l}X) is used to indicate which bonds that have been broken. A subscript is used to indicate where the chain is cleaved (A_i, B_i, C_i, X_j, Y_j, Z_j). The first glycosidic linkage from the reducing end is equivalent to i = 1 or j = 1. If the chain is branched the different antennae are distinguished by adding Greek letters to the subscript, with the longest antennae termed α.

4 Carbohydrate conformation

The conformation of carbohydrates is defined by the monosaccharide ring conformation and (for oligo- and polysaccharides) the conformation of the glycosidic linkages. In aqueous solution, the individual carbohydrate-water interactions are important to determine the conformation of carbohydrates (Engelsen *et al.*, 2001). These interactions are an interplay between intra-molecular hydrogen bonds and the amount of hydrogen bonding with water, also referred to as the hydration.

The conformation analysis of carbohydrates can be done by NMR spectroscopy, where NOEs and scalar coupling constants are essential for the determination of the conformation (Widmalm, 2013), as well as residual dipolar couplings, relaxation times and in the case of exchangeable protons also temperature variation of resonances and $^{1}H/^{2}H$ solvent exchange rates (Wormald *et al.*, 2002).

Usually an ensemble of conformations is present, due to the high flexibility of carbohydrates, and in the time scale of NMR spectroscopy an average of these conformations is observed. To obtain more detailed predictions, molecular dynamics (MD) simulations are used, which give a measure of the residence time of individual hydrogen bonds and Ramachandran plots of the angles of the glycosidic linkages (Widmalm, 2013). However, there is a need for experimental evidence to prove or disprove the predictions made by MD simulations.

In this chapter, the conformation of sugar rings and glycosidic linkages will be described briefly, followed by a description of hydroxy protons as a tool in the investigation of carbohydrate conformation by NMR spectroscopy.

4.1 Monosaccharide conformation

Pyranoside sugars prefer, similarly to cyclohexanes, the chair conformation, which is a rigid structure. The chair can be interconverted to another chair by a

"ring-flip", but this conversion is usually not observed on the NMR time scale for pyranoses. The two chairs are denoted $^4C_1$ and $^1C_4$, where the superscript number refers to the atom that lies on the side of a reference plane of the atoms C-2, C-3, C-5 and the ring oxygen, from which numbering appears clockwise, and the subscript refers to the atom on the other side (Figure 16). D-Pyranoses usually adopt the $^4C_1$ conformation and L-pyranoses adopt the $^1C_4$ conformation, due to the larger number of equatorial hydroxyl groups (Bubb, 2003). There are, however, examples of rapid interconversion between $^4C_1$ and $^1C_4$ forms, *e. g.* demonstrated on D-Glc*p*NAc (Sattelle & Almond, 2011).

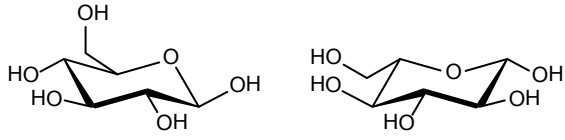

Figure 16. The two chair conformations $^4C_1$ and $^1C_4$ are illustrated for β-D-glucose and β-L-glucose, respectively.

Other less frequently found conformations of monosaccharides are, for example, the skew boat of sulfated iduronic acid (Ferro *et al.*, 1986) and the half chair of 4,5-unsaturated glucuronic acid (Jin *et al.*, 2009). Compared to pyranosides, furanosides have a higher degree of ring flexibility and are usually described as an equilibrium between twist (*T*) and envelope (*E*) forms (Bubb, 2003).

4.2 The glycosidic linkage

The glycosidic linkages of oligo- and polysaccharides are the main origin of flexibility in those structures. The conformation of the two bonds C-O-C that constitute the glycosidic linkage are defined by the torsion angles φ and ψ (Figure 17), and in the case of an exocyclic carbon, as in 1→6 linkages, the angle ω is added (Kamerling, 2007).

The torsion angle φ is restricted by the *exo*-anomeric effect, which favors a $\varphi_{H1\text{-}C1\text{-}On\text{-}Cn}$ (where *n* is the substitution position) of +40° in β-D- and α-L-hexopyranosides, and -40° in α-D- and β-L-hexopyranosides (Widmalm, 2013). The $\psi_{C1\text{-}On\text{-}Cn\text{-}Hn}$ angle is usually in the range +50° to -50°. These preferences lead to a *syn* conformation, where the anomeric proton is on the same side of plane as the proton on the substitution position of the adjacent sugar (H*n*). Usually a strong NOE can be observed between those protons and is often the only inter-residue NOE that can be used as a conformational constraint (Wormald *et al.*, 2002).

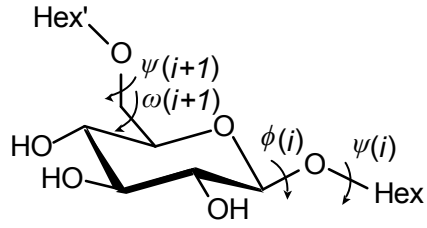

Figure 17. The torsion angles φ, ψ, and ω are shown on a 1- and 6-linked β-D-glucose.

There are rare examples of glycosidic linkages that exhibit minor amounts of an opposite orientation of the rings, called an *anti* conformation, with φ or ψ of about 180°. Experimental evidence of *anti* conformations have been reported for β-D-Gal-(1→3)-β-D-Glc-OMe (Dabrowski *et al.*, 1995), a methyl glycoside and a 1-phosphate derivative of α-cellobiose (Larsson *et al.*, 2004; Lipkind *et al.*, 1985), a β-D-Glc-(1→4)-α-D-Glc element of a core oligosaccharide from a LPS (Masoud *et al.*, 1994), and from the β-D-Glc-(1→2)-β-D-Glc element of a trisaccharide (Landersjö *et al.*, 1997). Hence, *anti* conformations have been observed in both disaccharides and in large oligosaccharides, and in both 1→2, 1→3, and 1→4 linkages, but only in linkages between a β-anomeric position and a position on a glucose.

4.3 Hydroxy protons

Hydroxy protons have an important role in the conformation of carbohydrates, by their hydration and participation in hydrogen bonding. NMR spectroscopy of hydroxy protons is used to characterize their hydrogen bonding and to obtain additional NOEs around the glycosidic linkages, which can be used to help define the conformation.

Hydroxy protons are not observed in D_2O solutions of carbohydrates by NMR spectroscopy, because of their rapid exchange with deuterium from the solvent. In an aprotic solvent, like DMSO, they are easily observed, but the conformation of the sugar may differ and hydrogen bonds that exist in DMSO may be found not to persist in aqueous solution (Leeflang *et al.*, 1992).

Instead H_2O solutions can be used under conditions where the rate of exchange with water is slowed down. This is achieved by lowering the temperature to below 0 °C, adjusting the pH to 6-7, and removing any traces of metal ions that can catalyze the exchange of hydroxy protons with water. Subzero temperatures have been used without freezing of the sample by means of supercooling (Poppe & Halbeek, 1994) or highly concentrated solutions (Batta & Kövér, 1999), but the most common strategy is to add 10-15% of an organic solvent such as acetone or methanol (Sandström & Kenne, 2006). It has been

shown that the addition of acetone-d_6 does not alter the conformation of carbohydrates (Bekiroglu *et al.*, 2003; Hawley *et al.*, 2002). Full solvation of dicarboxylic acids even occurred in a 90% acetone-d_6/10% H_2O solution (Lin & Frey, 2000).

Hydroxy protons in aqueous solutions resonate in a part of the ^1H NMR spectrum (δ 5-7.5 ppm) that is isolated from other protons, which facilitates their assignment. Hydroxy protons are further characterized by the use of chemical shifts, temperature coefficients, coupling constants, NOEs/ROEs and rate of exchange.

Protons involved in hydrogen bonds are usually deshielded due to their proximity to an electronegative acceptor atom. However, intra-molecular hydrogen bonds in aqueous solution are in most cases not persistent on the NMR time scale, due to the competing inter-molecular hydrogen bonding with water. There are only a few examples of persistent hydrogen bonding in aqueous solution evidenced by a downfield shift, mainly from phenols (Kontogianni *et al.*, 2013; Exarchou *et al.*, 2002).

Carbohydrates are strongly hydrated by hydrogen bonding between hydroxyl groups and water molecules, where the hydroxyl group can act both as acceptor and donator of hydrogen bonds. The chemical shifts of hydroxy protons will become a balance between deshielding due to enhanced intra-molecular hydrogen bonding and shielding due to reduced hydration (Bekiroglu *et al.*, 2004).

Chemical shift differences (Δδ), which is the difference between the chemical shift of a hydroxy proton of an oligosaccharide and the same hydroxy proton in the corresponding monosaccharide, have been measured in a variety of oligosaccharides to determine the influence of hydrogen bonding and hydration on the chemical shift (Bekiroglu *et al.*, 2003; Ivarsson *et al.*, 2000; Sandström *et al.*, 1998b; Sandström *et al.*, 1998a). A downfield shift ($\Delta\delta > 0$) was found to be associated with hydrogen bonding to another hydroxyl group, whereas an upfield shift ($\Delta\delta < 0$) is due to steric hindrance from bulk water or hydrogen bonding to a ring oxygen (Bekiroglu *et al.*, 2004). Thus, large $|\Delta\delta|$ (> 0.2 ppm) can be indicative of intra-molecular hydrogen bonding, but should be compared with other measures, for example temperature coefficients, before drawing any conclusions.

The chemical shift of a hydroxy proton involved in a hydrogen bond or with reduced hydration is less affected by temperature changes due to decreased interaction with the solvent. Thus, in aqueous solutions hydroxy protons with large $|d\delta/dT|$ (> 11 ppb/°C) are fully hydrated, whereas hydroxy protons with small $|d\delta/dT|$ (< 11 ppb/°C) are only partially hydrated. For hydroxy protons

involved in strong hydrogen bonding, |dδ/dT| of less than 3 ppb/°C has been measured (Poppe & Halbeek, 1991).

A modified version of the Karplus equation has been used to derive $^{3}J_{HCOH}$ depending on the H-C-O-H torsion angle (Zhao *et al.*, 2007). A $^{3}J_{HCOH}$ of 5.7-5.8 Hz was found to correspond to a freely rotating hydroxyl group around the C-O bond. Deviations from this average value is indicative of a preferred orientation of the hydroxyl group, which can correspond to hydrogen bonding (Sandström & Kenne, 2006; Poppe & Halbeek, 1994).

Hydroxy protons can be used to obtain additional inter-residue NOEs, which can be used to discriminate between different conformations. However, the extraction of quantitative distance information from NOE cross-peaks involving hydroxy protons is not straightforward, due to the chemical exchange with water. In a study on uniformly ^{13}C-enriched oligosaccharides NOESY- and ROESY-HSQC were used to determine ROEs and exchange rates of hydroxy protons, which were used to calculate distances by a full relaxation matrix approach (Harris *et al.*, 1997). The use of ^{13}C-enriched carbohydrates is however limited and the additional conformational restraints provided by hydroxy protons have not been routinely utilized.

Nevertheless, NOEs/ROEs and chemical exchange are useful parameters to determine spatial proximity, which can be indicative of hydrogen bonding (Sandström & Kenne, 2006). Chemical exchange between two hydroxy protons has been interpreted as evidence for transient inter-residue hydrogen bonding in sucrose (Sheng & Halbeek, 1995) and maltose (Bekiroglu *et al.*, 2003).

Hydroxy protons involved in strong hydrogen bonding have a lower rate of exchange with water, compared to other hydroxy protons in the same sample. Exchange rates can be measured by comparing the intensity of the cross-peaks between hydroxy protons and water in NOESY spectra at different mixing times (Dobson *et al.*, 1986). Exchange rates are sensitive to pH, solvent composition and catalysis by trace amounts of impurities, and comparisons should only be made between protons within the same sample (Sandström & Kenne, 2006).

5 Metabonomics

The concept of metabolic profiling by NMR spectroscopy and mass spectrometry was outlined in the 1990s and has grown to a widely used approach. In analogy to genomics, transcriptomics, and proteomics, metabonomics aims to describe the complete metabolome of an organism, or at least what can be observed by the analytical method employed.

The terms metabolomics and metabonomics are often used interchangeably, but whereas metabolomics is used to describe the metabolic composition of a sample (Fiehn, 2002), the term metabonomics is more precisely defined as the description of metabolic responses to perturbations through time, and how these responses can be described using analytical and statistical techniques (Nicholson *et al.*, 1999). The metabonomics approach has found its use particularly in toxicology (Lindon *et al.*, 2004), drug development (Lindon *et al.*, 2007), nutrition (Rezzi *et al.*, 2007), and clinical diagnostics (Nicholson *et al.*, 2012).

In metabonomics on animals and humans, most often easily available body fluids, such as blood and urine, are utilized. Tissue samples of different origin are also investigated with the same approach by HR-MAS NMR (Lindon *et al.*, 2009). NMR spectroscopy has, besides MS, been the technique of choice due to the minimal requirements of sample preparation and the simultaneous measurement of a wide range of metabolites with a possibility for quantifications. The large amount of data that is produced is treated by multivariate statistical methods to gain information about metabolic responses to a specific perturbation.

5.1 Sample preparation

Body fluids and tissue samples degrade over time. Degradation would falsely transform the desired snapshot from a certain time to another metabolic status.

The solution to avoid degradation is to keep the samples at low temperature (-80 °C) and to prepare the samples quickly before analysis, with as few steps as possible.

A number of protocols have been developed for urine (Bernini *et al.*, 2011; Beckonert *et al.*, 2007), blood plasma and serum (Bernini *et al.*, 2011; Beckonert *et al.*, 2007), and intact tissues (Beckonert *et al.*, 2010).

5.2 NMR experiments

NMR spectroscopy of blood plasma and serum present a challenge, because it contains both low and high molecular weight compounds. The macromolecules, represented by *e. g.* albumin, lipoproteins and glycoproteins, give broad signals in NMR spectra, which make the interpretation of other signals difficult. To overcome this problem different spectral editing techniques are employed. CPMG experiments can be used to observe the signals from small molecules by spin-spin relaxation editing, whereas diffusion-editing experiments can be used to enhance the signals from macromolecules (Figure 18).

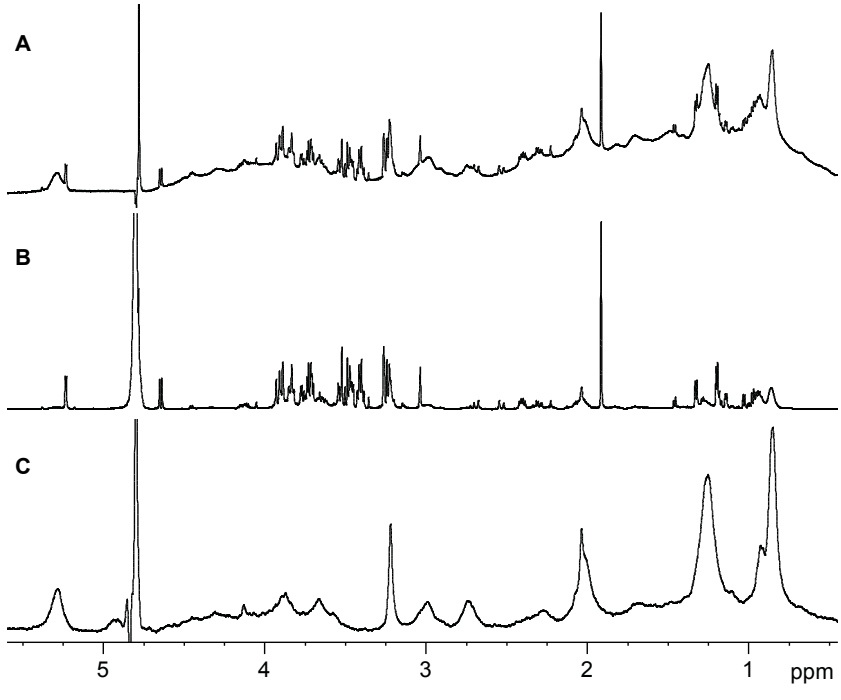

Figure 18. **A**) NOESY presaturation, **B**) CPMG, and **C**) BPP-LED spectra of cow blood serum (unpublished data). Broad signals from lipoproteins mainly, appear in spectrum **A** and **C**, whereas spectrum **B** is dominated by signals from glucose, amino acids and other small metabolites.

A disadvantage of the CPMG experiment is that the proportionality between concentration and proton signal integral is lost and so also the possibility of direct quantification. If a direct quantification is desired blood samples should be filtered to remove macromolecules.

5.3 Identification

The identification of metabolites is, despite the small molecular structures, not trivial. Often only one resolved ^{1}H signal is available due to overlap with other signals. The chemical shifts of common metabolites in human blood and urine have been tabulated (Fan, 1996; Nicholson *et al.*, 1995) and can also be compared to databases (Emwas *et al.*, 2013) and computer programs (Smolinska *et al.*, 2012). However, differences in pH and salinity can alter the chemical shift in a specific matrix and a supported identification is often necessary. This can be achieved by the use of reference samples and 2D NMR experiments. ^{1}H,^{1}H-TOCSY, ^{1}H,^{13}C-HSQC and DOSY experiments are particularly useful in the identification of small metabolites in complex mixtures.

5.4 Preprocessing methods

After phasing and baseline correction of the NMR data a number of steps have to be considered before multivariate analysis is performed. The NMR spectra are collected in a data matrix for further processing, where each row is a spectrum and the columns consist of data points or integrals over selected regions (termed binning).

First of all the spectral region of the water signal is usually excluded. Despite the use of water suppression techniques, there are still remains of the water signal that would interfere with the interpretation of other signals.

A normalization of the data matrix is made to take differences in dilution of the samples and differences in the receiver gain of the NMR experiment into account. The different degree of dilution is especially important when working with urine samples. The most often employed normalization method is to normalize each spectrum to a unit total integral of one, called integral normalization. However, the approximation that the total integral of all sample spectra is the same breaks down if large perturbations to intensities occur (Craig *et al.*, 2006). An alternative method is probabilistic quotient normalization, where a most probable dilution factor is calculated from the distribution of quotients of the amplitudes of a test spectrum by those of a reference spectrum (Dieterle *et al.*, 2006).

One, already mentioned, problem is the differences in chemical shift between samples, due to differences in pH and salinity. Citrate is well-known to cause such problems, but most metabolites have more or less pH dependant chemical shifts. Binning has been used to overcome this problem, which is to divide the spectrum into narrow segments, typically 0.04 ppm wide, that are integrated (Lindon *et al.*, 2001). Unfortunately, the multiplet pattern of the NMR signals is lost by this approach and a signal can be divided between different segments. Another way to solve the problem with misaligned signals is to use a peak alignment algorithm, that line up the signals by comparing the different spectra. There are several different peak alignment methods, *e. g.* interval correlated shifting (icoshift) (Savorani *et al.*, 2010), and recursive segment-wise peak alignment (RSPA) (Veselkov *et al.*, 2009). They are both based on segment-wise alignment of spectra to a reference spectrum, but whereas the icoshift algorithm relies on user-defined segments, the RSPA algorithm relies on a peak-picking routine.

Scaling is a kind of normalization of the data, but performed on the columns (the variables) instead of the rows (the spectra) of the data matrix. Each column can be given a mean of zero by subtracting the column mean from each value in the column, so-called mean-centering (Craig *et al.*, 2006). This scaling reflects the covariance of the variables and is advantageous in multivariate analysis.

Scaling can also be used to compensate for the low variance of small signals, so that not only the abundant signals show significant variance. A scaling to unit variance means that each column is divided by the standard deviation of the column, resulting in a weighting that reflects the correlation of the variables. However, this scaling can overestimate the significance of small signals and even noise, and often a third method is used, which is a compromise between mean-centering only and scaling to unit variance. This is called pareto scaling, where each column is divided by the square root of the standard deviation of the column. Pareto scaling has been used extensively on NMR data, but as in the case of unit variance scaling, the output variables (the loadings) of the multivariate analysis are distorted and the high variance variables have relatively greater weight (Cloarec *et al.*, 2005).

5.5 Multivariate analysis

The purpose of multivariate analysis is to extract meaningful information about systematic variation from the multivariate measurement that an NMR spectrum is. Usually only a limited number of variables show variation to a specific perturbation of the biological system investigated and these variables need to

be extracted. Initially, it should be tested whether data from the perturbed and unperturbed states can be separated by their variation.

Multivariate analysis methods are divided into unsupervised and supervised methods, depending on if the data are initially ungrouped or grouped based on the origin of the samples. An unsupervised method can be regarded as unbiased. Among the unsupervised methods, principal component analysis (PCA) is by far the most encountered.

PCA is a projection-based method with the underlying assumption that the system is driven by a small number of multivariate latent variables (Wold *et al.*, 1987). By calculating these latent variables a low-dimensional model can be constructed from the multidimensional matrix **X**, formed by objects (spectra) and variables (intensity in each point). From the initial data matrix, two new matrices are constructed: the loadings and score matrices **P** and **T**. Principal components (PC) are linear combinations of the original data, but expressed as scores and loadings, instead of objects and variables. The first PC describes the maximum variance between the objects, the second PC the next highest variance, and so on. Each PC is orthogonal to the preceding and thus exhibits new variance.

The two matrices with scores and loadings can be visualized by using the principal components (Figure 19). The score plot shows how the objects are related to each other by variance explained by the PCs. Each point represents a single spectrum. The loadings plot shows the connections between the variables and can be used to interpret differences displayed by the score plot.

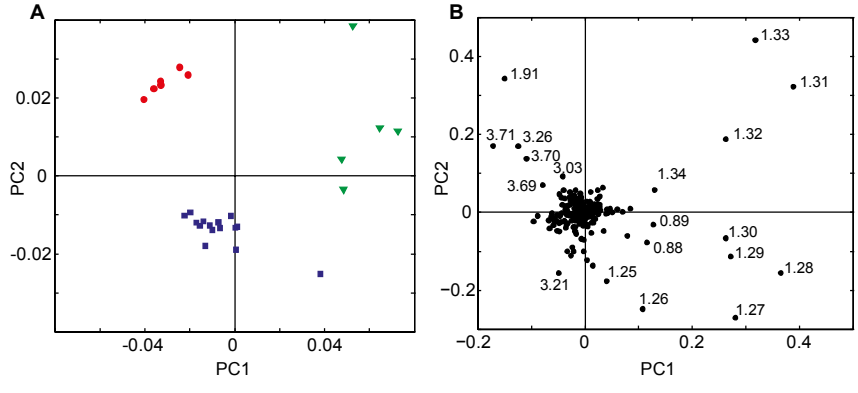

Figure 19. Example of **A**) score and **B**) loadings plot from PCA of human (blue), rat (green), and cow (red) blood serum (unpublished data). The species are clearly separated in the score plot and the loadings plot can be used to determine the differentiating metabolites.

Supervised models are, in contrast to unsupervised models, built on *a priori* knowledge about the structure of the data set. A model is constructed by

regression of continuous parameters or classification of discrete parameters, and then validated to estimate its prediction capability.

Partial least square (PLS)-regression is a projection-based supervised model for relating two data matrices, **X** and **Y**, by a linear multivariate analysis (Wold *et al.*, 2001). **X** is, as in PCA, the data matrix, whereas **Y** is a matrix of response variables. If the **Y** matrix contains discrete variables, partial least square discriminant analysis (PLS-DA) can be employed (Trygg *et al.*, 2007). Orthogonal PLS-DA (OPLS-DA) is a further modification of PLS-DA, where an orthogonal filter has been included to remove within-class variation from between-class variation (Bylesjö *et al.*, 2006).

In analogy to PCA, loadings and scores are generated by OPLS-DA, but the scores are separated into Y-predictive and Y-orthogonal components. The Y-predictive component is linearly related to **Y** and predicts the between-class variation, whereas the Y-orthogonal component is orthogonal to the Y-predictive component and thus predicts the within-class variation. The interpretation of OPLS-DA results is simplified by the feature that all predicted between-class variation is summarized in one component.

The visualization of the corresponding loadings was further improved by Cloarec *et al.* (2005). The predictive component scaled to unit variance was 'back-scaled' by multiplication with the standard deviation, thus producing a mean-centered component. This predictive component, equivalent to a covariance spectrum, was then color-coded by the unit variance scaled predictive component, equivalent to a correlation spectrum. In the 'back-scaling' approach the appearance of the NMR spectrum is retained, but with a color-coding pointing out signals with high correlation (Figure 20). The mean-centered and unit variance scaled spectrum from OPLS-DA is directly scalable to the correlation between **X** and **Y**, and thus correlation coefficients can be derived (Fonville *et al.*, 2010).

The results of OPLS-DA models are not interpretable unless the model has been satisfactorily validated. It should be kept in mind that supervised models on multivariate data will always extract differences between the classes, even in cases where the true difference is negligible and what is fitted is only noise. To prevent over-fitting, the predictive ability of the model is calculated by validation. Ideally, a second independent data set is used for validation. Alternatively, cross-validation is used, where parts of the samples are temporarily left out to form a validation test set (Wold *et al.*, 2001). The result of the cross-validation is expressed as the modeled variation of **X** (R^2X) and the cross-validated prediction of **Y** (Q^2Y).

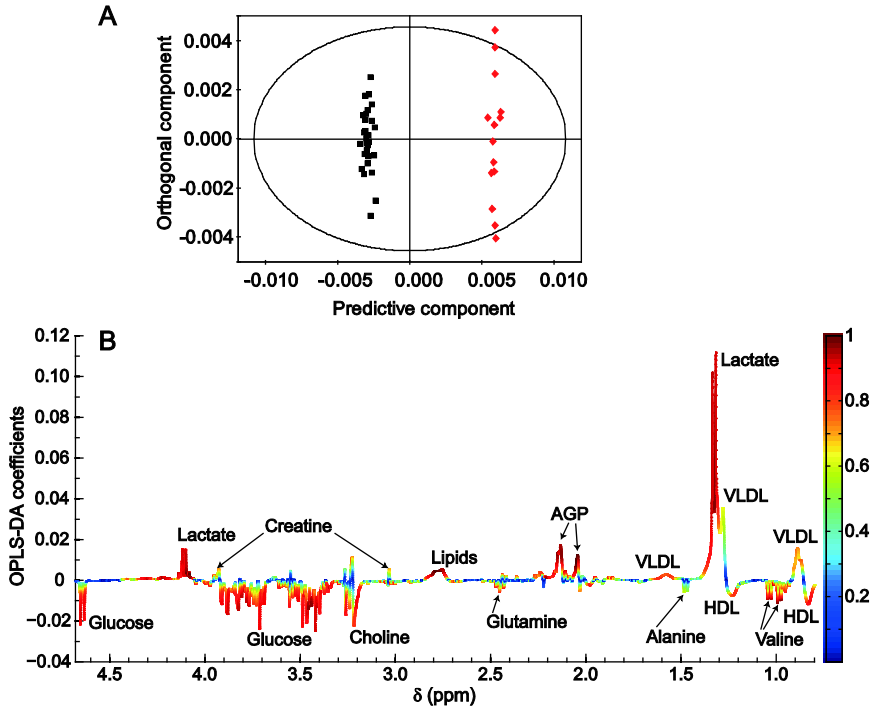

Figure 20. Example of **A**) score and **B**) loadings plots from OPLS-DA of human (black) and rat (red) blood serum (unpublished data). The loadings plot is color-coded by 'back-scaling' and metabolites discriminating between rats (positive) and humans (negative) are highlighted. R^2X = 0.94 and Q^2Y = 0.97.

6 Structure analysis of a lipopolysaccharide from *Plesiomonas shigelloides* (Paper I)

6.1 Background

6.1.1 Lipopolysaccharides

LPSs are endotoxins situated on the outer membrane of Gram-negative bacteria. In addition to a protective function, they are potent virulence factors. The role of LPSs as antigens and immune activators makes them interesting as targets in vaccine development (Bernardi *et al.*, 2013).

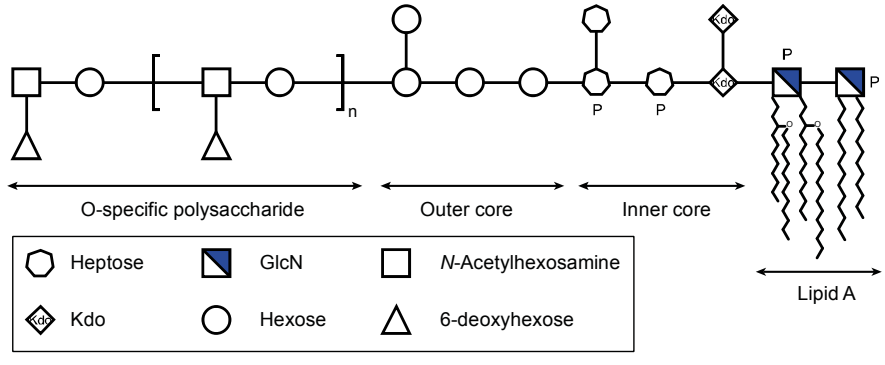

Figure 21. Schematic structure of a typical LPS. Phosphate groups are denoted by P.

LPSs (Figure 21) consist of a lipophilic part, called lipid A, a core oligosaccharide and an O-specific polysaccharide (Raetz & Whitfield, 2002). Lipid A is anchored to the bacterial membrane via fatty acids, which are linked to two GlcN residues through amide and ester bonds. The two GlcN residues are usually linked to the core oligosaccharide through a Kdo. The inner core part is constituted by Kdo and heptose residues, often substituted by phosphate

groups. The outer core is dominated by hexoses and is linked to the O-specific polysaccharide (Caroff *et al.*, 2002).

The extent of structural variation of LPS structures is increasing when going further away from the membrane (Raetz & Whitfield, 2002). The O-specific polysaccharide shows a remarkable diversity and defines the O-antigen specificity of a bacterial strain. The core oligosaccharide is more conserved within and between species, even though a number of different glycoforms can occur within the same species. Lipid A is more or less conserved throughout the bacterial world, with differences only found in the nature of the fatty acids (Erridge *et al.*, 2002).

LPSs are divided into smooth, semi-rough and rough forms. Smooth LPS have all the constituents mentioned above, whereas semi-rough LPS has just one RU of the O-specific polysaccharide, and rough LPS is just composed of lipid A and the core oligosaccharide (Wilkinson, 1996).

LPSs are isolated by hot phenol/water extraction (Westphal & Jann, 1965), in which LPS and nucleic acids are usually obtained in the water phase, and proteins and lipids are obtained in the phenol phase. However, rough-type LPS can also be found in the phenol phase due to the larger contribution of lipid A to its lipophilicity. The fraction containing LPS is further purified by dialysis and ultracentrifugation to obtain the pure LPS.

The hydrophilic carbohydrate structure and the lipophilic lipid A, making LPSs amphiphilic, is responsible for their aggregation in aqueous solution (Wilkinson, 1996). To increase the solubility in water, a delipidation step is performed, where lipid A is cleaved off by mild acidic hydrolysis (see section 3.1). The resulting delipidated LPS is fractionated by size-exclusion chromatography before analysis by NMR spectroscopy and MS. Smooth-type LPS often consists of minor fractions of rough or semi-rough forms, which can be separated from the smooth form and characterized.

6.1.2 *Plesiomonas shigelloides*

Plesiomonas shigelloides is a Gram-negative, rod-shaped bacterium of the *Enterobacteriaceae* family, which causes gastrointestinal and localized infections with diarrhea as the main symptom. *P. shigelloides* is found in freshwater and surface water in tropical and temperate climates (Levin, 2008), but has also been identified in the Nordic countries (González-Rey *et al.*, 2004). Outbreaks of human infections of *P. shigelloides* are most often associated with seafood, especially uncooked shellfish or raw oysters (Stock, 2004). Infections of *P. shigelloides* are reported at irregular intervals and there is probably an underestimation of the number of infected subjects (Stock, 2004).

The pathogenesis of *P. shigelloides* is yet not understood in detail. A number of possible virulence factors from *P. shigelloides* have been described, including a cholera-like toxin (Gardner *et al.*, 1987), a thermostable and a thermolabile enterotoxin (Sears & Kaper, 1996), a β-hemolysin (Janda & Abbott, 1993) and a cytotoxic protein (Tsugawa *et al.*, 2008; Okawa *et al.*, 2004), which forms a complex with LPS on the outer bacterial membrane.

Strains of *P. shigelloides* have been classified into 102 O serotypes, based on their O-antigens, and 50 H serotypes, which are based on their H-antigens in the form of flagellar proteins (Aldova & Shimada, 2000). Only a few structures of LPSs from these different strains have been published to date and were recently reviewed by Nazarenko *et al.* (2011). The complete LPS of serotype O54:H2 (Lukasiewicz *et al.*, 2006b; Niedziela *et al.*, 2002; Czaja *et al.*, 2000), O74:H5 (Lukasiewicz *et al.*, 2006a; Niedziela *et al.*, 2006) and O37 (Kaszowska *et al.*, 2013a) have been characterized, as well as the core oligosaccharide of serotype O13 (Kaszowska *et al.*, 2013b), the core oligosaccharide substituted to a RU of the O-specific polysaccharide of serotype O17 (Maciejewska *et al.*, 2013; Kubler-Kielb *et al.*, 2008) and O1 (Pieretti *et al.*, 2010; Pieretti *et al.*, 2009; Pieretti *et al.*, 2008), and the O-specific polysaccharide of serotype O51 (Maciejewska *et al.*, 2009), strains 22074 and 12254 (Linnerborg *et al.*, 1995), and strain AM36565 (Säwén *et al.*, 2012).

LPSs of *P. shigelloides* are characterized by the absence of phosphate groups in the inner core, but the presence of uronic acids in the outer core provides negative charges that stabilize the bacterial membrane (Niedziela *et al.*, 2006). O-specific polysaccharides from *P. shigelloides* are often hydrophobic and the LPSs have been collected from the phenol fraction instead of the water fraction during phenol/water extraction of the crude LPS. This hydrophobicity can be explained by the presence of several deoxy sugars with *O*- and *N*-acetylations (Niedziela *et al.*, 2006). All characterized LPSs from *P. shigelloides* have been smooth except the O37 LPS, which was semi-rough (Kaszowska *et al.*, 2013a).

The aim of this project was to determine the structure of the core oligosaccharide and the O-specific polysaccharide from the *P. shigelloides* strain CNCTC 34/89 LPS, associated to the serotype O33:H3 (Shimada & Sakazaki, 1985), which is a clinical isolate collected from a patient from Cuba.

6.2 Experimental procedures

LPS was obtained from bacterial cells by the hot phenol/water extraction, followed by dialysis and ultracentrifugation. LPS was delipidated with acetic acid and fractionated by size-exclusion chromatography in two steps (Figure 22):

The O-specific polysaccharide was separated from core oligosaccharides with a Superdex 75 column and the core oligosaccharides were then further fractionated on a Superdex 30 column. The fraction with only core oligosaccharide was then further separated on a strong cation exchange column.

The structures of the different fractions were analyzed by chemical analysis, NMR spectroscopy and mass spectrometry as described in chapter 3. The structure of the O-specific polysaccharide was confirmed by ^{1}H HR-MAS NMR spectroscopy on bacteria and purified LPS.

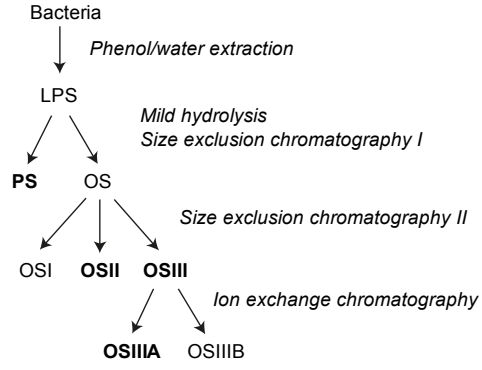

Figure 22. Schematic representation of the work-flow to yield LPS fractions for further analysis. Fractions in bold are discussed below.

6.3 Results and discussion

6.3.1 O-specific polysaccharide

The O-specific polysaccharide was found to contain the following tetrasaccharide RU, denoted by **P-O-N-M**:

→2)-β-D-Gal*p*-(1→3)-β-D-Glc*p*NAc-(1→4)-β-D-Glc*p*A-(1→3)-β-D-Glc*p*NAc-(1→

The sugar analysis showed the presence of Gal and GlcNAc in a 1:2 ratio, which were D sugars according to determination of the absolute configuration on the trimethylsilylated (*S*)-butyl glycosides. D-GlcA was also observed as the (*S*)-butyl glycoside. Methylation analysis revealed the presence of 2-substituted Gal*p* and 3-substituted Gal*p*NAc (Figure 23).

NMR spectroscopy on the O-specific polysaccharide confirmed the presence of one Gal, two GlcNAc and one GlcA. The sequence of the residues was determined by ^{1}H,^{13}C-HMBC and ^{1}H,^{1}H-NOESY (Figure 24) experiments and the chemical shifts were compared with predictions made by the CASPER program.

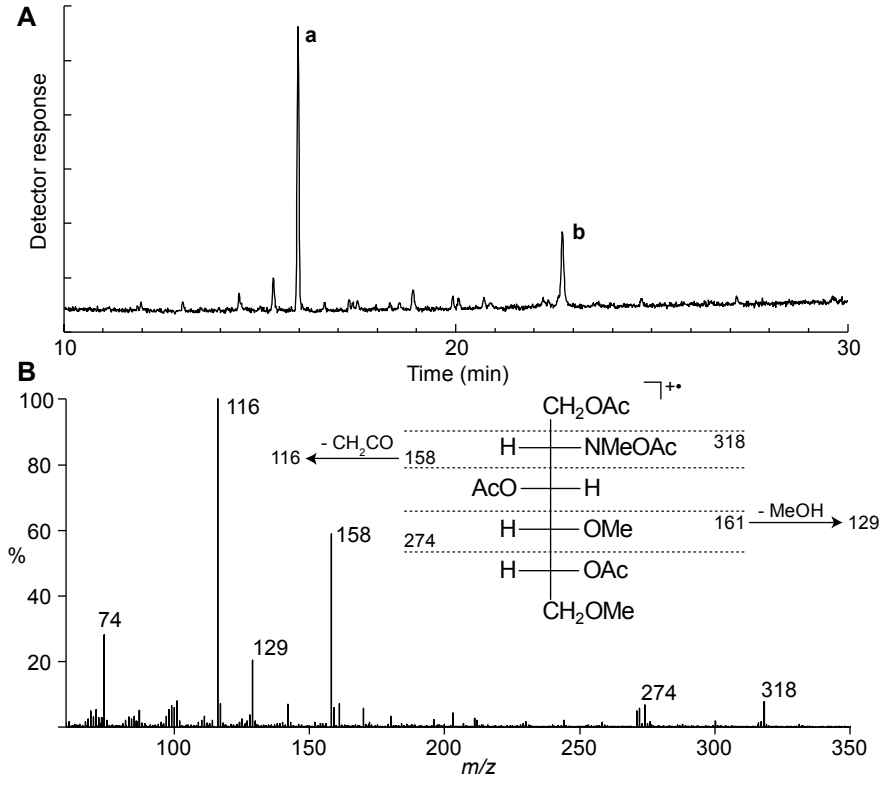

Figure 23. GC-MS total ion current chromatogram (**A**) of PMAA from the O-specific polysaccharide. The mass spectrum of peak **a**, corresponding to 1,2,5-tri-*O*-acetyl-3,4,6-tri-*O*-methyl-galactitol, is shown in Figure 13, whereas the mass spectrum of peak **b**, corresponding to 1,3,5-tri-*O*-acetyl-2-deoxy-4,6-di-*O*-methyl-2-(*N*-methylacetamido)glucitol, is shown here (**B**). Minor peaks in the chromatogram were mainly due to core oligosaccharide residues.

HR-MAS NMR spectroscopy was used to confirm the identical appearance of the O-antigen structure *in situ* on bacteria and in extracted LPS, compared to purified O-specific polysaccharide. Chemical shifts of signals from polysaccharide residues were in agreement with those for bacterial O-antigen and extracted LPS (Figure 25).

6.3.2 Core oligosaccharide OSIII

Core oligosaccharide fractions were termed OSI, OSII, and OSIII according to the order of elution from the size-exclusion column. OSI corresponded to core substituted by two RU, OSII to core substituted by one RU, and OSIII to unsubstituted core oligosaccharide.

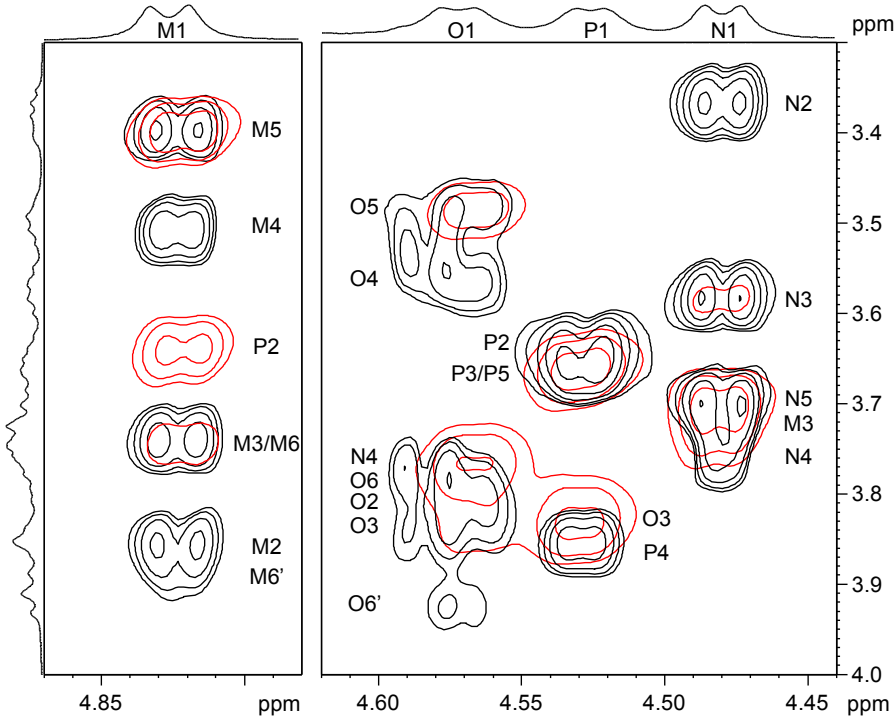

Figure 24. Selected regions of TOCSY (black) and NOESY (red) spectra of the O-specific polysaccharide. Mixing times were 120 ms (TOCSY) and 100 ms (NOESY). The uppercase letters refer to designation of carbohydrate residues.

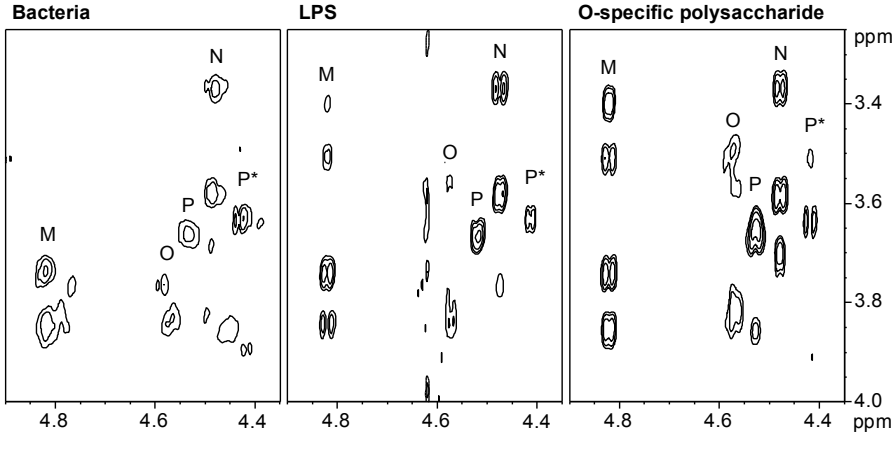

Figure 25. Selected regions of TOCSY spectra. Bacteria and LPS were studied by HR-MAS with 60 ms mixing time, whereas the O-specific polysaccharide was studied in solution with 80 ms mixing time. The uppercase letters refer to designation of carbohydrate residues, where **P*** is the non-reducing end form of **P**.

Fraction OSIII was subjected to chemical analysis, which revealed the presence of 2,3,7-substituted, 3,4-substituted and 7-substituted L,D-Hep*p*, 6-substituted D-Glc*p*N, and non-substituted D-Gal*p*, D-Glc*p*, D-Gal*p*N, and D-Gal*p*NAc. Minor amounts of 3,7-substituted L,D-Hep*p* and 6-substituted D-Glc*p* indicated heterogeneity.

The heterogeneity of OSIII was further confirmed by ESI-MS in negative ion mode (Figure 26). The charge-deconvoluted spectrum showed a main species at 2039.63 Da, which corresponds to an undecasaccharide built of one Kdo in anhydro form, three Hep, two Hex, two HexA, two HexN, and one *O*-Ac-HexNAc. The peaks at 1877.58 and 1997.62 Da indicated the absence of a Hex and an *O*-acetyl group, respectively.

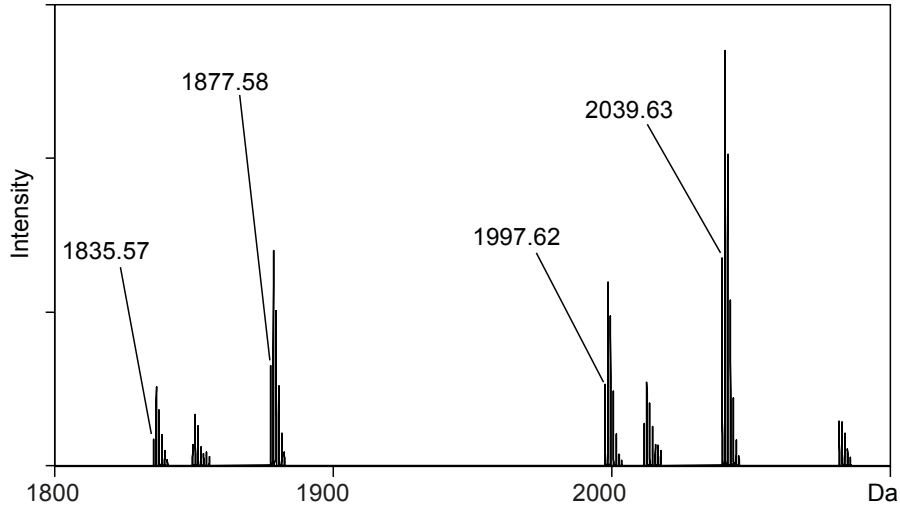

Figure 26. Charge-deconvoluted ESI-MS spectrum of OSIII in negative ion mode.

NMR spectra of OSIII showed many similarities to the core oligosaccharide of serotype O17 investigated by Kubler-Kielb *et al.* (2008). Residue **A**-**K** were identical to the O17 core oligosaccharide, whereas a 6-*O*-Ac-α-D-Gal*p*NAc (residue **L***) was observed only in the O33 core oligosaccharide (Figure 27).

The α-pyranoside *galacto* configuration of residue **L*** was deduced from a $^{1}J_{\text{C-1,H-1}}$ of 173 Hz and from TOCSY spectra. An upfield shift of the C-2 signal (50.5 ppm) and a downfield shift of the H-2 signal (4.20 ppm) indicated *N*-acetylation at position 2 (Figure 28), which was supported by connectivities in the HMBC spectra between H-2 and C=O (175.7 ppm), and between C=O and a methyl group (2.05/22.8 ppm). The presence of an *O*-acetyl group at position 6 was supported by downfield shifts of H-6/H-6' (4.25/4.33 ppm) and C-6 (64.9 ppm), and by HMBC correlations between H-6 and C=O (175.0 ppm),

and between C=O and a methyl group (2.11/21.1 ppm). De-*O*-acetylation with ammonia afforded an oligosaccharide without the signals at 2.11/21.1 ppm and 4.25, 4.33/64.9 ppm.

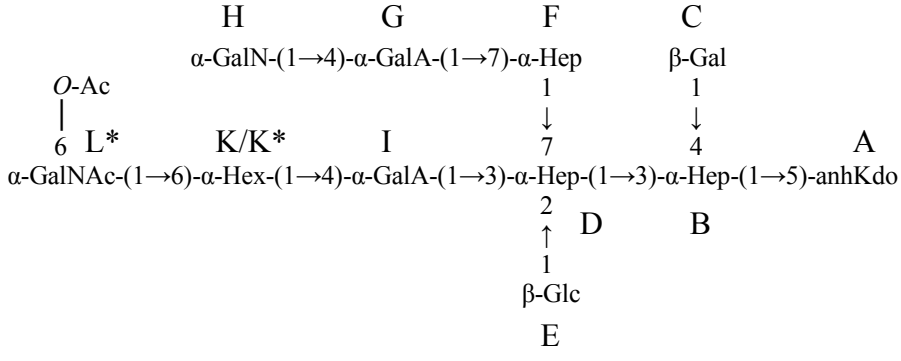

Figure 27. Structure of OSIII, where **K** is GlcN and **K*** is Glc. Residue **A**-**K** were identical to the core oligosaccharide of serotype O17 (Kubler-Kielb *et al.*, 2008).

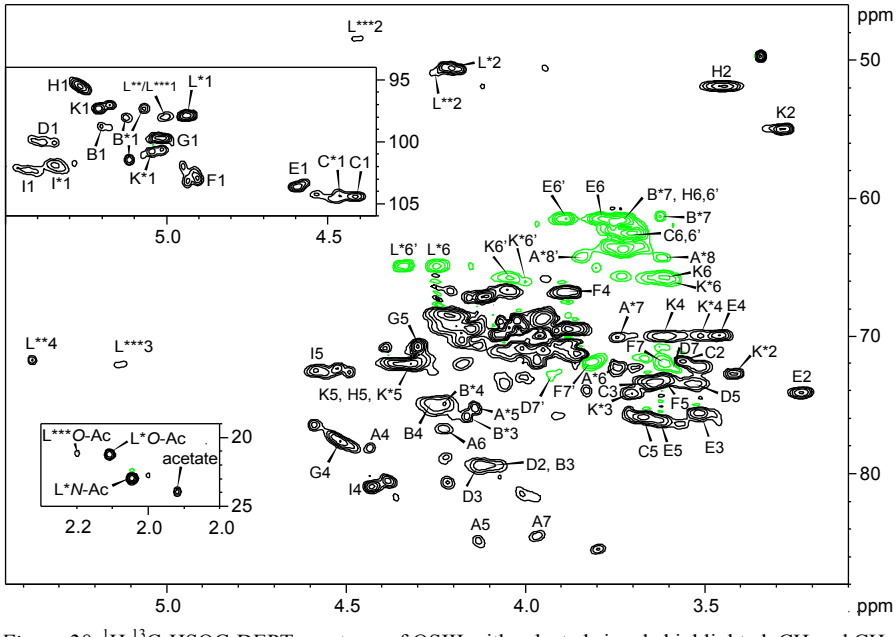

Figure 28. $^{1}H,^{13}C$-HSQC-DEPT spectrum of OSIII with selected signals highlighted. CH and CH_3 protons are positive (black) and CH_2 protons are negative (green). Insets represent the anomeric region and the methyl region. The uppercase letters refer to designation of carbohydrate residues (Figure 27). Minor forms of residue **A**, **B**, **C** and **I** are denoted by asterisks.

The heterogeneous appearance of OSIII had several different origins: To begin with, Kdo (residue **A**) was partially dehydrated to a mixture of Kdo, 4,7-anhydro Kdo, and 4,8-anhydro Kdo (Figure 29).

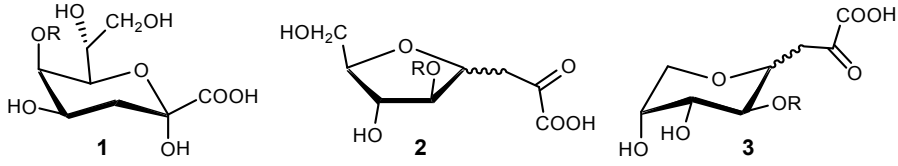

Figure 29. Structures of 5-substituted α-Kdo (**1**), 4,7-anhydro Kdo (**2**), and 4,8-anhydro Kdo (**3**).

4,7-Anhydro Kdo was the major component, which was recognized by the downfield shifts of C-4 (78.1 ppm), C-5 (84.8 ppm), C-6 (76.7 ppm), and C-7 (84.4 ppm). The high chemical shifts are consistent with a furanose ring, since carbons in furanose rings are less shielded than carbons in pyranose rings (Bubb, 2003). The anhydro form was also supported by the absence of H-3 signals, which is due to exchange with deuterium from D_2O. These protons are more acidic when situated adjacent to a carbonyl C-2, instead of the hemi-ketal C-2 of a normal reducing Kdo (Carlson *et al.*, 1995).

A phosphate group substitution at position 4 of Kdo has been attributed to the formation of 4,7- and 4,8-anhydro Kdo (Vinogradov *et al.*, 1993; Auzanneau *et al.*, 1991). However, enterobacterial inner core regions contain a second Kdo substituted at position 4 of Kdo (Holst, 2007):

L,D-Hep-(1→7)-L,D-Hep-(1→3)-L-α-D-Hep-(1→5)-[α-Kdo-(2→4)]-α-Kdo

This lateral Kdo residue has been observed in core oligosaccharides from the *P. shigelloides* O54 (Lukasiewicz *et al.*, 2006b), O74 (Lukasiewicz *et al.*, 2006a), and O1 (Pieretti *et al.*, 2009) LPS. In the O1 core oligosaccharide this Kdo residue was partially replaced by D-*glycero*-D-*talo*-oct-2-ulopyranosonic acid (Ko) (Pieretti *et al.*, 2009).

The determination of lateral Kdo, as well as the GlcN residues of lipid A, is made by de-*O*-acylation of the LPS in anhydrous hydrazine. However, when mild acidic hydrolysis is used not only lipid A is cleaved off, but also other Kdo residues are hydrolyzed. This hydrolysis of Kdo could thus be followed by the elimination of water and subsequent 1,4-addition to 4,7- and 4,8-anhydro Kdo (Figure 30).

Other reasons for heterogeneity of the OSIII fraction were a partial lack of Glc **E** residue, a partial lack of *O*-acetylation on residue **L***, and minor forms of 4-*O*-Ac and 3-*O*-Ac-GalNAc (termed **L**** and **L*****). After consideration of these reasons for heterogeneity, the $^{1}H,^{13}C$-HSQC spectrum still contained unassigned cross-peaks, thus indicating additional glycoforms. In the anomeric

region the signal at 5.04/100.7 ppm remained unassigned and appeared to come from an isomer of GlcN **K**. However, this residue (termed **K***) lacked the up-field shift of C-2 of **K** (55.0 ppm), which is characteristic of amino sugars. It was assigned as →6)-α-D-Glc-(1→ and showed HMBC connectivities to position 4 of GalA **I**. Unfortunately, the presumed glycosidic linkage between residue **K*** and residue **L** was difficult to determine due to the similar chemical shifts of H-6/6' from residue **K** and **K***.

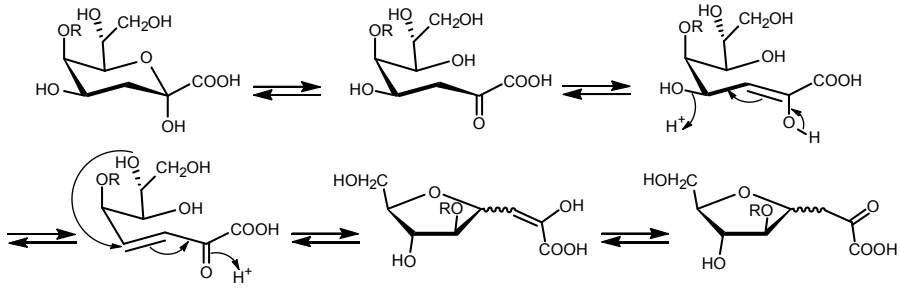

Figure 30. Proposed reaction mechanism of acid catalyzed elimination of 5-substituted α-Kdo and subsequent 1,4-addition to 4,7-anhydro Kdo. The initial hydrolysis of the two Kdo residues is not shown. A similar mechanism was proposed by Auzanneau *et al.* (1991) for phosphorylated Kdo. R represents the rest of the core oligosaccharide.

This kind of replacement of a sugar residue in the carbohydrate backbone of a core oligosaccharide (**K** to **K*** in this case) has not been previously reported and must be proved unequivocally. To do this, ESI mass spectra in positive ion mode were evaluated (Figure 31). Since the mass difference between the two glycoforms would be 1, the additional glycoform should be hidden in the isotopic peaks of OSIII. The isotopic pattern of the $[M + H + Na]^{2+}$ ion (Figure 31A) was compared with the theoretical pattern (Figure 31C and D) and it was found to be equal to about 30% of **K*** and 70% **K**.

Subsequently, an attempt was made to separate the two glycoforms, to obtain a clear proof of the replacement. Because of the different number of positive charges in the two glycoforms when a positively charged GlcN is changed to a neutral Glc, a strong cation exchange resin (Dowex 50WX8) was chosen. The **K*** containing glycoform eluted first, as expected, and was termed fraction OSIIIA, whereas the later eluting **K** containing glycoform was termed OSIIIB. However, the two glycoforms did not separate, but the fraction of **K*** increased from ~30% in OSIII to at most *ca*. 59% in OSIIIA.

The degree of cross-linkage of the cation resin has been found to have a large effect on the adsorption of erythromycin (Dechow, 1989), which is an antibiotic with an amino sugar that is sterically hindered. Dowex 50WX4, with 4% cross-linkage gave a much better adsorption of erythromycin than Dowex

50WX8 with 8% cross-linkage, in spite of a better exchange capacity of Dowex 50WX8 (Dechow, 1989). Since the positive charge of GlcN **K** is probably also, by some degree, sterically hindered, Dowex 50WX4 was tested. This ion exchange resin yielded an OSIIIA fraction of at most *ca*. 88% **K*** glycoform, instead of *ca*. 59% with Dowex 50WX8.

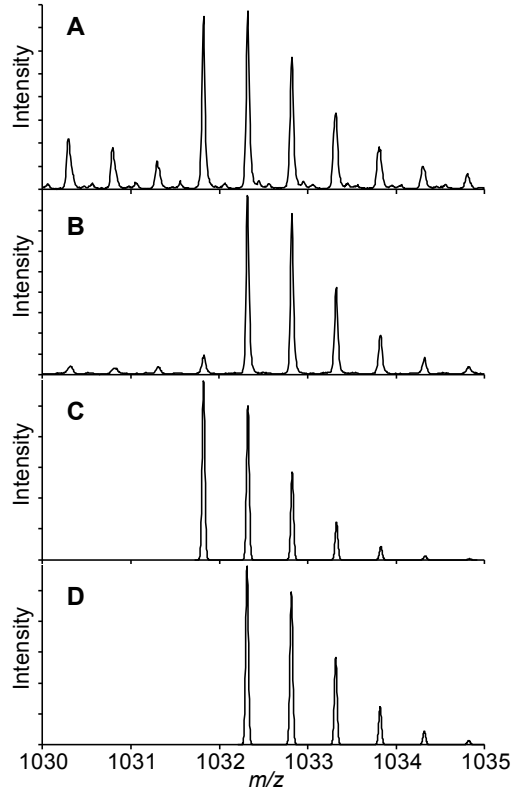

Figure 31. The experimental isotopic pattern of the $[M + H + Na]^{2+}$ ion of the OSIII fraction (A) and the OSIIIA fraction (B), and calculated isotopic patterns of OSIII with 100% **K** (C), and with 100% **K*** (D).

Fraction OSIIIA was used for ESI MS analysis and the mass was equivalent to Glc **K*** glycoform (*m/z* 1032.32; Figure 30B). MS/MS analysis on the ion corresponding to the sodium adduct $[M + 2Na]^{2+}$ of OSIIIA (*m/z* 1043.31), yielded $B_{2\alpha}$ (*m/z* 430.13) and $Y_{5\alpha}Y_{5\beta}$ (*m/z* 840.22) fragments, which could be used to trace the additional mass unit, compared to OSIIIB, to residue **K*** (Figure 32 and Table 2).

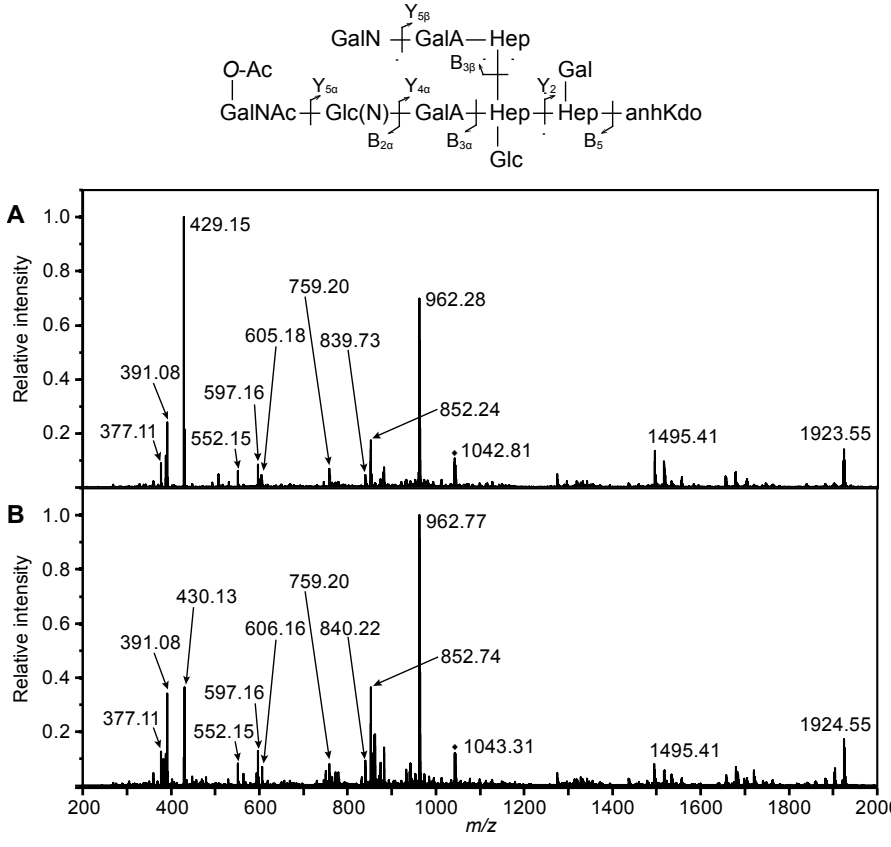

Figure 32. MS/MS spectra of OSIIIB (**A**) and OSIIIA (**B**). The precursor ion was $[M + 2Na]^{2+}$.

Table 2. *Structural assignments of fragment ions from MS/MS analysis of OSIIIA and OSIIIB.*

OSIIIA		OSIIIB			
Observed	Calculated	Observed	Calculated	Proposed composition	Charge
377.1078	377.1054	377.1074	377.1054	B_5Y_2	Na^+
391.0868	391.0847	391.0865	391.0847	$B_{3\beta}Y_{5\beta}$	Na^+
430.1348	430.1320	429.1489	429.1480	$B_{2\alpha}$	Na^+
552.1514	552.1535	552.1536	552.1535	$B_{3\beta}$	Na^+
597.1639	597.1637	597.1648	597.1637	Y_2	Na^+
606.1676	606.1641	605.1834	605.1801	$B_{3\alpha}$	Na^+
759.1980	759.1983	759.1953	759.1983	$Y_{4\alpha}Y_{5\beta}$	$2Na^+$
840.2221	840.2248	839.7335	839.7328	$Y_{5\alpha}Y_{5\beta}$	$2Na^+$
852.7445	852.7406	852.2489	852.2486	$B_5Y_{5\beta}$	$2Na^+$
962.7700	962.7697	962.2794	962.2777	$Y_{5\beta}$	$2Na^+$
1495.4096	1495.4075	1495.4115	1495.4075	$Y_{4\alpha}Y_{5\beta}$	Na^+
1924.5439	1924.5321	1923.5536	1923.5481	$Y_{5\beta}$	$2Na^+ - H^+$

NMR analysis of OSIIIA confirmed the increase in **K*** residue and the decrease in **K** residue (Figure 33). The linkage between Glc **K*** and 6-*O*-Ac-GalNAc **L*** was supported by NOEs and HMBC connectivities.

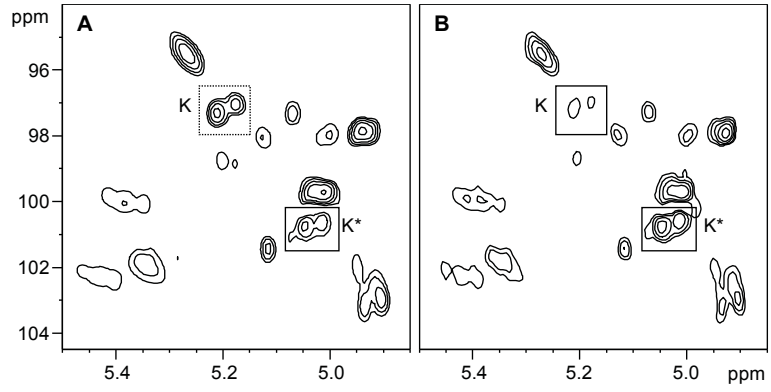

Figure 33. Parts of the anomeric region of HSQC spectra of A) OSIII and B) OSIIIA. **K** and **K*** anomeric protons are highlighted.

6.3.3 Oligosaccharide OSII

Oligosaccharide OSII corresponded to core oligosaccharide substituted by one RU of the O-specific polysaccharide, and was used to determine the linkage between them. The RU was found to be linked via GlcNAc (**M**) to position 4 of residue **L**. However, residue **L** was *O*-acetylated on position 3 instead of position 6, as in the OSIII fraction. A minor fraction of oligosaccharide without *O*-acetylation (~30%) illustrated the influence of the *O*-acetylation on the chemical shift of H-3, which was shifted downfield by almost 1.2 ppm in residue **L**, compared to the same residue without *O*-acetylation (**L'**, 4.06 ppm).

De-*O*-acetylation of OSII with ammonia confirmed the conversion of residue **L** to residue **L'**, and revealed the effects of *O*-acetylation of residue **L** on the chemical shifts of the neighboring residues **M** and **N** (Figure 34).

The reason for the difference in the position of the *O*-acetyl group can be found in migration of substituents under certain conditions. The presence of minor amounts of 3- and 4-*O*-Ac forms in the OSIII fraction, in addition to the 6-*O*-Ac form, indicates that the *O*-acetyl group has migrated from position 3, via position 4, to position 6 (Figure 35). In OSII such a migration is not possible, due to the glycosidic linkage at position 4.

A similar migration of an *O*-acetyl group in a core oligosaccharide has previously been observed for 2-*O*-Ac-Rha (Knirel *et al.*, 1996). Studies on acyl group migrations in β-galactopyranosides have shown acyl group migrations at alkaline (Roslund *et al.*, 2008) and acidic pH (Horrobin *et al.*, 1998), and a slower migration at neutral pH (Roslund *et al.*, 2008). Thus, the migration

could probably occur during the mild acidic hydrolysis with acetic acid, but migrations already on the bacterial cell membrane of rough-type LPS cannot be excluded.

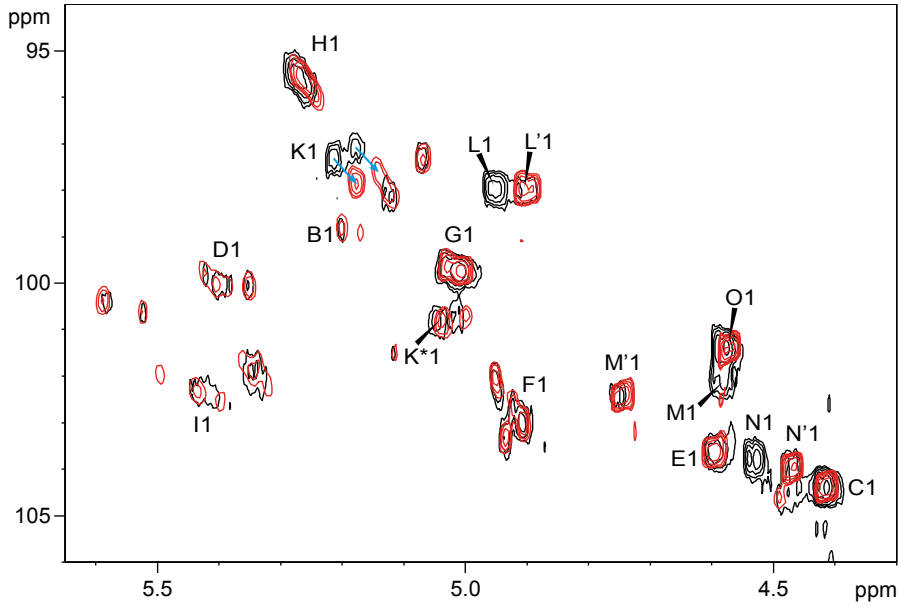

Figure 34. Anomeric region of HSQC spectra of OSII before (black) and after (red) de-*O*-acetylation with ammonia. Residue **L'**, **M'** and **N'** refer to OSII without *O*-acetylation. The chemical shifts of residue **K** signals were altered due to differences in pH.

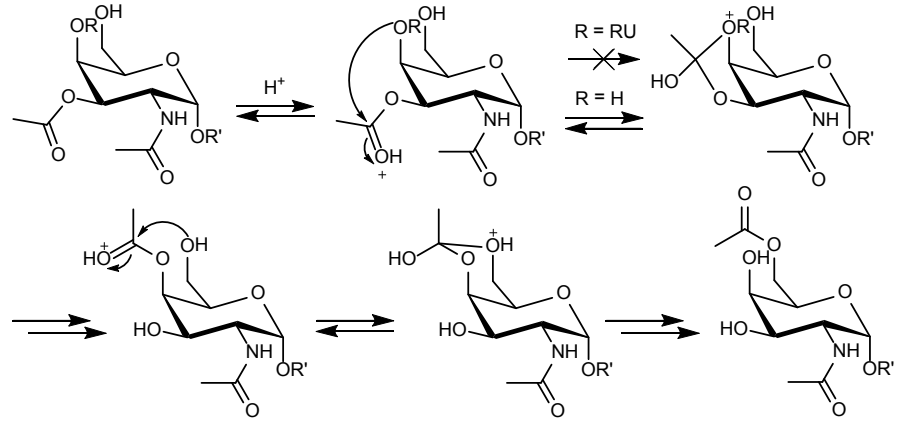

Figure 35. Mechanism of acid catalyzed *O*-acetyl migration to form 6-*O*-Ac-Gal*p*NAc from 3-*O*-Ac-Gal*p*NAc. A similar mechanism was proposed by Horrobin *et al.* (1998) for acetylated glucoses.

7 Hydroxy protons of hyaluronan oligosaccharides (Paper II)

7.1 Background

HA is one of the most studied polysaccharides, with many biomedical applications. It is the only glycosaminoglycan that lacks sulphation and it is a linear, unbranched chain of the repeating unit →4)-β-GlcA-(1→3)-β-GlcNAc-(1→, with all sugars in the D pyranoside configuration.

HA was first discovered in the vitreous humor of cattle eyes in 1934 (Meyer & Palmer, 1934), but the complete structure of the repeating unit was not discovered until 1954 with HA from human umbilical cord (Weissmann & Meyer, 1954). The extraction, purification and identification of HA from different natural sources has been the topic for many investigations (Lapčik *et al.*, 1998). HA occurs in the extracellular matrix of most mammalian tissues and is the dominant polysaccharide in vitreous humor, synovial fluid, umbilical cords and rooster combs. It has also been isolated from *Streptococcus* bacteria, which gives a cleaner preparation and is nowadays the main source of HA in pharmaceutical applications (Liu *et al.*, 2011).

HA is used in ophthalmologic surgery, injections in osteoarthritis patients, in wound healing, and in cosmetic applications. The use of HA is due to its remarkably high viscosity and water-retaining properties. Many attempts have been made to relate these properties to the conformation of HA, but often with contradictory results (Hargittai & Hargittai, 2008; Lapčik *et al.*, 1998).

Techniques such as X-ray diffraction, viscometry, electron microscopy, circular dichroism and NMR spectroscopy have been used to explore the secondary and tertiary structure of HA (Cowman & Matsuoka, 2005). NMR spectroscopy has been used to analyze aliphatic protons and carbons, amide and hydroxy protons of HA oligosaccharides to get information on hydrogen bonds, conformational restraints, and flexibility of the structure.

On the macroscopic level, the structure of HA was early described as a somewhat rigid, random coil (Laurent & Gergely, 1955). Scott *et al.* (1984) proposed a network of inter-residue hydrogen bonds, based on ^{1}H NMR of HA oligosaccharides in DMSO-d_6 solution, which could explain the stiffness of the structure. Four hydrogen bonds per disaccharide unit were predicted: one between the amide proton of GlcNAc and the neighboring carboxylate group of GlcA, two between ring oxygens and hydroxyl groups across the glycosidic linkages, and one between a hydroxyl group of GlcA and the carbonyl oxygen of the *N*-acetyl group of the adjacent GlcNAc.

DMSO is an aprotic solvent, which facilitates formation of intra-molecular hydrogen bonds in the dissolved molecules. In aqueous solution, however, intra-molecular hydrogen bonds are more easily disrupted by competition with hydrogen bonding with the solvent. Thus, it can be argued that the network of inter-residue hydrogen bonds in DMSO solution is an extreme case and that the situation in water is completely different. The amide protons of HA in aqueous solution have been thoroughly investigated by NMR spectroscopy (Blundell & Almond, 2007; Blundell *et al.*, 2006a; Cowman *et al.*, 1984), and the proposed hydrogen bond between the amide proton of GlcNAc and the carboxylate group of GlcA was found not to persist in aqueous solution.

Studies on the hydroxy protons of HA by NMR spectroscopy have been limited due to their rapid exchange with water. Siciňska *et al.* (1993) studied the hydroxy protons of the methyl glycoside of a HA disaccharide dissolved in water/acetone-d_6 (50:50) and found no evidence for long-lived intra-molecular hydrogen bonds. However, the finding of end effects caused by the terminal residues has increased the interest in studying longer HA oligomers (Blundell *et al.*, 2006b). Hexasaccharides or longer oligomers of HA have been proposed to mimic the true secondary structure of HA satisfactorily (Almond *et al.*, 2006).

In this project, the hydroxy protons of unsaturated di-, tetra-, hexa-, and octasaccharides of HA (referred to as ΔHA_2, ΔHA_4, ΔHA_6 and ΔHA_8; Figure 36) were studied in aqueous solution to gain insight into hydration, hydrogen bonds and flexibility of the HA secondary structure.

7.2 Experimental procedures

HA oligosaccharides were obtained from bacterial hyaluronan treated with hyaluronidase, which introduced an unsaturation in the non-reducing end of the oligosaccharides. The HA oligomers were separated by size-exclusion chromatography in ammonium acetate buffer and remaining ammonium ions were

removed with a strong cation exchange resin. Prior to NMR analysis, pH was adjusted to 6.6-6.8.

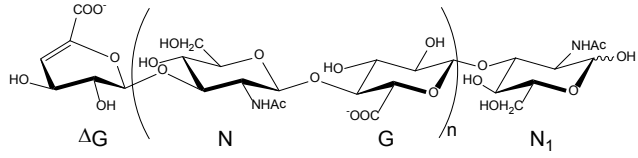

Figure 36. Chemical structure of ΔHA oligosaccharides: ΔHA_2 (n = 0), ΔHA_4 (n = 1), ΔHA_6 (n = 2), and ΔHA_8 (n = 3).

NMR experiments were performed on HA oligomers in D_2O and in H_2O/acetone-d_6 (85:15). $^1H,^1H$-TOCSY experiments were run at several different temperatures between -10 °C and 5 °C to obtain chemical shifts and temperature coefficients of the hydroxy protons. $^1H,^1H$-NOESY and ROESY experiments at several mixing times were run to obtain NOEs/ROEs and chemical exchange involving hydroxy protons. DOSY was used in an attempt to visualize the different rates of exchange of hydroxy protons. NMR experiments were also performed on the monosaccharides (GlcNAc and GlcA) to be able to calculate chemical shift differences (Δδ).

7.3 Results and discussion

The hydroxy protons of HA oligomers were visible after cation exchange and adjustment of pH (Figure 37). The rate of exchange was high, resulting in broad signals, and $^3J_{HCOH}$ could not be measured. Nor the rate of exchange could be determined, because of severe overlap of hydroxy protons. However, Δδ and dδ/dT could be measured, as well as NOEs and chemical exchange involving hydroxy protons.

To be able to mimic the HA polymer the interior parts of the oligomers were examined. The terminal residues were ruled out due to end effects and unsaturation at the non-reducing end. Hydroxy proton signals of G_{n-2} (GlcA, n = length of the oligomer) of ΔHA_4, ΔHA_6, and ΔHA_8, G_{n-4} of ΔHA_6 and ΔHA_8, and G_{n-6} of ΔHA_8 were chosen, as well as N_{n-3} (GlcNAc) of ΔHA_6 and ΔHA_8, and N_{n-5} of ΔHA_8, based on their similar chemical shifts. It should be mentioned that the signals from the interior residues of ΔHA_8 were overlapping.

The results for the interior residues of ΔHA_8 are summarized in Figure 38 and show upfield shifts of O(4)H (Δδ = -0.74 ppm), O(3')H (Δδ = -0.43 ppm), O(2')H (Δδ = -0.29 ppm), and NH (Δδ = -0.12 ppm), and a downfield shift of O(6)H (Δδ = 0.20 ppm). The |dδ/dT| were slightly lower than average for

O(4)H (10.2 ppb/°C) and O(3')H (11.0 ppb/°C), and higher for O(6)H (14.1 ppb/°C) and O(2')H (14.5 ppb/°C).

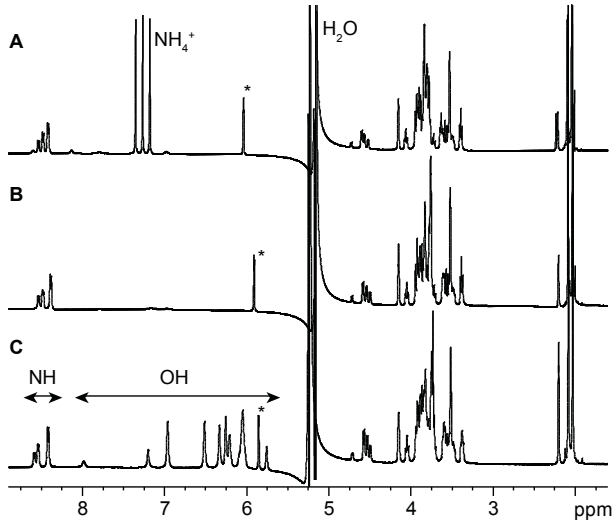

Figure 37. ^{1}H NMR spectra of ΔHA_4 in 85% H_2O/15% acetone-d_6 A) before cation exchange (-10 °C), B) after cation exchange (pH 4.5, -10 °C), and C) after cation exchange and adjustment of pH to 6.6 (-8 °C). The asterisks refer to the olefinic proton of non-reducing end ΔGlcA.

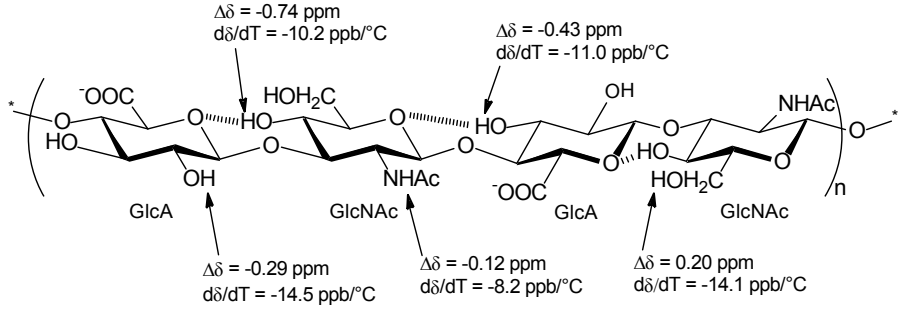

Figure 38. Δδ and dδ/dT for exchangeable protons of the interior residues of ΔHA_8. Hydrogen bonds discussed in the text are indicated. Protons from GlcA are denoted by prim in the text.

The upfield shifts and slightly decreased |dδ/dT| of O(4)H and O(3')H signals are consistent with reduced hydration due to inter-residue hydrogen bonding with the adjacent ring oxygens. The larger |Δδ| and the lower |dδ/dT| of O(4)H, compared to O(3')H, suggest that the hydration of this hydroxy proton is more reduced. In both cases, the relatively high |dδ/dT| indicates that these hydrogen bond interactions are weak. These two interactions, O(4)H-O(5') and O(3')H-O(5), have been predicted to occur in MD simulations incorporating explicit water molecules (Almond *et al.*, 2006; Almond & Sheehan, 2003; Almond *et*

al., 2000). This is the first experimental evidence of hydrogen bond interactions in aqueous solution of HA oligosaccharides.

The upfield shift of the O(2')H signal can be explained by the proximity to the neighboring *N*-acetyl group, thus leading to reduced hydration. NOEs between O(2')H and both the amide proton and the methyl group of the *N*-acetyl group confirmed such interaction. No strong hydrogen-bond interaction could be deduced, based on the high |dδ/dT|.

The downfield shift of the O(6)H signal suggests hydrogen bonding to another hydroxyl group. Indeed, a hydrogen bond between O(6)H and O(3')H over the β(1→4)-linkage has been proposed from MD simulations, but with short residence time (Almond *et al.*, 2000). The large |dδ/dT| and the absence of NOEs involving O(6)H indicate a relatively freely rotating hydroxymethyl group. Only a small Δδ of 0.07 ppm was observed for O(6)H in the reducing end of ΔHA_8, where no interaction with O(3')H occurs.

A number of inter-residue NOEs were observed over the β(1→3)-linkage, but not over the β(1→4)-linkage. This difference was due to spectral overlap of possible NOE signals over the β(1→4)-linkage. Several NOEs, which have not been observed before at room temperature, were observed at -5 °C (Figure 39).

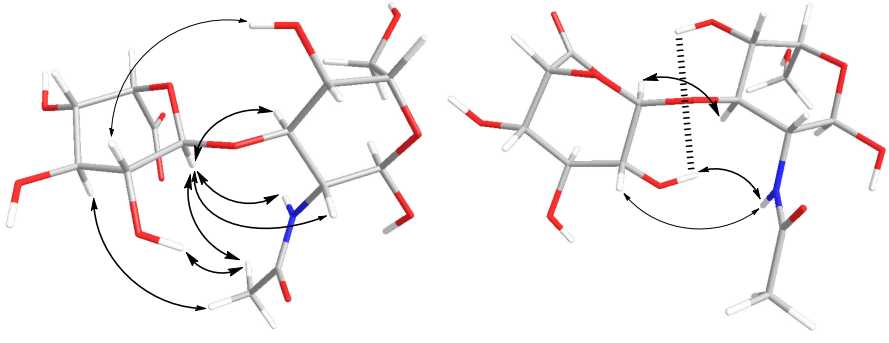

Figure 39. Inter-residue NOEs (arrows) and chemical exchange (dashed line) observed over the β(1→3)-linkage of ΔHA_8 at -5 °C. The glycosidic angles (φ, ψ) were set to (50.7°, 9.7°) for the major syn conformation (left) and (-30°, -25°) for a minor syn conformation (right). The angles were taken from Almond *et al.* (2006). The indicated NOEs and chemical exchange were visible at 50 ms mixing time and the arrow widths are adjusted according to the intensity of the cross-peaks.

The NOEs over the β(1→3)-linkage indicated the presence of additional conformations. C(1')H showed NOE with C(2)H, C(3)H, and the amide proton, which is in accordance to other NMR studies of HA oligomers (Almond *et al.*, 2006; Donati *et al.*, 2001; Holmbeck *et al.*, 1994). Also NOEs between the methyl group of GlcNAc and both C(1')H and O(2')H were observed, which were expected from a *syn* conformation. However, NOEs observed between

C(2')H and both O(4)H and the amide proton were not expected according to the global minimum conformation that has been calculated by MD simulations (Almond *et al.*, 2006).

Furthermore, a chemical exchange cross-peak was observed between O(4)H and O(2')H (Figure 40). The intensity of the cross-peak, which was observable already at a mixing time of 50 ms, was at a maximum at 100 ms mixing time and decreased considerably with longer mixing times. This appearance is inconsistent with spin diffusion, which would give an increasing intensity with longer mixing times.

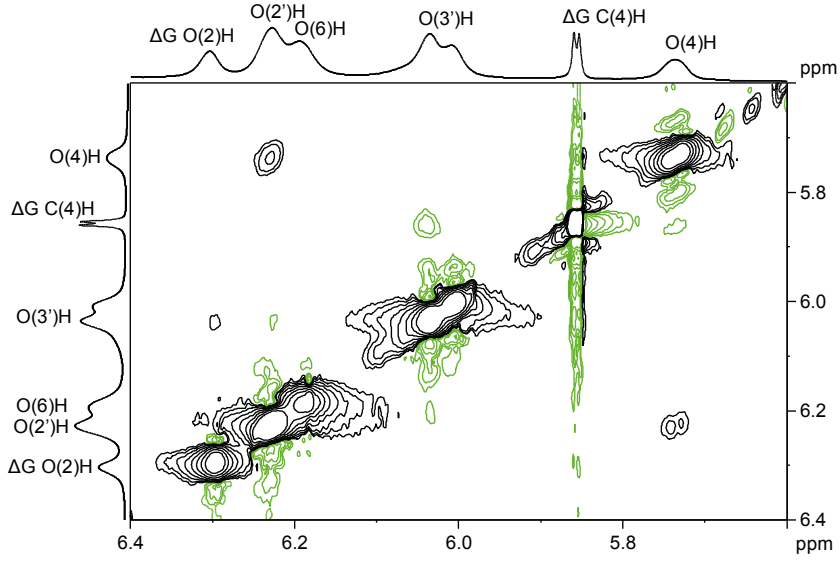

Figure 40. Selected region of a ROESY spectrum of ΔHA_6 obtained at -5 °C and 100 ms mixing time, illustrating cross peaks between O(4)H and O(2')H.

The interpretation of the chemical exchange between O(4)H and O(2')H is not straightforward, because these protons are situated on different sides of the glycosidic linkage and should not be close to each other in a normal *syn* conformation. The distance between the oxygens was measured to 5.4 Å in an average structure of a HA octasaccharide calculated by MD simulations and deposited in the Protein Data Bank (2BVK) by Almond *et al.* (2006). This is too long for a direct exchange. The exchange could rather be explained by: (i) water molecules bridging the two hydroxyl groups, (ii) a minor *syn* conformation, where the two hydroxyl groups are closer to each other, or (iii) an *anti* conformation.

In an attempt to monitor the rates of exchange of different hydroxy protons, DOSY experiments were run. It has previously been shown that DOSY can be

qualitatively used to study exchange phenomena (Cabrita & Berger, 2002). The diffusion coefficients of the hydroxy protons are averaged between the carbohydrate and water, with respect to their rate of exchange. A hydroxy proton with slow exchange appears closer to the non-exchangeable protons, whereas a hydroxy proton with faster exchange appears closer to the water signal. As illustrated in Figure 41 for GlcNAc, the diffusion time (Δ) can be adjusted to increase this dispersion in the diffusion dimension.

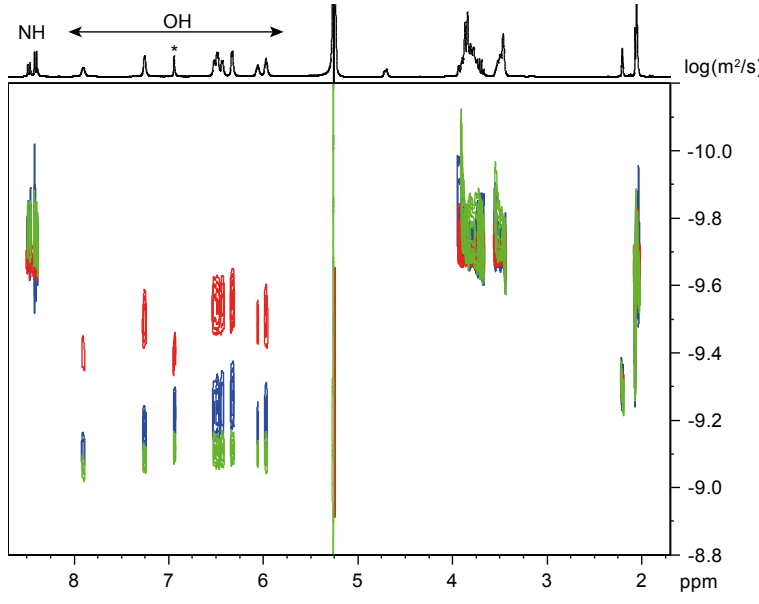

Figure 41. DOSY experiments of GlcNAc in H_2O/acetone-d_6 (85:15) at -10 °C. The diffusion time (Δ) was set to 50 ms (red), 200 ms (blue), and 500 ms (green). The asterisk refers to the hydrated form of acetone-d_6.

The DOSY experiment using WATERGATE suppression of the water signal suffered from phase distortions, which significantly affected the interpretation of the signals. HA oligomers larger than the disaccharide also had severe overlap in the ^{1}H dimension.

The high viscosity and water-retaining properties of HA can probably in part be explained by hydrogen bonding over the glycosidic linkages and water caging around the glycosidic linkages, but should also be dependent on the tertiary structure.

8 HR-MAS NMR of intact Arctic char muscle (Paper III)

8.1 Background

Marine lipid sources are unique compared to other lipid sources due to their content of polyunsaturated fatty acids (PUFA), such as EPA (eicosapentaenoic acid, 20:5 *n*-3) and DHA (docosahexaenoic acid, 22:6 *n*-3; Figure 42). These PUFA are reported to reduce arterial disease (Vanschoonbeek *et al.*, 2003), have a positive effect on the brain and nervous system, and to stimulate the immune system (Wahrburg, 2004; Connor, 2000). Thus, the nutritional value of the fish is linked to the amount of PUFA, and these compounds are present in relatively high levels in muscles of fatty fish like salmon and char.

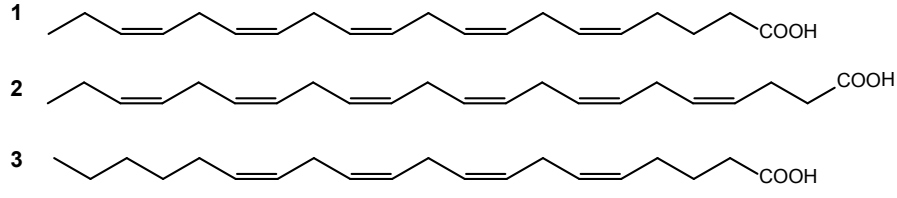

Figure 42. Chemical structures of **1**) EPA (20:5 *n*-3), **2**) DHA (22:6 *n*-3), and **3**) arachidonic acid (20:4 *n*-6).

Except the fatty acid content, there is increasing interest in the small metabolite pattern of fish to assess its quality. Free amino acids contribute to the flavor of the fish meat (Haard, 1992) and inosine monophosphate can be used as a marker of degradation processes (Howgate, 2006).

The FA composition of fish muscle is usually determined by GC analysis, but there are also methods developed to study FA profiles by NMR spectroscopy (Gribbestad *et al.*, 2005). The lipid ^{1}H NMR profile, which is obtained from lipid extracts of the fish muscle, contains information on different lipid

classes, the global unsaturation level, and PUFA. Information about the content of small hydrophilic metabolites can be obtained from aqueous extracts.

By the use of HR-MAS NMR spectroscopy on intact fish muscle, both lipids and small metabolites can be analyzed at the same time, without pre-treatment of the sample. ^{1}H HR-MAS NMR has previously been used on Atlantic salmon (*Salmo salar*) to obtain the *n*-3 FA content (Aursand *et al.*, 2006). EPA and DHA levels have previously been determined by ^{1}H NMR spectroscopy on fish oils (Guillén *et al.*, 2008; Tyl *et al.*, 2008).

The aim of this study was to develop a HR-MAS NMR method that can be used for quantification of *n*-3 FA, EPA and DHA on intact fish muscle, and at the same time give a profile of small metabolites. The method was applied on the relatively new aquaculture species Arctic char (*Salvelinus alpinus*), for which the NMR profiles of FA and small metabolites have not been previously investigated.

8.2 Experimental procedures

Tissue samples from Arctic char muscle (*ca.* 15 mg) were inserted into 4-mm zirconia rotors and 20 μL of D_2O was added. NOESY presaturation, BPP-LED and CPMG experiments were performed at 4 kHz spinning rate.

8.3 Results and discussion

NOESY presaturation and BPP-LED experiments (Figure 43) were used for quantification of *n*-3 FA, EPA and DHA, whereas CPMG experiments were used to monitor the small metabolite profile.

The signal of the terminal methyl group of *n*-3 FA (signal 2 in Figure 43) has a higher chemical shift than other FA, which is induced by the double bond on carbon 3 from the omega end. The relative amount of *n*-3 FA can be calculated by the formula (Sacchi *et al.*, 1993):

$$n\text{-}3\% = 100 \times \frac{S2}{S1 + S2}$$

where S1 is the methyl signal of other FA than *n*-3 FA.

Most individual FA are impossible to distinguish by ^{1}H NMR due to their equivalent chemical shifts. Fortunately, the two essential PUFA in fish, DHA and EPA, have typical signals, which can be used for quantification. The proton signals from the α- and β-carbon of DHA (S8) have different chemical shifts because of the double bond on the γ-carbon. These signals are more upfield shifted for other FA (S7 and S4). The amount of DHA can thus be calculated by the formula (Igarashi *et al.*, 2000):

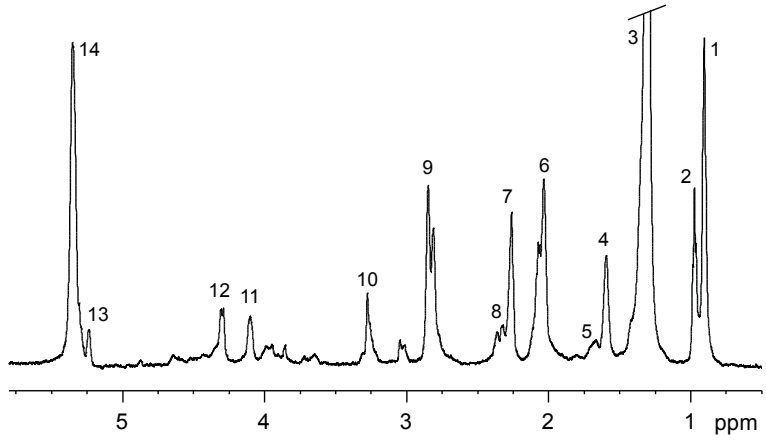

Figure 43. BPP-LED spectrum of Arctic char muscle showing the fatty acid profile: 1) CH_3 (except *n*-3), 2) *n*-3 CH_3, 3) CH_2, 4) β-CH_2, 5) β-CH_2 of EPA, 6) C*H*$_2$-CH=CH, 7) α-CH_2, 8) α- and β-CH_2 of DHA, 9) =CH-C*H*$_2$-CH=, 10) $N^+(CH_3)_3$ of phosphatidylcholine, 11) and 12) glyceryl CH_2, 13) glyceryl CH, and 14) CH=CH.

$$\mathrm{DHA\%} = 100 \times \frac{(\mathrm{S8})/2}{(\mathrm{S8})/2 + \mathrm{S7}}$$

EPA has a double bond on the δ-carbon, which induces a downfield shift of the signal from protons attached on the β-carbon (S5), compared to that of other FA (S4). The amount of EPA can be calculated by the formula (Guillén *et al.*, 2008; Tyl *et al.*, 2008):

$$\mathrm{EPA\%} = 100 \times \frac{\mathrm{S5}}{\mathrm{S4} + \mathrm{S5} + (\mathrm{S8})/2}$$

Also β-protons from arachidonic acid contribute to signal 5, as it contains the same structural element. However, the amount of arachidonic acid in fish is usually negligible, with the exception of tuna (Tyl *et al.*, 2008).

Triplicate samples from seven different fishes showed 25-31% *n*-3 FA, 10-17% DHA and 7-12% EPA, which were similar to the amounts determined by GC. The amounts calculated from NOESY presaturation and BPP-LED experiments did not differ significantly. As observed in previous studies (Tyl *et al.*, 2008; Aursand *et al.*, 2006; Igarashi *et al.*, 2000; Sacchi *et al.*, 1993), the *n*-3 FA content is higher when measured by GC, compared to NMR spectroscopy. This dissimilarity can be due to the different treatment of the samples, where the FA in the HR-MAS sample are still parts of triglycerides, phospholipids and sterols within the cell and the cell membrane. The composition of the FA methyl esters (FAME) that are analyzed by GC on the other hand, may be altered during the multiple-step procedure of lipid extraction, hydrolysis of lipids, and derivatization to yield FAME.

To observe the small metabolite profile, the CPMG pulse sequence was used to attenuate the contribution from macromolecules with short spin-spin relaxation times (Figure 44). The broad signals from lipids were not completely suppressed, suggesting that the muscle tissue contains a fraction of highly mobile lipids, *e. g.* in the form of non-esterified fatty acids (NEFA).

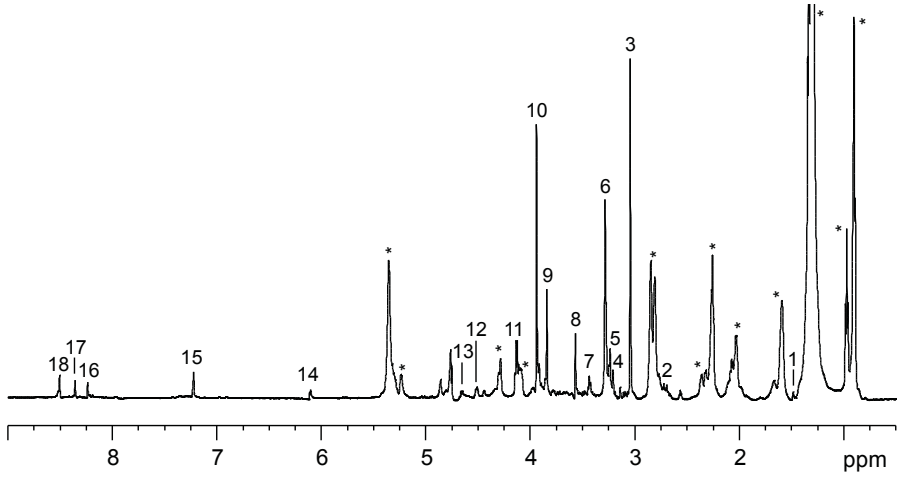

Figure 44. CPMG spectrum of Arctic char muscle showing the small metabolite profile. Asterisks refer to signals from lipids. The small metabolite signals were assigned as follows: 1) alanine, 2) anserine, 3) creatine/phosphocreatine, 4) anserine, 5) taurine, 6) choline, 7) taurine, 8) glycine, 9) anserine, 10) creatine/phosphocreatine, 11) lactate, 12) anserine, 13) β-glucose, 14) inosine, 15) anserine, 16) and 17) inosine, and 18) anserine.

Signals from lactate, anserine, choline, creatine/phosphocreatine, amino acids (alanine, glycine, taurine), glucose, acetate and inosine were identified, where creatine/phosphocreatine, anserine and taurine were the most abundant. The metabolite profile was similar to that of intact muscle of Atlantic salmon (*Salmo salar*), which has previously been investigated by ^{1}H NMR spectroscopy (Gribbestad *et al.*, 2005).

9 Metabonomic study on rat blood serum (Paper IV)

9.1 Background

Caloric restriction (CR) is regarded as healthy and life-extending in most cultures and religious fasting has been practiced for thousands of years. Increased lifespan through CR was first established in rats by McCay *et al.* (1935) and since then a considerable amount of research has been focused on the underlying mechanisms and the possible presence of similar effects in humans (Speakman & Mitchell, 2011; Spindler, 2010; Masoro, 2005).

The metabonomics approach has increased the possibilities to elucidate metabolic changes due to CR, and metabonomics with NMR spectroscopy has been used to evaluate acute CR in mice (Wijeyesekera *et al.*, 2012; Selman *et al.*, 2006) and long-term CR in non-human primates (Rezzi *et al.*, 2009).

The increase in lifespan is expected to be proportional to the level of CR (Merry, 2002), but Speakman and Mitchell (2011) pointed out that there should be a level where CR becomes negative.

The aim of this study was to investigate the metabolic effects of graded CR on rats, by a metabonomics approach with NMR spectroscopy.

9.2 Experimental procedures

Blood serum from 16-month old obese female rats (n = 15) was collected after 5 days of 0% (control), 20% and 40% CR. The serum was analyzed by CPMG and BPP-LED NMR experiments and data were treated by different multivariate methods (PCA and OPLS-DA) to extract information about metabolic changes as a response to CR.

9.3 Results and discussion

The NMR spectra of rat serum (Figure 45) showed clear differences between controls and 40% CR. The concentration of 3-hydroxybutyrate was increased, whereas the levels of VLDL and LDL were decreased after CR. BPP-LED spectra were used to distinguish lipoproteins and glycoproteins from other signals, but since these signals also appeared in the CPMG spectra, they were not further used.

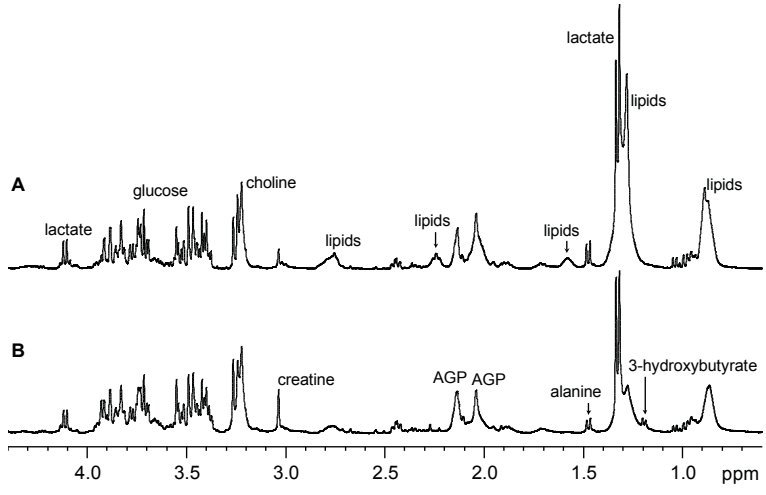

Figure 45. Representative CPMG ^{1}H NMR spectra of blood serum from obese rats after **A**) 0% CR (control) and **B**) 40% CR. AGP = "acute-phase" glycoproteins.

The spectral data were initially normalized by integral normalization before OPLS-DA, but an unexpected increase in glucose with CR showed that the approximation of unit total integral was not true. Probabilistic quotient normalization (Dieterle *et al.*, 2006) was used instead, which, after OPLS-DA, did not show any significant difference in glucose concentration (Figure 46).

Differences in chemical shifts between spectra were observed by phase distortions in the OPLS-DA loadings plot (Figure 46A). Peak alignment was obtained by the use of the icoshift algorithm (Savorani *et al.*, 2010), which changed the appearance of the alanine methyl signal (Figure 46 and 47) from being not significant to becoming significantly decreasing with CR.

The PCA score plot of the three groups (controls, 20% and 40% CR) showed a clear separation between controls and the CR groups, but no clear separation between 20% and 40% CR (Figure 48). This pattern was confirmed by OPLS-DA analysis, where pairwise comparisons of the three groups resulted in models with the best prediction power between controls and 40%

CR (Q^2Y = 0.84), followed by controls and 20% CR (Q^2Y = 0.76) and 20% and 40% CR (Q^2Y = 0.32).

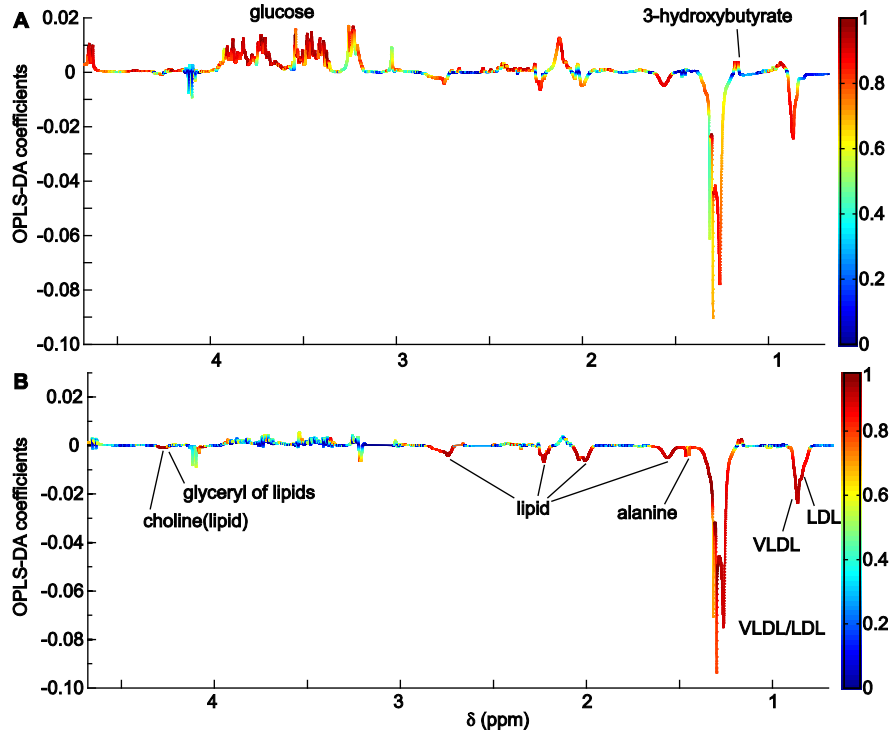

Figure 46. OPLS-DA cross-validated loadings of CPMG ^{1}H NMR spectra of blood serum from obese rats (0% and 40% CR) **A**) with integral normalization and no peak alignment and **B**) with probabilistic quotient normalization and peak alignment. The color-code of the loadings plot corresponds to unit variance model weights. Metabolites discriminating between 40% CR (positive) and 0% CR (negative) are highlighted. R^2X = 0.93 (**A**) and 0.88 (**B**), and Q^2Y = 0.35 (**A**) and 0.84 (**B**).

Discriminating metabolites from the OPLS-DA model of 40% CR, compared to controls, are highlighted in Figure 46B. After 40% CR an increase in 3-hydroxybutyrate signals and a decrease in alanine and lipid signals, including LDL, VLDL, glyceryl of lipids and lipid-bound choline, were observed. After 20% CR only signals from choline and glyceryl of lipids were decreased and creatine signals were increased.

The decrease in lipid signals reflects an increased β-oxidation and a decreased lipogenesis as a response to CR. The significant decrease in signals from phospholipid choline and glyceryl of lipids already at 20% CR is interesting. These compounds are degraded in the first step in the fatty acid

catabolism, when triacylglycerols and phospholipids are hydrolyzed into glycerol, NEFA and phosphocholine.

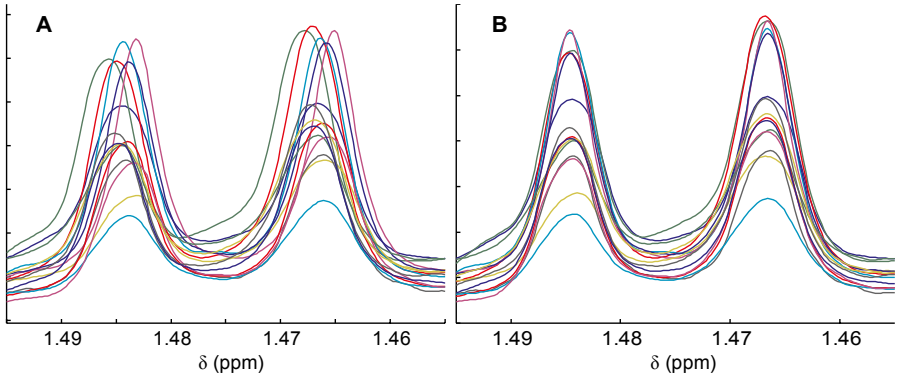

Figure 47. Expansion of the CPMG ^{1}H NMR spectra of blood serum from obese rats **A**) before peak alignment and **B**) after peak alignment, showing the methyl signal from alanine.

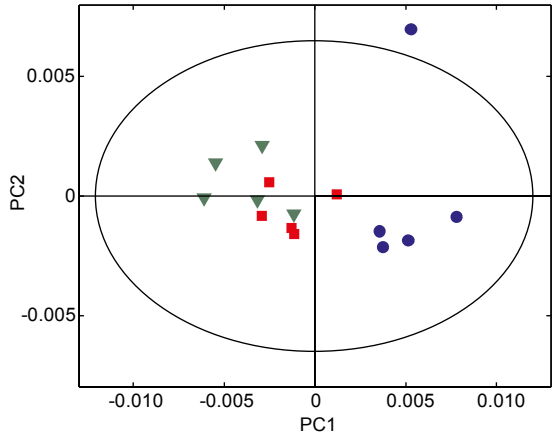

Figure 48. PCA score plot of PC1 vs. PC2 from obese rat blood serum after 0% CR (blue), 20% CR (red) and 40% CR (green). PC1 explained 72% and PC2 21% of the variance.

The increase in 3-hydroxybutyrate also reflects an increased β-oxidation and a limited access to glucose. The decrease in alanine can be associated with an increased hepatic gluconeogenesis.

The results are similar to a previous metabonomic CR study on mice (Selman *et al.*, 2006), except for the decrease in alanine. However, a CR study on overweight rats has shown a decrease in alanine concentration (Simón *et al.*, 2002) and a net hepatic uptake of alanine was also shown during prolonged fasting in humans (Felig *et al.*, 1969).

10 Conclusions and outlook

This thesis is a contribution to carbohydrate and metabonomic NMR spectroscopy. It is aimed to give a brief introduction to the NMR technique with special focus on carbohydrate and metabonomic applications. Conclusions of the four studies and ideas about further research are summarized here.

The structural analysis of the core oligosaccharide and the O-specific polysaccharide from the *P. shigelloides* O33 LPS was presented in paper I. The O-specific polysaccharide was built up of a tetrasaccharide RU, whereas the core oligosaccharide contained an undecasaccharide. At the linkage between the O-specific polysaccharide and the core oligosaccharide a 3-*O*-Ac-D-Gal*p*NAc residue was found. Further investigations of the minor glycoforms revealed a 30% replacement of GlcN to Glc in the core carbohydrate backbone. This diversity has not been observed before among core oligosaccharides, and motivates the search for it in other strains and species, as well as to investigate its origin in the biosynthesis of LPSs.

The first NMR spectroscopic investigation of hydroxy protons of HA oligosaccharides, up to octasaccharide, in aqueous solution was presented in paper II. It shows that weak hydrogen bonds exist between O(4)H of GlcNAc and O(5) of GlcA across the β(1→3) glycosidic linkage and between O(3)H of GlcA and O(5) of GlcNAc across the β(1→4) linkage. A chemical exchange was observed between O(4)H of GlcNAc and O(2)H of GlcA over the β(1→3) linkage. This investigation will continue in order to distinguish between intra- and inter-molecular hydrogen bonding and to find a molecular answer on the high viscosity and water-retaining ability of HA.

HR-MAS NMR spectroscopy of intact Arctic char muscle to obtain lipid and small metabolite profiles was presented in paper III. Quantitative analysis of *n*-3 FA, EPA and DHA was done, which gave similar results compared to GC analysis. By this technique the nutritional value of the fish could rapidly be obtained without any pretreatment.

The metabolic response to graded levels of short term CR in obese rats was investigated by NMR spectroscopy of blood serum and presented in paper IV. Multivariate analysis was used to determine a decrease in signals from lipids and alanine, and an increase in signals from creatine and 3-hydroxybutyrate, as a response to CR.

References

Aldova, E. & Shimada, T. (2000). New O and H antigens of the international antigenic scheme for *Plesiomonas shigelloides*. *Folia Microbiologica* 45(4), 301-304.

Almond, A., Brass, A. & Sheehan, J.K. (2000). Oligosaccharides as model systems for understanding water-biopolymer interaction: Hydrated dynamics of a hyaluronan decamer. *Journal of Physical Chemistry B* 104(23), 5634-5640.

Almond, A., DeAngelis, P.L. & Blundell, C.D. (2006). Hyaluronan: The local solution conformation determined by NMR and computer modeling is close to a contracted left-handed 4-fold helix. *Journal of Molecular Biology* 358(5), 1256-1269.

Almond, A. & Sheehan, J.K. (2003). Predicting the molecular shape of polysaccharides from dynamic interactions with water. *Glycobiology* 13(4), 255-264.

Aursand, M., Gribbestad, I.S. & Martinez, I. (2006). Omega-3 fatty acid content of intact Muscle of farmed Atlantic salmon (*Salmo salar*) examined by ^{1}H NMR spectroscopy. In: Webb, G.A. (Ed.) *Modern Magnetic Resonance: Part I: Applications in Chemistry, Biological and Marine Sciences*. 1st. ed. pp. 941-945 Springer Netherlands.

Auzanneau, F.I., Charon, D. & Szabó, L. (1991). Phosphorylated sugars. Part 27. Synthesis and reactions, in acid-medium, of 5-*O*-substituted methyl 3-deoxy-α-D-*manno*-oct-2-ulopyranosidonic acid 4-phosphates. *Journal of the Chemical Society-Perkin Transactions 1* (3), 509-517.

Batta, G. & Kövér, K.E. (1999). Heteronuclear coupling constants of hydroxyl protons in a water solution of oligosaccharides: trehalose and sucrose. *Carbohydrate Research* 320(3-4), 267-272.

Bax, A. & Davis, D.G. (1985a). MLEV-17-based two-dimensional homonuclear magnetization transfer spectroscopy. *Journal of Magnetic Resonance* 65(2), 355-360.

Bax, A. & Davis, D.G. (1985b). Practical aspects of two-dimensional transverse NOE spectroscopy. *Journal of Magnetic Resonance* 63(1), 207-213.

Bax, A., Sklenár, V. & Summers, M.F. (1986). Direct identification of relayed nuclear Overhauser effects. *Journal of Magnetic Resonance* 70(2), 327-331.

Beckonert, O., Coen, M., Keun, H.C., Wang, Y., Ebbels, T.M.D., Holmes, E., Lindon, J.C. & Nicholson, J.K. (2010). High-resolution magic-angle-spinning NMR spectroscopy for metabolic profiling of intact tissues. *Nature Protocols* 5(6), 1019-1032.

Beckonert, O., Keun, H.C., Ebbels, T.M.D., Bundy, J.G., Holmes, E., Lindon, J.C. & Nicholson, J.K. (2007). Metabolic profiling, metabolomic and metabonomic procedures for NMR spectroscopy of urine, plasma, serum and tissue extracts. *Nature Protocols* 2(11), 2692-2703.

Bekiroglu, S., Kenne, L. & Sandström, C. (2003). H-1 NMR studies of maltose, maltoheptaose, alpha-, beta-, and gamma-cyclodextrins, and complexes in aqueous solutions with hydroxy protons as structural probes. *Journal of Organic Chemistry* 68(5), 1671-1678.

Bekiroglu, S., Sandström, A., Kenne, L. & Sandström, C. (2004). Ab initio and NMR studies on the effect of hydration on the chemical shift of hydroxy protons in carbohydrates using disaccharides and water/methanol/ethers as model systems. *Organic & Biomolecular Chemistry* 2(2), 200-205.

Bernardi, A., Jiménez-Barbero, J., Casnati, A., De Castro, C., Darbre, T., Fieschi, F., Finne, J., Funken, H., Jaeger, K.E., Lahmann, M., Lindhorst, T.K., Marradi, M., Messner, P., Molinaro, A., Murphy, P.V., Nativi, C., Oscarson, S., Penades, S., Peri, F., Pieters, R.J., Renaudet, O., Reymond, J.L., Richichi, B., Rojo, J., Sansone, F., Schäffer, C., Turnbull, W.B., Velasco-Torrijos, T., Vidal, S., Vincent, S., Wennekes, T., Zuilhof, H. & Imberty, A. (2013). Multivalent glycoconjugates as anti-pathogenic agents. *Chemical Society Reviews* 42(11), 4709-4727.

Bernini, P., Bertini, I., Luchinat, C., Nincheri, P., Staderini, S. & Turano, P. (2011). Standard operating procedures for pre-analytical handling of blood and urine for metabolomic studies and biobanks. *Journal of Biomolecular Nmr* 49(3-4), 231-243.

Berzelius, J.J. (1806). *Föreläsningar i djurkemien*. Stockholm; 1).

Bloch, F., Hansen, W.W. & Packard, M. (1946). Nuclear induction. *Physical Review* 69(3-4), 127-127.

Blundell, C.D. & Almond, A. (2007). Temperature dependencies of amide ^{1}H- and ^{15}N-chemical shifts in hyaluronan oligosaccharides. *Magnetic Resonance in Chemistry* 45(5), 430-433.

Blundell, C.D., DeAngelis, P.L. & Almond, A. (2006a). Hyaluronan: the absence of amide-carboxylate hydrogen bonds and the chain conformation in aqueous solution are incompatible with stable secondary and tertiary structure models. *Biochem J* 396(3), 487-498.

Blundell, C.D., Reed, M.A.C. & Almond, A. (2006b). Complete assignment of hyaluronan oligosaccharides up to hexasaccharides. *Carbohydrate Research* 341(17), 2803-2815.

Brand, T., Cabrita, E.J. & Berger, S. (2005). Intermolecular interaction as investigated by NOE and diffusion studies. *Progress in Nuclear Magnetic Resonance Spectroscopy* 46(4), 159-196.

Bubb, W.A. (2003). NMR spectroscopy in the study of carbohydrates: Characterizing the structural complexity. *Concepts in Magnetic Resonance Part A* 19A(1), 1-19.

Bylesjö, M., Rantalainen, M., Cloarec, O., Nicholson, J.K., Holmes, E. & Trygg, J. (2006). OPLS discriminant analysis: combining the strengths of PLS-DA and SIMCA classification. *Journal of Chemometrics* 20(8-10), 341-351.

Cabrita, E.J. & Berger, S. (2002). HR-DOSY as a new tool for the study of chemical exchange phenomena. *Magnetic Resonance in Chemistry* 40, S122-S127.

Carlson, R.W., Reuhs, B., Chen, T.B., Bhat, U.R. & Noel, K.D. (1995). Lipopolysaccharide core structures in *Rhizobium etli* and mutants deficient in O-antigen. *Journal of Biological Chemistry* 270(20), 11783-11788.

Caroff, M., Karibian, D., Cavaillon, J.M. & Haeffner-Cavaillon, N. (2002). Structural and functional analyses of bacterial lipopolysaccharides. *Microbes and Infection* 4(9), 915-926.

Carr, H.Y. & Purcell, E.M. (1954). Effects of diffusion on free precession in nuclear magnetic resonance experiments. *Physical Review* 94(3), 630-638.

Ciucanu, I. & Kerek, F. (1984). A simple and rapid method for the permethylation of carbohydrates. *Carbohydrate Research* 131(2), 209-217.

Cloarec, O., Dumas, M.E., Trygg, J., Craig, A., Barton, R.H., Lindon, J.C., Nicholson, J.K. & Holmes, E. (2005). Evaluation of the orthogonal projection on latent structure model limitations caused by chemical shift variability and improved visualization of biomarker changes in H-1 NMR spectroscopic metabonomic studies. *Analytical Chemistry* 77(2), 517-526.

Connor, W.E. (2000). Importance of n-3 fatty acids in health and disease. *American Journal of Clinical Nutrition* 71(1), 171S-175S.

Cowman, M.K., Cozart, D., Nakanishi, K. & Balazs, E.A. (1984). ^{1}H NMR of glycosaminoglycans and hyaluronic acid oligosaccharides in aqueous solution: The amide proton environment. *Archives of Biochemistry and Biophysics* 230(1), 203-212.

Cowman, M.K. & Matsuoka, S. (2005). Experimental approaches to hyaluronan structure. *Carbohydrate Research* 340(5), 791-809.

Craig, A., Cloareo, O., Holmes, E., Nicholson, J.K. & Lindon, J.C. (2006). Scaling and normalization effects in NMR spectroscopic metabonomic data sets. *Analytical Chemistry* 78(7), 2262-2267.

Cui, S.W. (2005). Structural analysis of polysaccharides. In: *Food Carbohydrates* CRC Press. ISBN 978-0-8493-1574-9.

Czaja, J., Jachymek, W., Niedziela, T., Lugowski, C., Aldova, E. & Kenne, L. (2000). Structural studies of the O-specific polysaccharide from *Plesiomonas shigelloides* strain CNCTC 113/92. *European Journal of Biochemistry* 267(6), 1672-1679.

Dabrowski, J., Kožár, T., Grosskurth, H. & Nifant'ev, N.E. (1995). Conformational mobility of oligosaccharides: Experimental evidence for the existence of an "anti" conformer of the Galβ1-3Glcβ1-OMe disaccharide. *Journal of the American Chemical Society* 117(20), 5534-5539.

Dechow, F.J. (1989). *Separation and Purification Techniques in Biotechnology*: William Andrew Publishing/Noyes. ISBN 978-0-8155-1197-7.

Dieterle, F., Ross, A., Schlotterbeck, G. & Senn, H. (2006). Probabilistic quotient normalization as robust method to account for dilution of complex biological mixtures. Application in H-1 NMR metabonomics. *Analytical Chemistry* 78(13), 4281-4290.

Dirac, P.A.M. (1928). The quantum theory of the electron. *Proceedings of the Royal Society of London. Series A, Containing Papers of a Mathematical and Physical Character* 117(778), 610-624.

Dobson, C.M., Lian, L.Y., Redfield, C. & Topping, K.D. (1986). Measurement of hydrogen exchange rates using 2D NMR spectroscopy. *Journal of Magnetic Resonance* 69(2), 201-209.

Domon, B. & Costello, C.E. (1988). A systematic nomenclature for carbohydrate fragmentations in FAB-MS/MS spectra of glycoconjugates. *Glycoconjugate Journal* 5(4), 397-409.

Donati, A., Magnani, A., Bonechi, C., Barbucci, R. & Rossi, C. (2001). Solution structure of hyaluronic acid oligomers by experimental and theoretical NMR, and molecular dynamics simulation. *Biopolymers* 59(6), 434-445.

Duus, J.O., Gotfredsen, C.H. & Bock, K. (2000). Carbohydrate structural determination by NMR spectroscopy: Modern methods and limitations. *Chemical Reviews* 100(12), 4589-4614.

Emwas, A.H.M., Salek, R.M., Griffin, J.L. & Merzaban, J. (2013). NMR-based metabolomics in human disease diagnosis: applications, limitations, and recommendations. *Metabolomics* 9(5), 1048-1072.

Engelsen, S.B., Monteiro, C., de Penhoat, C.H. & Pérez, S. (2001). The diluted aqueous solvation of carbohydrates as inferred from molecular dynamics simulations and NMR spectroscopy. *Biophysical Chemistry* 93(2-3), 103-127.

Erridge, C., Bennett-Guerrero, E. & Poxton, I.R. (2002). Structure and function of lipopolysaccharides. *Microbes and Infection* 4(8), 837-851.

Exarchou, V., Troganis, A., Gerothanassis, I.P., Tsimidou, M. & Boskou, D. (2002). Do strong intramolecular hydrogen bonds persist in aqueous solution? Variable temperature gradient H-1, H-1-C-13 GE-HSQC and GE-HMBC NMR studies of flavonols and flavones in organic and aqueous mixtures. *Tetrahedron* 58(37), 7423-7429.

Fan, W.M.T. (1996). Metabolite profiling by one- and two-dimensional NMR analysis of complex mixtures. *Progress in Nuclear Magnetic Resonance Spectroscopy* 28, 161-219.

Felig, P., Owen, O.E., Wahren, J. & Cahill, G.F. (1969). Amino acid metabolism during prolonged starvation. *Journal of Clinical Investigation* 48(3), 584-594.

Ferro, D.R., Provasoli, A., Ragazzi, M., Torri, G., Casu, B., Gatti, G., Jacquinet, J.C., Sinaÿ, P., Petitou, M. & Choay, J. (1986). Evidence for conformational equilibrium of the sulfated L-iduronate residue in heparin and in synthetic heparin monosaccharides and oligosaccharides - NMR and force-field studies. *Journal of the American Chemical Society* 108(21), 6773-6778.

Fiehn, O. (2002). Metabolomics - the link between genotypes and phenotypes. *Plant Molecular Biology* 48(1-2), 155-171.

Fonville, J.M., Richards, S.E., Barton, R.H., Boulange, C.L., Ebbels, T.M.D., Nicholson, J.K., Holmes, E. & Dumas, M.-E. (2010). The evolution of partial least squares models and related chemometric approaches in metabonomics and metabolic phenotyping. *Journal of Chemometrics* 24(11-12), 636-649.

Freeman, R. (1988). *A handbook of nuclear magnetic resonance*. Harlow: Longman Scientific & Technical. ISBN 0-582-00574-4.

Freeman, R. (1997). *Spin choreography: basic steps in high resolution NMR*. Oxford: Spektrum. ISBN 0-935702-95-4.

Gardner, S.E., Fowlston, S.E. & George, W.L. (1987). *In vitro* production of cholera-toxin like activity by *Plesiomonas shigelloides*. *Journal of Infectious Diseases* 156(5), 720-722.

Gerwig, G.J., Kamerling, J.P. & Vliegenthart, J.F.G. (1978). Determination of the D and L configuration of neutral monosaccharides by high-resolution capillary G.L.C. *Carbohydrate Research* 62(2), 349-357.

Gheysen, K., Mihai, C., Conrath, K. & Martins, J.C. (2008). Rapid identification of common hexapyranose monosaccharide units by a simple TOCSY matching approach. *Chemistry - A European Journal* 14(29), 8869-8878.

Gibbs, S.J. & Johnson, C.S. (1991). A PFG NMR experiment for accurate diffusion and flow studies in the presence of eddy currents. *Journal of Magnetic Resonance* 93(2), 395-402.

González-Rey, C., Svenson, S.B., Bravo, L., Siitonen, A., Pasquale, V., Dumontet, S., Ciznar, I. & Krovacek, K. (2004). Serotypes and anti-microbial susceptibility of *Plesiomonas shigelloides* isolates from humans, animals and aquatic environments in different countries. *Comparative Immunology Microbiology and Infectious Diseases* 27(2), 129-139.

Gribbestad, I.S., Aursand, M. & Martinez, I. (2005). High-resolution ^{1}H magnetic resonance spectroscopy of whole fish, fillets and extracts of farmed Atlantic salmon (*Salmo salar*) for quality assessment and compositional analyses. *Aquaculture* 250(1-2), 445-457.

Guillén, M.D., Carton, I., Goicoechea, E. & Uriarte, P.S. (2008). Characterization of cod liver oil by spectroscopic techniques. New approaches for the determination of compositional parameters, acyl groups, and cholesterol from H-1 nuclear magnetic resonance and Fourier transform infrared spectral data. *Journal of Agricultural and Food Chemistry* 56(19), 9072-9079.

Haard, N.F. (1992). Control of chemical-composition and food quality attributes of cultured fish. *Food Research International* 25(4), 289-307.
Hahn, E.L. (1950). Spin echoes. *Physical Review* 80(4), 580-594.
Hakomori, S.I. (1964). A rapid permethylation of glycolipid, and polysaccharide catalyzed by methylsulfinyl carbanion in dimethyl sulfoxide. *Journal of Biochemistry* 55(2), 205-208.
Hargittai, I. & Hargittai, M. (2008). Molecular structure of hyaluronan: an introduction. *Structural Chemistry* 19(5), 697-717.
Harris, R., Rutherford, T.J., Milton, M.J. & Homans, S.W. (1997). Three-dimensional heteronuclear NMR techniques for assignment and conformational analysis using exchangeable protons in uniformly C-13-enriched oligosaccharides. *Journal of Biomolecular Nmr* 9(1), 47-54.
Harris, R.K., Becker, E.D., De Menezes, S.M.C., Goodfellow, R. & Granger, P. (2001). NMR nomenclature. Nuclear spin properties and conventions for chemical shifts - (IUPAC recommendations 2001). *Pure and Applied Chemistry* 73(11), 1795-1818.
Hawley, J., Bampos, N., Aboitiz, N., Jimenez-Barbero, J., de la Paz, M.L., Sanders, J.K.M., Carmona, P. & Vicent, C. (2002). Investigation of the hydrogen bonding properties of a series of monosaccharides in aqueous media by H-1 NMR and IR spectroscopy. *European Journal of Organic Chemistry* (12), 1925-1936.
Hennel, J. & Klinowski, J. (2005). Magic-angle spinning: a historical perspective. In: Klinowski, J. (Ed.) *New Techniques in Solid-State NMR*. pp. 1-14 Springer Berlin Heidelberg. (Topics in Current Chemistry; 246). ISBN 978-3-540-22168-5.
Holmbeck, S.M.A., Petillo, P.A. & Lerner, L.E. (1994). The solution conformation of hyaluronan: A combined NMR and molecular dynamics study. *Biochemistry* 33(47), 14246-14255.
Holst, O. (2007). The structures of core regions from enterobacterial lipopolysaccharides - an update. *Fems Microbiology Letters* 271(1), 3-11.
Horrobin, T., Tran, C.H. & Crout, D. (1998). Esterase-catalysed regioselective 6-deacylation of hexopyranose per-acetates, acid-catalysed rearrangement to the 4-deprotected products and conversions of these into hexose 4- and 6-sulfates. *Journal of the Chemical Society-Perkin Transactions 1* (6), 1069-1080.
Howgate, P. (2006). A review of the kinetics of degradation of inosine monophosphate in some species of fish during chilled storage. *International Journal of Food Science and Technology* 41(4), 341-353.
Hwang, T.L. & Shaka, A.J. (1995). Water suppression that works. Excitation sculpting using arbitrary wave forms and pulsed field gradients. *Journal of Magnetic Resonance Series A* 112(2), 275-279.
Igarashi, T., Aursand, M., Hirata, Y., Gribbestad, I.S., Wada, S. & Nonaka, M. (2000). Nondestructive quantitative determination of docosahexaenoic acid and n-3 fatty acids in fish oils by high-resolution H-1 nuclear

magnetic resonance spectroscopy. *Journal of the American Oil Chemists Society* 77(7), 737-748.
Ivarsson, I., Sandström, C., Sandström, A. & Kenne, L. (2000). H-1 NMR chemical shifts of hydroxy protons in conformational analysis of disaccharides in aqueous solution. *Journal of the Chemical Society-Perkin Transactions 2* (10), 2147-2152.
Janda, J.M. & Abbott, S.L. (1993). Expression of hemolytic activity by *Plesiomonas shigelloides*. *Journal of Clinical Microbiology* 31(5), 1206-1208.
Jansson, P.-E., Kenne, L. & Widmalm, G. (1987). Casper—a computerised approach to structure determination of polysaccharides using information from n.m.r. spectroscopy and simple chemical analyses. *Carbohydrate Research* 168(1), 67-77.
Jin, L., Hricovini, M., Deakin, J.A., Lyon, M. & Uhrin, D. (2009). Residual dipolar coupling investigation of a heparin tetrasaccharide confirms the limited effect of flexibility of the iduronic acid on the molecular shape of heparin. *Glycobiology* 19(11), 1185-1196.
Johnson, C.S. (1999). Diffusion ordered nuclear magnetic resonance spectroscopy: principles and applications. *Progress in Nuclear Magnetic Resonance Spectroscopy* 34(3-4), 203-256.
Kamerling, J.P. (2007). 1.01 - Basics concepts and nomenclature recommendations in carbohydrate chemistry. In: Kamerling, H. (Ed.) *Comprehensive Glycoscience*. pp. 1-38. Oxford: Elsevier. ISBN 978-0-444-51967-2.
Kaszowska, M., Jachymek, W., Lukasiewicz, J., Niedziela, T., Kenne, L. & Lugowski, C. (2013a). The unique structure of complete lipopolysaccharide isolated from semi-rough *Plesiomonas shigelloides* O37 (strain CNCTC 39/89) containing (2S)-O-(4-oxopentanoic acid)-α-D-Glcp (α-D-Lenose). *Carbohydrate Research* 378, 98-107.
Kaszowska, M., Jachymek, W., Niedziela, T., Koj, S., Kenne, L. & Lugowski, C. (2013b). The novel structure of the core oligosaccharide backbone of the lipopolysaccharide from the *Plesiomonas shigelloides* strain CNCTC 80/89 (serotype O13). *Carbohydrate Research* 380, 45-50.
Knirel, Y.A., Moll, H. & Zähringer, U. (1996). Structural study of a highly *O*-acetylated core of *Legionella pneumophila* serogroup 1 lipopolysaccharide. *Carbohydrate Research* 293(2), 223-234.
Kontogianni, V.G., Charisiadis, P., Primikyri, A., Pappas, C.G., Exarchou, V., Tzakos, A.G. & Gerothanassis, I.P. (2013). Hydrogen bonding probes of phenol -OH groups. *Organic & Biomolecular Chemistry* 11(6), 1013-1025.
Kubler-Kielb, J., Schneerson, R., Mocca, C. & Vinogradov, E. (2008). The elucidation of the structure of the core part of the LPS from *Plesiomonas shigelloides* serotype O17 expressing O-polysaccharide chain identical to the *Shigella sonnei* O-chain. *Carbohydrate Research* 343(18), 3123-3127.
Landersjö, C., Stenutz, R. & Widmalm, G. (1997). Conformational flexibility of carbohydrates: A folded conformer at the phi dihedral angle of a

glycosidic linkage. *Journal of the American Chemical Society* 119(37), 8695-8698.

Lapčik, L.J., Lapčik, L., De Smedt, S., Demeester, J. & Chabreček, P. (1998). Hyaluronan: Preparation, structure, properties, and applications. *Chemical Reviews* 98(8), 2663-2684.

Larsson, E.A., Staaf, M., Soderman, P., Hoog, C. & Widmalm, G. (2004). Determination of the conformational flexibility of methyl alpha-cellobioside in solution by NMR spectroscopy and molecular simulations. *Journal of Physical Chemistry A* 108(18), 3932-3937.

Laurent, T.C. & Gergely, J. (1955). Light scattering studies on hyaluronic acid. *Journal of Biological Chemistry* 212(1), 325-333.

Leeflang, B.R., Vliegenthart, J.F.G., Kroon-Batenburg, L.M.J., Eijck, B.P.v. & Kroon, J. (1992). A H-1-NMR and MD study of intramolecular hydrogen bonds in methyl β-cellobioside. *Carbohydrate Research* 230(1), 41-61.

Levin, R.E. (2008). *Plesiomonas shigelloides* - An aquatic food borne pathogen: A review of its characteristics, pathogenicity, ecology, and molecular detection. *Food Biotechnology* 22(1-2), 189-202.

Li, L., Ly, M. & Linhardt, R.J. (2012). Proteoglycan sequence. *Molecular BioSystems* 8(6), 1613-1625.

Li, W. (2006). Multidimensional HRMAS NMR: a platform for in vivo studies using intact bacterial cells. *Analyst* 131(7), 777-781.

Lin, J. & Frey, P.A. (2000). Strong hydrogen bonds in aqueous and aqueous-acetone solutions of dicarboxylic acids: Activation energies for exchange and deuterium fractionation factors. *Journal of the American Chemical Society* 122(45), 11258-11259.

Lindon, J.C., Beckonert, O.P., Holmes, E. & Nicholson, J.K. (2009). High-resolution magic angle spinning NMR spectroscopy: Application to biomedical studies. *Progress in Nuclear Magnetic Resonance Spectroscopy* 55(2), 79-100.

Lindon, J.C., Holmes, E. & Nicholson, J.K. (2001). Pattern recognition methods and applications in biomedical magnetic resonance. *Progress in Nuclear Magnetic Resonance Spectroscopy* 39(1), 1-40.

Lindon, J.C., Holmes, E. & Nicholson, J.K. (2004). Toxicological applications of magnetic resonance. *Progress in Nuclear Magnetic Resonance Spectroscopy* 45(1-2), 109-143.

Lindon, J.C., Holmes, E. & Nicholson, J.K. (2007). Metabonomics in pharmaceutical R & D. *Febs Journal* 274(5), 1140-1151.

Linnerborg, M., Widmalm, G., Weintraub, A. & Albert, M.J. (1995). Structural elucidation of the O-antigen lipopolysaccharide from two strains of *Plesiomonas shigelloides* that share a type-specific antigen with *Shigella flexneri* 6, and the common group 1 antigen with *Shigella flexneri* spp and *Shigella dysenteriae* 1. *European Journal of Biochemistry* 231(3), 839-844.

Lipkind, G.M., Shashkov, A.S. & Kochetkov, N.K. (1985). Nuclear Overhauser effect and conformational states of cellobiose in aqueous solution. *Carbohydrate Research* 141(2), 191-197.

Liu, L., Liu, Y., Li, J., Du, G. & Chen, J. (2011). Microbial production of hyaluronic acid: current state, challenges, and perspectives. *Microbial Cell Factories* 10.

Lukasiewicz, J., Dzieciatkowska, M., Niedziela, T., Jachymek, W., Augustyniuk, A., Kenne, L. & Lugowski, C. (2006a). Complete lipopolysaccharide of *Plesiomonas shigelloides* O74:H5 (strain CNCTC 144/92). 2. Lipid A, its structural variability, the linkage to the core oligosaccharide, and the biological activity of the lipopolysaccharide. *Biochemistry* 45(35), 10434-10447.

Lukasiewicz, J., Niedziela, T., Jachymek, W., Kenne, L. & Lugowski, C. (2006b). Structure of the lipid A-inner core region and biological activity of *Plesiomonas shigelloides* O54 (strain CNCTC 113/92) lipopolysaccharide. *Glycobiology* 16(6), 538-550.

Lundborg, M. & Widmalm, G. (2011). Structural analysis of glycans by NMR chemical shift prediction. *Analytical Chemistry* 83(5), 1514-1517.

Lönngren, J. & Svensson, S. (1974). Mass spectrometry in structural analysis of natural carbohydrates. In: Tipson, R.S.*, et al.* (Eds.) *Advances in Carbohydrate Chemistry and Biochemistry*. pp. 41-106 Academic Press; Volume 29). ISBN 0065-2318.

Maciejewska, A., Lukasiewicz, J., Kaszowska, M., Man-Kupisinska, A., Jachymek, W. & Lugowski, C. (2013). Core oligosaccharide of *Plesiomonas shigelloides* PCM 2231 (serotype O17) lipopolysaccharide - structural and serological analysis. *Marine Drugs* 11(2), 440-454.

Maciejewska, A., Lukasiewicz, J., Niedziela, T., Szewczuk, Z. & Lugowski, C. (2009). Structural analysis of the O-specific polysaccharide isolated from *Plesiomonas shigelloides* O51 lipopolysaccharide. *Carbohydrate Research* 344(7), 894-900.

Masoro, E.J. (2005). Overview of caloric restriction and ageing. *Mechanisms of Ageing and Development* 126(9), 913-922.

Masoud, H., Perry, M.B., Brisson, J.R., Uhrin, D. & Richards, J.C. (1994). Structural elucidation of the backbone oligosaccharide from the lipopolysaccharide of *Moraxella catarrhalis* serotype A. *Canadian Journal of Chemistry-Revue Canadienne De Chimie* 72(6), 1466-1477.

McCay, C.M., Crowell, M.F. & Maynard, L.A. (1935). The effect of retarded growth upon the length of life span and upon the ultimate body size. *Journal of Nutrition* 10, 63-79.

Meiboom, S. & Gill, D. (1958). Modified spin-echo method for measuring nuclear relaxation times. *Review of Scientific Instruments* 29(8), 688-691.

Merry, B.J. (2002). Molecular mechanisms linking calorie restriction and longevity. *International Journal of Biochemistry & Cell Biology* 34(11), 1340-1354.

Meyer, K. & Palmer, J.W. (1934). The polysaccharide of the vitreous humor. *Journal of Biological Chemistry* 107, 629-634.

Nazarenko, E.L., Crawford, R.J. & Ivanova, E.P. (2011). The structural diversity of carbohydrate antigens of selected Gram-negative marine bacteria. *Marine Drugs* 9(10), 1914-1954.

Neuhaus, D., Ismail, I.M. & Chung, C.W. (1996). "FLIPSY" - A new solvent-suppression sequence for nonexchanging solutes offering improved integral accuracy relative to 1D NOESY. *Journal of Magnetic Resonance Series A* 118(2), 256-263.

Nicholson, J.K., Foxall, P.J.D., Spraul, M., Farrant, R.D. & Lindon, J.C. (1995). 750 MHz ^{1}H and ^{1}H-^{13}C NMR spectroscopy of human blood plasma. *Analytical Chemistry* 67(5), 793-811.

Nicholson, J.K., Holmes, E., Kinross, J.M., Darzi, A.W., Takats, Z. & Lindon, J.C. (2012). Metabolic phenotyping in clinical and surgical environments. *Nature* 491(7424), 384-392.

Nicholson, J.K., Lindon, J.C. & Holmes, E. (1999). 'Metabonomics': understanding the metabolic responses of living systems to pathophysiological stimuli via multivariate statistical analysis of biological NMR spectroscopic data. *Xenobiotica* 29(11), 1181-1189.

Niedziela, T., Dag, S., Lukasiewicz, J., Dzieciatkowska, M., Jachymek, W., Lugowski, C. & Kenne, L. (2006). Complete lipopolysaccharide of *Plesiomonas shigelloides* O74:H5 (strain CNCTC 144/92). 1. Structural analysis of the highly hydrophobic lipopolysaccharide, including the O-antigen, its biological repeating unit, the core oligosaccharide, and the linkage between them. *Biochemistry* 45(35), 10422-10433.

Niedziela, T., Lukasiewicz, J., Jachymek, W., Dzieciatkowska, M., Lugowski, C. & Kenne, L. (2002). Core oligosaccharides of *Plesiomonas shigelloides* O54:H2 (strain CNCTC 113/92) - Structural and serological analysis of the lipopolysaccharide core region, the *O*-antigen biological repeating unit, and the linkage between them. *Journal of Biological Chemistry* 277(14), 11653-11663.

Novoa-Carballal, R., Fernandez-Megia, E., Jiménez, C. & Riguera, R. (2011). NMR methods for unravelling the spectra of complex mixtures. *Natural Product Reports* 28(1), 78-98.

Okawa, Y., Ohtomo, Y., Tsugawa, H., Matsuda, Y., Kobayashi, H. & Tsukamoto, T. (2004). Isolation and characterization of a cytotoxin produced by *Plesiomonas shigelloides* P-1 strain. *Fems Microbiology Letters* 239(1), 125-130.

Pauling, L. & Corey, R.B. (1951). Configurations of polypeptide chains with favored orientations around single bonds - two new pleated sheets. *Proceedings of the National Academy of Sciences of the United States of America* 37(11), 729-740.

Pauling, L., Corey, R.B. & Branson, H.R. (1951). The structure of proteins - two hydrogen-bonded helical configurations of the polypetide chain.

Proceedings of the National Academy of Sciences of the United States of America 37(4), 205-211.

Pieretti, G., Carillo, S., Lindner, B., Lanzetta, R., Parrilli, M., Jimenez, N., Regué, M., Tomás, J.M. & Corsaro, M.M. (2010). The complete structure of the core of the LPS from *Plesiomonas shigelloides* 302-73 and the identification of its O-antigen biological repeating unit. *Carbohydrate Research* 345(17), 2523-2528.

Pieretti, G., Corsaro, M.M., Lanzetta, R., Parrilli, M., Canals, R., Merino, S. & Tomás, J.M. (2008). Structural studies of the O-chain polysaccharide from Plesiomonas shigelloides strain 302-73 (serotype O1). *European Journal of Organic Chemistry* (18), 3149-3155.

Pieretti, G., Corsaro, M.M., Lanzetta, R., Parrilli, M., Vilches, S., Merino, S. & Tomás, J.M. (2009). Structure of the core region from the lipopolysaccharide of *Plesiomonas shigelloides* strain 302-73 (serotype O1). *European Journal of Organic Chemistry* (9), 1365-1371.

Piotto, M., Saudek, V. & Sklenář, V. (1992). Gradient-tailored excitation for single-quantum NMR spectroscopy of aqueous solutions. *Journal of Biomolecular Nmr* 2(6), 661-665.

Poppe, L. & Halbeek, H.v. (1991). Nuclear magnetic resonance of hydroxyl and amido protons of oligosaccharides in aqueous solution: Evidence for a strong intramolecular hydrogen bond in sialic acid residues. *Journal of the American Chemical Society* 113(1), 363-365.

Poppe, L. & Halbeek, H.v. (1994). NMR spectroscopy of hydroxyl protons in supercooled carbohydrates. *Nat Struct Mol Biol* 1(4), 215-216.

Purcell, E.M., Torrey, H.C. & Pound, R.V. (1946). Resonance absorption by nuclear magnetic moments in a solid. *Physical Review* 69(1-2), 37-38.

Raetz, C.R.H. & Whitfield, C. (2002). Lipopolysaccharide endotoxins. *Annual Review of Biochemistry* 71, 635-700.

Rezzi, S., Martin, F.-P.J., Shanmuganayagam, D., Colman, R.J., Nicholson, J.K. & Weindruch, R. (2009). Metabolic shifts due to long-term caloric restriction revealed in nonhuman primates. *Experimental Gerontology* 44(5), 356-362.

Rezzi, S., Ramadan, Z., Fay, L.B. & Kochhar, S. (2007). Nutritional metabonomics: Applications and perspectives. *Journal of Proteome Research* 6(2), 513-525.

Roslund, M.U., Aitio, O., Wärnå, J., Maaheimo, H., Murzin, D.Y. & Leino, R. (2008). Acyl group migration and cleavage in selectively protected β-D-galactopyranosides as studied by NMR spectroscopy and kinetic calculations. *Journal of the American Chemical Society* 130(27), 8769-8772.

Roslund, M.U., Säwén, E., Landström, J., Rönnols, J., Jonsson, K.H.M., Lundborg, M., Svensson, M.V. & Widmalm, G. (2011). Complete ^{1}H and ^{13}C NMR chemical shift assignments of mono-, di-, and trisaccharides as basis for NMR chemical shift predictions of polysaccharides using the computer program CASPER. *Carbohydrate Research* 346(11), 1311-1319.

Sacchi, R., Medina, I., Aubourg, S.P., Addeo, F. & Paolillo, L. (1993). Proton nuclear magnetic resonance rapid and structure specific determination of omega-3 polyunsaturated fatty acids in fish lipids. *Journal of the American Oil Chemists Society* 70(3), 225-228.

Sandström, C., Baumann, H. & Kenne, L. (1998a). NMR spectroscopy of hydroxy protons of 3,4-disubstituted methyl alpha-D-galactopyranosides in aqueous solution. *Journal of the Chemical Society-Perkin Transactions 2* (4), 809-815.

Sandström, C., Baumann, H. & Kenne, L. (1998b). The use of chemical shifts of hydroxy protons of oligosaccharides as conformational probes for NMR studies in aqueous solution. Evidence for persistent hydrogen bond interaction in branched trisaccharides. *Journal of the Chemical Society-Perkin Transactions 2* (11), 2385-2393.

Sandström, C. & Kenne, L. (2006). Hydroxy Protons in Structural Studies of Carbohydrates by NMR Spectroscopy. In: *NMR Spectroscopy and Computer Modeling of Carbohydrates*. pp. 114-132 American Chemical Society. (ACS Symposium Series; 930). ISBN 0-8412-3953-3.

Sattelle, B.M. & Almond, A. (2011). Is *N*-acetyl-D-glucosamine a rigid $^{4}C_{1}$ chair? *Glycobiology* 21(12), 1651-1662.

Sawardeker, J.S., Sloneker, J.H. & Jeanes, A. (1965). Quantitative determination of monosaccharides as their alditol acetates by gas liquid chromatography. *Analytical Chemistry* 37(12), 1602-1604.

Savorani, F., Tomasi, G. & Engelsen, S.B. (2010). icoshift: A versatile tool for the rapid alignment of 1D NMR spectra. *Journal of Magnetic Resonance* 202(2), 190-202.

Schwarzmann, G.O.H. & Jeanloz, R.W. (1974). Separation by gas-liquid chromatography, and identification by mass spectrometry, of methyl ethers of 2-deoxy-2-(*N*-methylacetamido)-D-glucose. *Carbohydrate Research* 34(1), 161-168.

Scott, J.E., Heatley, F. & Hull, W.E. (1984). Secondary structure of hyaluronate in solution. A ^{1}H-n.m.r. investigation at 300 and 500 MHz in [$^{2}H_{6}$]dimethyl sulphoxide solution. *Biochem. J.* 220(1), 197-205.

Sears, C.L. & Kaper, J.B. (1996). Enteric bacterial toxins: Mechanisms of action and linkage to intestinal secretion. *Microbiological Reviews* 60(1), 167-215.

Selman, C., Kerrison, N.D., Cooray, A., Piper, M.D.W., Lingard, S.J., Barton, R.H., Schuster, E.F., Blanc, E., Gems, D., Nicholson, J.K., Thornton, J.M., Partridge, L. & Withers, D.J. (2006). Coordinated multitissue transcriptional and plasma metabonomic profiles following acute caloric restriction in mice. *Physiological Genomics* 27(3), 187-200.

Shaka, A.J., Lee, C.J. & Pines, A. (1988). Iterative schemes for bilinear operators; application to spin decoupling. *Journal of Magnetic Resonance* 77(2), 274-293.

Sheng, S.Q. & Halbeek, H.v. (1995). Evidence for a transient interresidue hydrogen bond in sucrose in aqueous solution obtained by rotating-frame

exchange NMR spectroscopy under supercooled conditions. *Biochemical and Biophysical Research Communications* 215(2), 504-510.
Shimada, T. & Sakazaki, R. (1985). New O and H antigens and additional serovars of *Plesiomonas shigelloides*. *Japanese Journal of Medical Science & Biology* 38(2), 73-76.
Siciňska, W., Adams, B. & Lerner, L. (1993). A detailed ^{1}H and ^{13}C NMR study of a repeating disaccharide of hyaluronan: the effects of temperature and counterion type. *Carbohydrate Research* 242, 29-51.
Simón, E., Portillo, M.P., Fernández-Quintela, A., Zulet, M.A., Martínez, J.A. & Del Barrio, A.S. (2002). Responses to dietary macronutrient distribution of overweight rats under restricted feeding. *Annals of Nutrition and Metabolism* 46(1), 24-31.
Smolinska, A., Blanchet, L., Buydens, L.M.C. & Wijmenga, S.S. (2012). NMR and pattern recognition methods in metabolomics: From data acquisition to biomarker discovery: A review. *Analytica Chimica Acta* 750, 82-97.
Speakman, J.R. & Mitchell, S.E. (2011). Caloric restriction. *Molecular Aspects of Medicine* 32(3), 159-221.
Spindler, S.R. (2010). Caloric restriction: From soup to nuts. *Ageing Research Reviews* 9(3), 324-353.
Stejskal, E.O. & Tanner, J.E. (1965). Spin diffusion measurements: spin echoes in the presence of a time-dependent field gradient. *Journal of Chemical Physics* 42(1), 288-292.
Stock, I. (2004). *Plesiomonas shigelloides*: an emerging pathogen with unusual properties. *Reviews in Medical Microbiology* 15(4), 129-139.
Säwén, E., Östervall, J., Landersjö, C., Edblad, M., Weintraub, A., Ansaruzzaman, M. & Widmalm, G. (2012). Structural studies of the O-antigenic polysaccharide from *Plesiomonas shigelloides* strain AM36565. *Carbohydrate Research* 348, 99-103.
Trygg, J., Holmes, E. & Lundstedt, T. (2007). Chemometrics in metabonomics. *Journal of Proteome Research* 6(2), 469-479.
Tsugawa, H., Ogawa, A., Takehara, S., Kimura, M. & Okawa, Y. (2008). Primary structure and function of a cytotoxic outer-membrane protein (ComP) of *Plesiomonas shigelloides*. *Fems Microbiology Letters* 281(1), 10-16.
Tyl, C.E., Brecker, L. & Wagner, K.H. (2008). H-1 NMR spectroscopy as tool to follow changes in the fatty acids of fish oils. *European Journal of Lipid Science and Technology* 110(2), 141-148.
Wahrburg, U. (2004). What are the health effects of fat? *European Journal of Nutrition* 43, 6-11.
Valentini, M., Ritota, M., Cafiero, C., Cozzolino, S., Leita, L. & Sequi, P. (2011). The HRMAS-NMR tool in foodstuff characterisation. *Magnetic Resonance in Chemistry* 49, S121-S125.
Vanschoonbeek, K., de Maat, M.P.M. & Heemskerk, J.W.M. (2003). Fish oil consumption and reduction of arterial disease. *Journal of Nutrition* 133(3), 657-660.

Varga, K. & Watts, A. (2008). Introduction to solid-state NMR and its application to membrane protein–ligand binding studies. In: *Biophysical Analysis of Membrane Proteins*. pp. 55-87 Wiley-VCH Verlag GmbH & Co. KGaA. ISBN 9783527621224.

Watson, J.D. & Crick, F.H.C. (1953). Molecular structure of nucleic acids - a structure for deoxyribose nucleic acid. *Nature* 171(4356), 737-738.

Weissmann, B. & Meyer, K. (1954). The structure of hyalobiuronic acid and of hyaluronic acid from umbilical cord. *Journal of the American Chemical Society* 76(7), 1753-1757.

Veselkov, K.A., Lindon, J.C., Ebbels, T.M.D., Crockford, D., Volynkin, V.V., Holmes, E., Davies, D.B. & Nicholson, J.K. (2009). Recursive segment-wise peak alignment of biological H-1 NMR spectra for improved metabolic biomarker recovery. *Analytical Chemistry* 81(1), 56-66.

Westphal, O. & Jann, K. (1965). Extraction with phenol-water and further applications of the procedure. In: Whistler, R.L. (Ed.) *Methods in carbohydrate chemistry*. pp. 83-91 Academic Press; V).

Widmalm, G. (2013). A perspective on the primary and three-dimensional structures of carbohydrates. *Carbohydrate Research* 378, 123-132.

Wijeyesekera, A., Selman, C., Barton, R.H., Holmes, E., Nicholson, J.K. & Withers, D.J. (2012). Metabotyping of long-lived mice using H-1 NMR spectroscopy. *Journal of Proteome Research* 11(4), 2224-2235.

Wilkinson, S.G. (1996). Bacterial lipopolysaccharides - Themes and variations. *Progress in Lipid Research* 35(3), 283-343.

Vinogradov, E.V., Stuikeprill, R., Bock, K., Holst, O. & Brade, H. (1993). The structure of the carbohydrate backbone of the core-lipid-A region of the lipopolysaccharide from *Vibrio cholerae* strain H11 (non-O1). *European Journal of Biochemistry* 218(2), 543-554.

Vliegenthart, J.F.G., Dorland, L. & Vanhalbeek, H. (1983). High-resolution H-1 nuclear magnetic resonance spectroscopy as a tool in the structural analysis of carbohydrates related to glycoproteins. *Advances in Carbohydrate Chemistry and Biochemistry* 41, 209-374.

Wold, S., Esbensen, K. & Geladi, P. (1987). Principal component analysis. *Chemometrics and Intelligent Laboratory Systems* 2(1–3), 37-52.

Wold, S., Sjöström, M. & Eriksson, L. (2001). PLS-regression: a basic tool of chemometrics. *Chemometrics and Intelligent Laboratory Systems* 58(2), 109-130.

Wormald, M.R., Petrescu, A.J., Pao, Y.L., Glithero, A., Elliott, T. & Dwek, R.A. (2002). Conformational studies of oligosaccharides and glycopeptides: Complementarity of NMR, X-ray crystallography, and molecular modelling. *Chemical Reviews* 102(2), 371-386.

Wu, D.H., Chen, A.D. & Johnson, C.S. (1995). An improved diffusion-ordered spectroscopy experiment incorporating bipolar-gradient pulses. *Journal of Magnetic Resonance Series A* 115(2), 260-264.

Zhao, H.Q., Pan, Q.F., Zhang, W.H., Carmichael, I. & Serianni, A.S. (2007). DFT and NMR studies of $^{2}J_{COH}$, $^{3}J_{HCOH}$, and $^{3}J_{CCOH}$ spin-couplings in

saccharides: C-O torsional bias and H-bonding in aqueous solution. *Journal of Organic Chemistry* 72(19), 7071-7082.

Acknowledgement

I would like to express my gratitude to those who have been of great importance for me during these years.

Corine Sandström, my supervisor, for all your support. You are an amazing scientist and I am very glad that I have got the chance to be in your team. Thank you for everything you have taught me about NMR, carbohydrates, how to deal with collaborations, a scientific approach, and not the least about positive thinking. I appreciate that you have encouraged me to try also the craziest ideas and when I have felt that the seemingly impossible is impossible you have encouraged me to try again. In this way, you have allowed me to develop self-confidence, motivation and courage. Thank you so much!

Anders Broberg, my assistant supervisor, for taking the time to answer my questions in the lab and for proof reading of this thesis. Even without being actively involved in my projects I have felt that you have always been easily available.

The late Lennart Kenne, my assistant supervisor, who left us too early, for sharing your enthusiasm and outstanding scientific knowledge. Numerous times during the last two years I have thought "*that* I would have asked Lennart about".

Jan Eriksson, my co-author and informal assistant supervisor, thanks a lot for sharing the probability dimension in research, as well as your reflections about everything from parenting to environmental pollutants.

Jolanta Lukasiewicz, my co-author and informal assistant supervisor some distance away, for answering all my questions about LPS without getting tired. Thank you also, together with Wojciech, Tomasz, and the rest of your group, for a very nice visit in Wrocław.

Other co-authors, including Johan Bankefors, for being helpful and relaxed, and Jana Pickova, Christian Schlechtriem and Kjell Malmlöf.

Ulf Holmbäck and Roger Olsson at Uppsala University for sharing their human blood serum samples that are included in Figure 19 and 20.

Thanks to my room mates, Eric Morssing Vilén and Lena Lundqvist for listening to me whenever I have to tell you about my extremely important results or the extremely bad outcome of yet another experiment. You have been invaluable, both as scientific partners and as friends during conferences, courses, and late evenings in our pleasant room.

Pierre Andersson, my former room mate and still friend, for all discussions about religion, politics, money and other things that will stay between us.

Other former room mates are Marta Kaszowska, who made my first year at the department more exciting – Thank you for being spontaneous and emotionally generous! – and Jun Xu, who let me know about Chinese brilliance.

David Hansson, I miss you. Thank you for many interesting conversations. Christina Nord, thanks for enjoyable discussions and keep your boots muddy. Other former and current PhD students for keeping a pleasant environment. That includes (in some kind of chronological order) Elena Ossipova, Gunnar Almkvist (initially you were also a graduate student), Olesya Nikonova, Natallia Torapava, Lars Eklund, Kai Wilkinson, Johan Mähler, Shahin Norbakhsh, Tobias Bölscher, Josephina Werner, Frida Wende, Elizabeth Polido Legaria, and Martin Palmqvist.

Thanks to Suresh Gohil for sharing your MS knowledge and sense of humor. Rolf Andersson for help in my initial attempts to get control over the NMR spectrometers and Peter Agback for tips and help when the NMR spectrometers were in a bad mood. Sonja Jansson and your forerunner, Lena Andersson, for keeping administrative stuff easy. Bernt Andersson (and Linus) for making the lab exercises going on smoothly.

Anders Sandström for a good climate of cooperation regarding teaching and for proof reading of this thesis. Anke Herrmann, Mattias Fredriksson, Ali Moazzami, and Daniel Lundberg for many nice lunches. Aahana Shrestha, Seda Demirel Topel, Elisabeth Müllner, Gulaim Seisenbaeva, Vadim Kessler, Ingmar Persson, and Yina Salamanca for keeping a nice atmosphere in our corridor.

I would like to thank former members of the Committee for appointing lecturers for your welcoming attitude when I was a student representative.

Elisabet Öberg for nice cooperation during the well-known Carey Sundberg course.

I know that I should stop now, because otherwise this would become an autobiography. However, I can not resist to thank my former supervisor Annika Björn at Water and Environmental Studies, Linköping University who

inspired me to keep on with chemistry. Also the staff at the former Department of Environmental Chemistry at Stockholm University for your friendly environment and for teaching me a lot about research.

Kristin Webling, for a nice collaboration and friendship. Good luck with PhD studies and childbearing! Axel, Erik and Matilda for being my friends.

Thanks to other relatives and friends, who I will come back to in my auto-biography.

Kerstin, my mother, to whom this thesis is dedicated, who abruptly passed away five years ago. I wish that you would have been able to experience this moment of my life. I know that you would have been proud of me.

Conny, my father, for your support. Thank you for reminding me of what is most important in life. Now is the time to come here more frequently and visit me and your grandchildren!

At last, I want to thank my wife, Elvira Caselunghe, for not being too mad at me, especially during these last months when I have been working days and nights, and you have taken care of our children during days and nights. I promise to pay back when you are in the final part of your PhD studies. Thank you for your support and unrestricted love. I love you!

My children, Vera and Ingrid, who are the most important. You make it easy for me to forget about work when I get home. Now we will have much time to play together!